Imperial College London

Development of Multifunctional Nano-probes for Neuroscience Research

Babak Babakinejad

Nano-medicine Laboratory

Experimental Physiology

A thesis submitted in fulfilment of the requirements for the degree of Doctor of Philosophy and the Diploma of Imperial College

Nanotechnology & Neuroscience

June 2013

The material presented in this thesis is of my own work under the supervision of Professor Yuri Korchev at Imperial College London. All the previous work & collaborative work have been appropriately acknowledged.

Babak Babakinejad

London 30 June 2013

Abstract

The contribution of nanotechnology to the field of Neuroscience is increasing exponentially. In order to understand the relationship of structure to function at the cellular level, and to decipher the mysteries of nervous system, development of new tools to manipulate and measure cellular function at a local level is necessary. It is a continuing challenge to develop easily fabricated, multipurpose nano-probes which are able to target neural nanostructures for the local manipulation and measurement of functional responses.

This thesis is focused on the fabrication, characterisation and implementation of a nano-pipette on a Scanning Ion Conductance Microscopy (SICM). The nano-pipette mounted on a SICM set-up acts as a proximity sensor for non-contact imaging of cellular features.

SICM platform to accommodate electrochemical experiments is discussed. In particular, the development of a novel electrochemical probe, fabricated by pyrolytic decomposition of carbon within a quartz nano-pipette is discussed. This method is simple and carbon nano-electrodes of variable size can be fabricated in a single step.

The nano-pipette‘s distance controlled feedback system was exploited for local delivery of chemicals to neuronal structures. Experimental and theoretical data are compared in order to calculate the concentration of molecules at the tip of the nano-pipette as a function of the driving force (voltage or pressure) and distance. The quantitative delivery of molecules from a 100 nm nano-pipette is demonstrated. In particular capsaicin-filled nano-pipette is used to trigger capsaicin-sensitive TRPV1 receptors in sensory neurons and transfected cells. Finally some preliminary results for the future development and potential application of nano-pipettes are shown. The nano-pipette is easily fabricated and is shown to be multi-functional. It provides an invaluable tool in the investigation of the nano-physiology of neurons. The SICM multipoint delivery competence can contribute to the various endeavours in drug discovery and to the yield of *in vitro* pharmacological assays.

Acknowledgement

I would like to thank my supervisor Professor Yuri Korchev for introducing me to the joys of fly fishing and for embodying the ideal of the independent-minded scientist and for his insightful comments throughout my research. I am indebted to Dr Paolo Actis for his sincere assistance and continual encouragement and for reading and commenting on multiple drafts of this thesis. I am particularly indebted to Dr Peter Jönsson of the University of Cambridge for showing me a real life example of what it means to be an ethical scientist and a perfect gentleman. I would like to thank Dr Pavel Novak for patiently giving his time to explain the SICM technique and software manipulation.

I would like to thank Dr Yasufumi Takahashi for his support and introducing me to electrochemistry. I would like to thank Dr Uma Anand for teaching me to dissect and prepare primary cultures of sensory neurons. I would like to thank Dr Julia Gorelik, Professor Max J Lab and Ms Francisca Schultz for reading and commenting on the draft of this thesis. I would like to thank Dr Andrew Shevchuk for his technical assistance. I would also like to thank Ms Ainara López Córdoba. I would like to thank Dr Charlie R Parkinson for his support. I would like to thank BBSRC & GSK for supporting this research and paying my salary. As scientists we are sometimes inclined to become lost in the intricacies of highly specific areas of human endeavour, and to lose perspective of the place of science in the wider context of the nature and society. I would like to thank my friend Mr. Kayvan Beklik notwithstanding that he is not a scientist, for providing me with invaluable opportunities to talk and think about life apart from science.

Table of content

List of figures

Abbreviations

AFM	Atomic Force Microscopy
AM	Acetoxymethyl
Cr	Chromium
DAC	Digital to Analog Converter
DC	Direct Current
DNA	Deoxyribonucleic acid
DRG	Dorsal root ganglia
DSP	Digital Signal Processor
EDTA	Ethylenediaminetetraacetic acid
EDX	Energy-dispersive X-ray Microscopy
FET	Field Effect Transistor
FRET	Fluorescence Resonance Energy Transfer microscopy
HBSS	Hank's Balanced Salt Solution
HEK	Human Embryonic Kidney cells
HPICM	Hopping Probe Ion Conductance Microscopy
ICM	Icon Conductance Microscope
MEAs	Microelectrode Arrays
NCLSCs	Neural Crest-Like Stem Cells

PALM	Photo-Activated Localization Microscopy
PAP	*p*-aminophenol
PAPP	*p*- aminophenyl phosphate
PBS	Phosphate Buffered Saline
PC12	Pheochromocytoma 12
PNS	Peripheral Nervous System
Pt	Platinum
SCINEs	Solid-Conductor Intracellular Nano-electrodes
SCM	Scanning Confocal Microscopy
SECM	Scanning electrochemical microscopy
SEM	Scanning Electron Microscopy
SICM	Scanning Ion Conductance Microscopy
SPM	Scanning probe microscopy
SSCM	Scanning Surface Confocal Microscopy
STED	Stimulated Emission Depletion
STORM	Stochastic optical reconstruction microscopy
TRP	Transient Receptor Potential
TRPV1	Transient Receptor Potential cation channel subfamily Vanilloid member 1
UME	Ultra-micro-electrode
VENA	Vertical nano-wire electrode array

Nomenclature and Units

k_B	Boltzmann factor
q	charge of the molecule
c	concentration of molecules
I_{ss}	current reduction value
CV	Cyclic Voltammetry
D	diffusivity
R_+	distance from the tip
E	electric field
E_t	electric field tangential to the wall
Ψ	electrical potential
μ_{eo}	electro-osmotic mobility
μ_{ep}	electro-phoretic mobility
J	flux of molecules
ϑ	inner half-cone angle of the pipette
kHz	Kilohertz
kPa	kilopascal
ms	Millisecond
mV	Millivolt
mW	Milliwatt
nm	Nanometer

nM	nanomolar
Ω	Ohm
ε_0	permittivity of vacuum
Δp	pressure drop
R	radius
Rg	ratio of the quartz capillary's outer and inner
ε_r	relative permittivity of the electrolyte solution
T	temperature
u_{eo}	velocity field due to electro-osmosis
u_{ep}	velocity field due to electro-phoresis
u_p	velocity field due to pressure-driven flow
η	viscosity of the liquid
ζ	zeta potential of the pipette wall

Chapter 1

Introduction

Understanding how the nervous system works is a major challenge that has yet to be overcome. One reason for this is the sheer complexity of the central nervous system; there are approximately 85 billion neurons and 100 trillion synapses in the human brain (Azevedo et al., 2009). Having a comprehensive understanding of the function of the brain is essential in the development of new medicines for neurological disorders. For this finding the structure-function relationship in the small scale is essential. This challenged can only be overcome by developing nano-scale tools to examine electrochemical communications by manipulating cellular interaction and also by measuring responses with nano-scale resolution (Alivisatos et al., 2013).

Patch clamp electrophysiology is one of the earliest and the most widely used methods to study ion channels (Neher and Sakmann, 1976). This method is highly sensitive since single ion channel activity can be probed; however there are drawbacks in this method. It is invasive, and routine analysis relies on highly skilled operators which limits the widespread adoption of this technique. The maintenance of contact for prolonged periods of time is also a disadvantage. Several groups have developed methods to overcome these limitations. In particular the fabrication of nano-probes to reduce the damage to the cell membrane have been developed for intra and extracellular recordings, but these methods generally give a

poor read out due to the low signal to noise ratio in the recorded signal (Wirth and Luscher, 2004; Li et al., 2003; Banks et al., 2002; Kwiat et al., 2013).

Recent development in nano-technology has made it possible to fabricate devices such as nano-particles for therapeutic purposes (Krol et al., 2013), nano-sensing devices and probes (Cui et al., 2001) small enough, for targeted interactions with biological cells to investigate the nano-physiology of cells and neurons.

Angle and Shaefer recently showed the fabrication of Solid-Conductor Intracellular Nano-electrodes (SCINEs), by milling tungsten micro-electrodes using a focused ion beam to achieve a tip diameter as small as <300nm (Figure 1.1). They have managed to shown recordings of transmembrane potential changes in brain tissue using these probes (Angle and Schaefer, 2012).

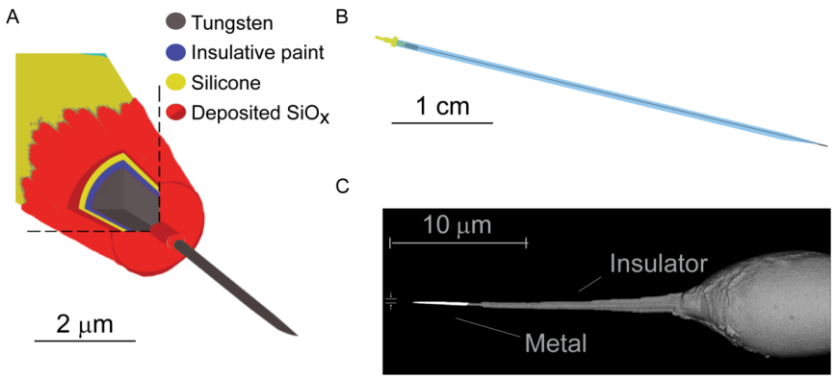

Figure 1.1 Cartoon showing the fabrication of SCINEs electrodes (Angle and Schaefer, 2012).

A similar approach was followed by Yoon and co-workers (Yoon et al., 2013). They have developed a reusable needle-shaped carbon nano-tube, from an electrochemically etched tungsten wire. The fabricate probe requires further improvement in terms of geometry and

insulation layers and implementation of capacitance compensation methods, to become suitable for *in vitro* and *in vivo* assays.

Lieber's group have applied semi-conductor fabrication technology to fabricate a miniaturized field effect transistor (FET), capable of intracellular recording of action potential in cardiomyocytes (Tian et al., 2010). This work pioneered the application of transistors for electrophysiology but the very complex fabrication procedure limits its use by other research groups.

Xie and colleagues have used nano-pillar electrode arrays for intra and extra cellular recordings of action potential from cardiomyocyte by means of electro-poration (Figure 1.2). The recordings were performed with high sensitivity and over a long period of time. Intra cellular Vertical nano-wire electrode array (VENA) have been developed and used to record and stimulate neurons *in vitro* (Robinson et al., 2012).

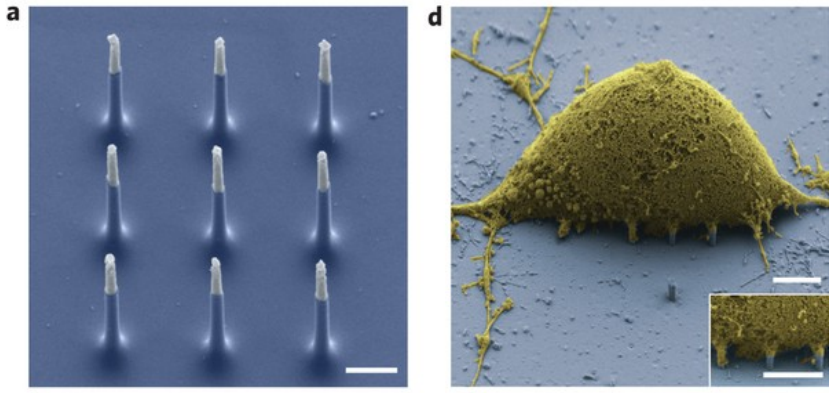

Figure 1.2. (A) SEM image of a representative silicon nano-wires (scale bar, 1 µm). Grey region, constitutes the active site. **(B)** Interface of cell membrane and the vertical silicon electrodes array (VNEA; scale bar, 2.5 µm), (Robinson et al., 2012).

Extracellular and intracellular single nano-electrode fabrication research is promising, however at its present state the fabrication process of single probe is technologically complicated and at the same time does not provide the needed integrated approach required for understanding neuronal processes. The microelectrode arrays (MEAs) and FET devices have the advantage of stimulating and measuring neuronal activities from different points, compared to single probes. However Nano-wires may spontaneously penetrate or in cases permealise cell membrane following the application of short pulse (Xie et al., 2012). Protruding arrays may interact with cell membrane and interfere with the normal biochemical processes of cells that are seeded on them (Kwiat et al., 2013).

Pipette mediated local delivery

Micro-pipettes, have been extensively used over the past decades for intra- and extra-cellular perfusions, whole cell and single channel current recordings, cell injection, local delivery of chemicals, suction of cellular contents, or as biosensors (Stone T.W., 1985; Adam Seger et al., 2012; Vilozny et al., 2011). This has made micro-pipettes a unique research tool in cell physiology.

Researchers mostly rely on visual means to operate and position micro-pipettes - which consequently in the best case scenario provide an accuracy of about a micron. Micro-pipettes can be used for local delivery of chemicals. Traditionally delivery of molecules to cells, relies on pressure mediated and micro-iontophoresis, where small charged compounds within glass micro-pipettes of a few micrometers in diameter are released under the application of voltage or pressure (Lalley, 1999). This method is now routinely

applied especially for the administration of neuro-active compounds both *in vivo* and *in vitro* with single cell resolution (Lalley, 1994; Nicoll et al., 1990; Zhang and Mifflin, 1997). However the large size of the micro-pipette opening prevents targeting a specific regions on the cellular structures. In addition the lack of a positioning system and with nano-meter resolution prevent quantitative dosing since it is not possible to precisely control the distance between the pipette and the sample, with uncontrolled diffusional dilution (Bagher et al., 2011.; Kovacs et al., 2005).

Different groups have started to combine nano-pipettes with scanning probe microscopy methods (Loh et al., 2009; Meister et al., 2009). In particular, the integration of nano-pipettes into the Scanning Ion Conductance Microscopy, allows for the creation of molecular arrays or local stimulation or mapping of molecular complexes outside and inside living cells (Adam Seger et al., 2012; Bruckbauer et al., 2004; Bruckbauer et al., 2007; Piper et al., 2008; Rodolfa et al., 2005).

Development of SICM for biology and biomedical research

Scanning Ion Conductance Microscopy (SICM) (Hansma et al., 1989; Korchev et al., 1997; Shevchuk et al., 2011) is a member of the Scanning probe family of microscopy, which uses a nano-pipette as a probe. The basic SICM setup consists of a nano-pipette filled with an electrolyte solution that is immersed in an electrolytic bath. An electrode is introduced into the nano-pipette and a reference electrode is placed in the bath. The ion current flowing through the nano-pipette, determined by the resistance between the tip and surface, is measured and reduces as the tip approaches the sample surface. The reduction in ion

current is used as a feedback to control the distance between the nano-pipette and the sample. This distance is set as a constant while the nano-pipette scans across a surface. Information from the position of the nano-pipette across the sample is used to construct a detailed topographical image, comparable to scanning electron microscopy (Chen et al., 2012; Korchev et al., 1997; Rheinlaender et al., 2010). The noncontact and robust feedback system of the SICM nano-probe, makes it suitable for imaging biological samples without causing damage. The SICM system can be incorporated with multiple research tools and modalities, which makes it a powerful discovery tool in the field of biomedical science (Figure 1.3).

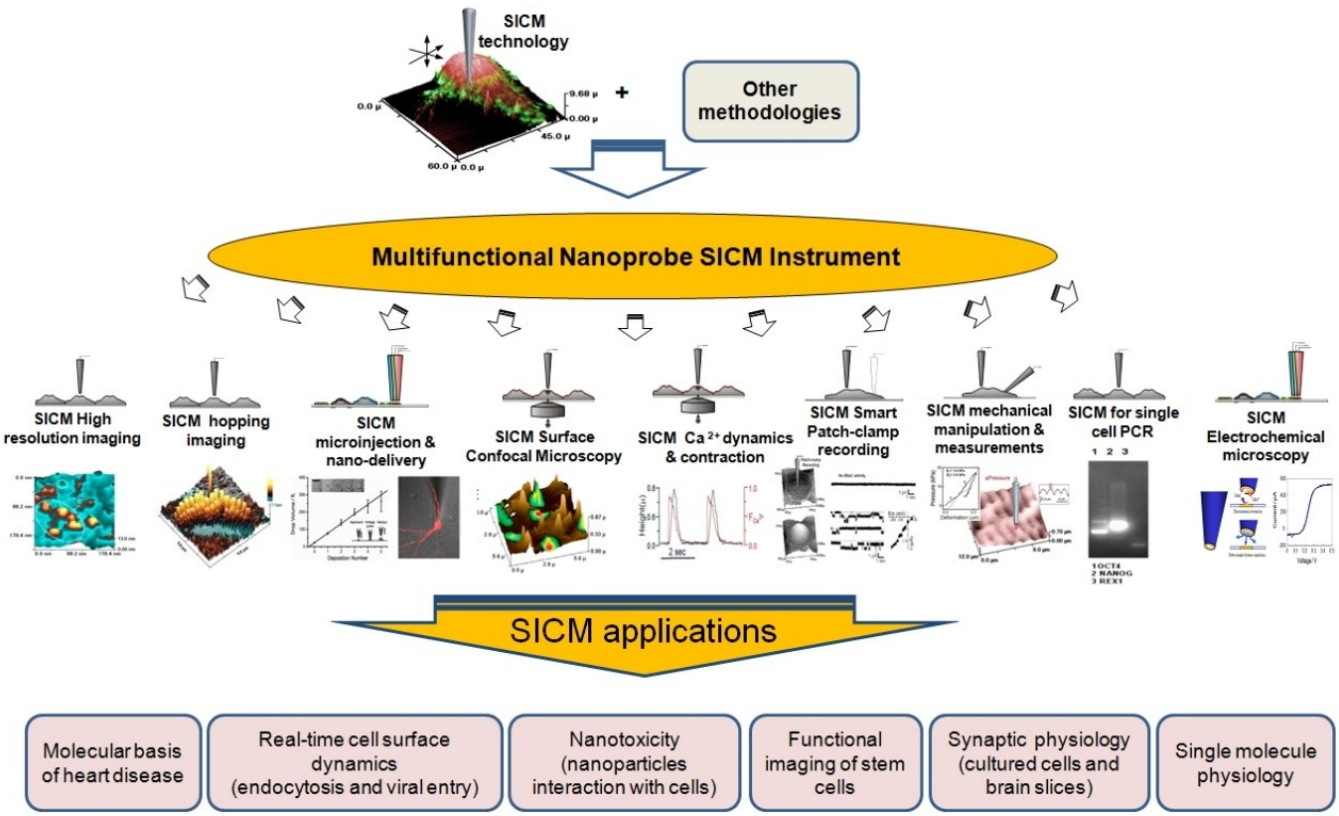

Figure 1.3. Schematic representation of SICM as a multifunctional tool and its versatility in combination with other techniques (Shevchuk et al., 2011).

Combined Fluorescence Imaging

The combination of SICM and fluorescence imaging has provided molecular specificity, as well as the possibility to map and characterise receptor mediated fluorescence responses by single molecule imaging in functional studies. Local delivery from the SICM nano-pipette in combination with Fluorescence Resonance Energy Transfer (FRET) microscopy, has enabled mapping of adrenergic receptors, in healthy and diseased cardiyomyocytes models. This was made possible by accurate positioning of the pipette for localized delivery of agonist solutions with pressure (Nikolaev et al., 2010).

Smart patch Clamp

Functional recordings from single ion channels (Smart-Patch), is a technique which implements patch-clamp electrophysiology into the SICM system, which allows targeted ion channel recording with the SICM pipette, in areas that were unreachable by micro-manipulation methods (Gorelik et al., 2002).

Mechanical mapping

SICM can be used to probe the mechanical properties of cellular structure by applying pressure. Positive and negative hydrostatic pressure, is applied with the same imaging probe, to investigate the local mechanical properties of the cell while the feedback system is used to measure the elasticity and mechanical properties of the sample Pressure application can also be applied directly, with the pipette tip making a direct physical contact to the cell membrane (Sanchez et al., 2008; Sanchez et al., 2007) (Figure 1.4).

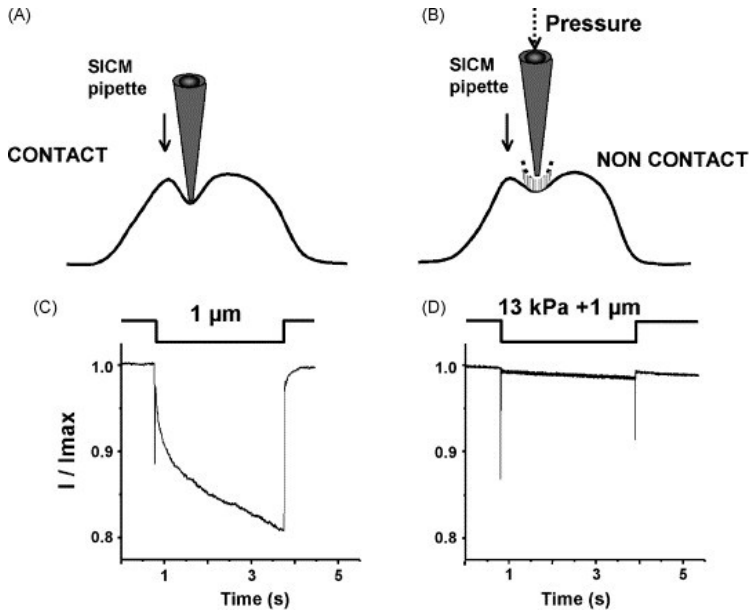

Figure 1.4. (A) and **(B)** are schematic representations of contact and non-contact modes of mechanical stimulation with a SICM pipette. **(C)** and **(D)** show normalised current through the pipette pore in contact and non contact modes respectively (Sanchez et al., 2007).

Combination of SICM with SECM

Scanning electrochemical microscopy (SECM) (Bard et al., 2006) in combination with SICM feedback control can be used to position the carbon probe in the proximity of synaptic boutons or active neurotransmitter release sites, for topographical and electrochemical analysis. Carbon probes have been used previously for detection of neurotransmitter release (Robinson et al., 2008). SECM uses an ultra-micro-electrode (UME) to detect electro-active substances, and has been used to image biological samples in combination with other forms of SPMs (Amemiya et al., 2008; Takahashi et al., 2009; Takahashi et al., 2010; Takahashi et al., 2011; Kueng et al., 2003; Avdic et al., 2011). The SECM probe has long distance sensitivity to the changes in the redox current. This prevents it to be utilised for simultaneous electrochemical measurement and for distance feedback. This is the reason

that SECM are generally performed on flat surfaces. Development of sharp UMEs and combination of SICM with SECM has provided a robust feedback mechanism for high resolution topographical and electrochemical imaging (Comstock et al., 2010; Takahashi et al., 2010).

SICM and local chemical delivery

The SICM nano-probe, and more importantly its distance-control capacity make it an ideal tool for controlled, targeted drug delivery and mechanical manipulation (Shevchuk et al., 2011). The high resolution structural information obtained by SICM can be used to position the probe to target local areas and deliver reagents from the SICM nano-pipette via electrophoresis and electro-osmosis ("nano-iontophoresis") or by using pressure.

This process can be automated to allow pre- and post-treatment topographical imaging that can be repeated after single or multipoint delivery to different regions within a frame. Distance information is essential to infer the concentration that the underlying structure experiences. By keeping this distance constant it is possible to collect consistent and comparable data from different structures.

The multi functional capacity of nano-pipette makes it a simple and reliable nano-probe, accessible to most scientists. Integration of nano-pipette probes into the SICM for local nano-physiology of neurons, allows repeated experiments on similar specimens, increases the yield of experimental data on rare primary culture neurons *in vitro*, and is ultimately more humane because it reduces the number of experimental animal required for testing.

References

Adam Seger R, Actis P, Penfold C, Maalouf M, Vilozny B, Pourmand N. Voltage controlled nano-injection system for single-cell surgery. Nano-scale 2012;4(19):5843-6.

Alivisatos A, Andrews AM, Boyden ES, Chun M, Church GM, Deisseroth K, et al. Nanotools for Neuroscience and Brain Activity Mapping. Acs Nano 2013;7(3):1850-66.

Amemiya S, Bard AJ, Fan FR, Mirkin MV, Unwin PR. Scanning Electrochemical Microscopy. Annual Review of Analytical Chemistry 2008;1:95-131.

Angle MR, Schaefer AT. Neuronal recordings with solid-conductor intracellular nano-electrodes (SCINEs). PloS one 2012;7(8):e43194.

Avdic A, Lugstein A, Wu M, Gollas B, Pobelov I, Wandlowski T, et al. Fabrication of cone-shaped boron doped diamond and gold nano-electrodes for AFM-SECM. Nanotechnology 2011;22(14).

Azevedo FA, Carvalho LR, Grinberg LT, Farfel JM, Ferretti RE, Leite RE, et al. Equal Numbers of Neuronal and Nonneuronal Cells Make the Human Brain an Isometrically Scaled-Up Primate Brain. Journal of Comparative Neurology 2009;513(5):532-41.

Bagher P, Polo-Parada L, Segal SS. Micro-iontophoresis and micromanipulation for intravital fluorescence imaging of the microcirculation. JoVE 11 A.D. Oct 6.

Bard AJ, Li X, Zhan W. Chemically imaging living cells by scanning electrochemical microscopy. Biosensors & Bioelectronics 2006;22(4):461-72.

Bruckbauer A, James P, Zhou D, Yoon JW, Excell D, Korchev Y, et al. Nano-pipette delivery of individual molecules to cellular compartments for single-molecule fluorescence tracking. Biophys J 2007 Nov 1;93(9):3120-31.

Bruckbauer A, Zhou D, Kang DJ, Korchev YE, Abell C, Klenerman D. An addressable antibody nanoarray produced on a nanostructured surface. J Am Chem Soc 2004 Jun 2;126(21):6508-9.

Chen CC, Zhou Y, Baker LA. Scanning ion conductance microscopy. Annual review of analytical chemistry (Palo Alto, Calif) 2012;5(1):207-28.

Comstock DJ, Elam JW, Pellin MJ, Hersam MC. Integrated Ultramicro-electrode-Nanopipet Probe for Concurrent Scanning Electrochemical Microscopy and Scanning Ion Conductance Microscopy. Analytical Chemistry 2010;82(4):1270-6.

Deisseroth K, Feng G, Majewska AK, Miesenbock G, Ting A, Schnitzer MJ. Next-generation optical technologies for illuminating genetically targeted brain circuits. Journal of Neuroscience 2006;26(41):10380-6.

Deisseroth K. Optogenetics. Nat Methods 2011 Jan;8(1):26-9.

Gorelik J, Gu Y, Spohr HA, Shevchuk AI, Lab MJ, Harding SE, et al. Ion channels in small cells and subcellular structures can be studied with a smart patch-clamp system. Biophys J 2002 Dec;83(6):3296-303.

Hansma PK, Drake B, Marti O, Gould SAC, Prater CB. The Scanning Ion-Conductance Microscope. Science 1989;243(4891):641-3.

Holmes D, Gawad S. The Application of Micro-fluidics in Biology. 2010.

Korchev YE, Bashford CL, Milovanovic M, Vodyanoy I, Lab MJ. Scanning ion conductance microscopy of living cells. Biophys J 1997 Aug;73(2):653-8.

Kovacs P, Denes V, Kellenyi L, Hernadi I. Micro-iontophoresis electrode location by neurohistological marking: Comparison of four native dyes applied from current balancing electrode channels. J Pharmacol Toxicol Methods 2005 Mar;51(2):147-51.

Kueng A, Kranz C, Lugstein A, Bertagnolli E, Mizaikoff B. Integrated AFM-SECM in tapping mode: Simultaneous topographical and electrochemical imaging of enzyme activity. Angewandte Chemie-International Edition 2003;42(28):3238-40.

Lalley P. Micro-iontophoresis and Pressure Ejection. In: Windhorst U, Johansson H+, editors. Modern Techniques in Neuroscience Research. Springer Berlin Heidelberg; 1999. p. 193-212.

Lalley PM. The excitability and rhythm of medullary respiratory neurons in the cat are altered by the serotonin receptor agonist 5-methoxy-N,N, dimethyltryptamine. Brain Res 1994 Jun 13;648(1):87-98.

Loh O, Lam R, Chen M, Moldovan N, Huang H, Ho D, et al. Nanofountain-probe-based high-resolution patterning and single-cell injection of functionalized nanodiamonds. Small 2009 Jul;5(14):1667-74.

Meister A, Gabi M, Behr P, Studer P, Voros J, Niedermann P, et al. FluidFM: combining atomic force microscopy and nanofluidics in a universal liquid delivery system for single cell applications and beyond. Nano Lett 2009 Jun;9(6):2501-7.

Neher E, Sakmann B. Single-Channel Currents Recorded from Membrane of Denervated Frog Muscle-Fibers. Nature 1976;260(5554):799-802.

Nicoll RA, Malenka RC, Kauer JA. Functional comparison of neurotransmitter receptor subtypes in mammalian central nervous system. Physiol Rev 1990 Apr;70(2):513-65.

Nikolaev VO, Moshkov A, Lyon AR, Miragoli M, Novak P, Paur H, et al. Beta2-adrenergic receptor redistribution in heart failure changes cAMP compartmentation. Science 2010 Mar 26;327(5973):1653-7.

Park JW, Kim HJ, Kang MW, Jeon NL. Advances in micro-fluidics-based experimental methods for neuroscience research. Lab on A Chip 2013;13(4):509-21.

Park JW, Vahidi B, Taylor AM, Rhee SW, Jeon NL. Micro-fluidic culture platform for neuroscience research. Nature Protocols 2006;1(4):2128-36.

Piper JD, Li C, Lo CJ, Berry R, Korchev Y, Ying L, et al. Characterization and application of controllable local chemical changes produced by reagent delivery from a nanopipet. J Am Chem Soc 2008 Aug 6;130(31):10386-93.

Rheinlaender J, Geisse NA, Proksch R, Scha¦êffer TE. Comparison of Scanning Ion Conductance Microscopy with Atomic Force Microscopy for Cell Imaging. Langmuir 2010 Dec 15;27(2):697-704.

Robinson DL, Hermans A, Seipel AT, Wightman R. Monitoring rapid chemical communication in the brain. Chemical Reviews 2008;108(7):2554-84.

Robinson JT, Jorgolli M, Shalek AK, Yoon MH, Gertner RS, Park H. Vertical nano-wire electrode arrays as a scalable platform for intracellular interfacing to neuronal circuits. Nat Nano 2012 Mar;7(3):180-4.

Rodolfa KT, Bruckbauer A, Zhou D, Korchev YE, Klenerman D. Two-component graded deposition of biomolecules with a double-barreled nano-pipette. Angew Chem Int Ed Engl 2005 Oct 28;44(42):6854-9.

Sanchez D, Anand U, Gorelik J, Benham CD, Bountra C, Lab M, et al. Localized and non-contact mechanical stimulation of dorsal root ganglion sensory neurons using scanning ion conductance microscopy. J Neurosci Methods 2007 Jan 15;159(1):26-34.

Sanchez D, Johnson N, Li C, Novak P, Rheinlaender J, Zhang Y, et al. Noncontact measurement of the local mechanical properties of living cells using pressure applied via a pipette. Biophys J 2008 Sep 15;95(6):3017-27.

Shevchuk AI, Novak P, Takahashi Y, Clarke R, Miragoli M, Babakinejad B, et al. Realizing the biological and biomedical potential of nano-scale imaging using a pipette probe. Nanomedicine (Lond) 2011 Apr;6(3):565-75.

Stone T.W. Micro-iontophoresis And Pressure Ejection. The International Brain Research Organization; 1985.

Takahashi Y, Shevchuk AI, Novak P, Murakami Y, Shiku H, Korchev YE, et al. Simultaneous noncontact topography and electrochemical imaging by SECM/SICM featuring ion current feedback regulation. J Am Chem Soc 2010 Jul 28;132(29):10118-26.

Takahashi Y, Shevchuk AI, Novak P, Zhang Y, Ebejer N, Macpherson JV, et al. Multifunctional Nano-probes for Nano-scale Chemical Imaging and Localized

Chemical Delivery at Surfaces and Interfaces. Angew Chem Int Ed 2011 Oct 4;50(41):9638-42.

Takahashi Y, Shiku H, Murata T, Yasukawa T, Matsue T. Transfected Single-Cell Imaging by Scanning Electrochemical Optical Microscopy with Shear Force Feedback Regulation. Analytical Chemistry 2009;81(23):9674-81.

Taylor AM, Blurton-Jones M, Rhee SW, Cribbs DH, Cotman CW, Jeon NL. A micro-fluidic culture platform for CNS axonal injury, regeneration and transport. Nat Methods 2005 Aug;2(8):599-605.

Tian B, Cohen-Karni T, Qing Q, Duan X, Xie P, Lieber CM. Three-Dimensional, Flexible Nano-scale Field-Effect Transistors as Localized Bioprobes. Science 2010 Aug 13;329(5993):830-4.

Vilozny B, Actis P, Seger R, Pourmand N. Dynamic Control of Nanoprecipitation in a Nano-pipette. Acs Nano 2011;5(4):3191-7.

Wolfe D, Mata M, Fink DJ. Targeted drug delivery to the peripheral nervous system using gene therapy. Neuroscience Letters 2012;527(2):85-9.

Xie C, Lin Z, Hanson L, Cui Y, Cui B. Intracellular recording of action potentials by nanopillar electroporation. Nature Nanotechnology 2012;7(3):185-90.

Yoon I, Hamaguchi K, Borzenets IV, Finkelstein G, Mooney R, Donald BR. Intracellular Neural Recording with Pure Carbon Nanotube Probes. PloS one 2013 Jun 19;8(6):e65715.

Zhang J, Mifflin SW. Influences of excitatory amino acid receptor agonists on nucleus of the solitary tract neurons receiving aortic depressor nerve inputs. J Pharmacol Exp Ther 1997 Aug;282(2):639-47.

CHAPTER 2

Materials and Methods

Materials for cell culture

Culture dishes

14 mm Microwell, No. 0 coverglass (0.085-0.13 mm), Glass bottom culture dish (MatTek Corporation, UK) Part No: P35G-014-C, or 35mm petri-dish were used for experiments. To coat the glass with collagen, 250 µl solution is added to the petri-dish/cover slip and incubated for 1 hour in the fume hood. The solution is then aspirated and left to dry.

0.5% Rat tail collagen is prepared in acetic acid (10 mM) and passed through 0.45 micron filter. 250 µl is added to each glass covered MatTek dish/cover-slip, and left at room temperature for 1 hour before washing with distilled water containing 100 ng/ml Penicillin and streptomycin.

Cell preparations

Sensory neurons dissection and preparation

Bilateral dorsal root ganglia (DRG) neurons were isolated from all spinal levels of neonatal (P0-P02), and adult Wistar rats (60 days old , 250 g), and transferred to in Dulbecco's modified Eagle's medium (DMEM, Life Technologies, UK). Dissected ganglions were then incubated in 0.5% dispase enzyme in 0.2% collagenase at 37°C for 3 hours to digest and were dissociated in modified BSF2 medium with 2% fetal calf serum (1 mg/ml). Cells were centrifuged and resuspended in DMEM with 10% FBS, penicillin and streptomycin and NGF (100 ng/ml), before plating (type I, 50 µg/ml) and incubated at 37° humidified incubator with 0.5% CO_2 (Anand et al., 2008). Isolation procedures were performed in accordance with the guidelines of the UK Home-Office Animal (Scientific Procedures) Act 1986. It should be

noted that DRG neurons used in this research have been obtained from animals that were already sacrificed for other research purposes.

Rat hippocampal neurons

Hippocampal neurons experiments were carried out in collaboration with Dr Guy Moss at the University College London. Primary cultures of rat hippocampal neurons were prepared as described in here: (Shah and Haylett, 2000).Imaging of hippocampal neurons were carried out in media containing (in mM): NaCl 145; KCl 3; $CaCl_2$ 2.5; $MgCl_2$ 1.2; Glucose 10; HEPES 10. The loading solution for Fluo-4 staining in (mM): NaCl 103; KCl 45; $CaCl_2$ 2.5; $MgCl_2$ 1.2; Glucose 10; HEPES 10.

Primary neurons and the neuronal cultured used for fluorescence imaging are kept in 37 ºC and 95% air with 5 % CO_2 incubator. Experiments are generally done on day 2-4 for DRGs and 1-2 weeks for hippocampal neurons, after cell culture, cells are removed from the incubator, and washed with external solution. Experiments are carried out within 90 minutes at room temperature.

Neuronal system animal stem cells

Embryonic neural crest cells are pluripotent and can generate the peripheral nervous system, melanocytes, and some connective tissues. Neural Crest-Like Stem Cells (NCLSCs) were used from neonatal mouse epidermis, to stimulate their differentiation into neurons (Sviderskaya *et al*., 2009). A mixture of neurotrophic factors (described below), is used to differentiate neuronal crest cells to sensory neurons. Most of the differentiated cells

express neurofilaments and a minority express transient receptor potential vanilloid subtype 1 (TRPV1) channels.

Primary cultures were made from mouse trunk skin (Neonatal *misty* (*m/m*)) (Sviderskaya *et al*., 1995). The *misty* mutation increases the pigmentation and impairs the proliferation of melanocytes. Trypsin and EDTA were used to dissociate the epidermal sheets into cell suspension. The cells were then seeded on keratinocyte feeder cells. For details of establishment and passage of melanocyte cell cultures please refer to (Sviderskaya et al., 2009).

Maintenance and differentiation of immortal cell lines

Medium containing fetal calf serum was used to maintain the cultures in addition to 200 nM of TPA that was added before resuspension of the cells in the culture. The medium was changed twice a week. For differentiation into sensory like neurons, NCLSCs were incubated in the media containing 2 nM TPA, 50 ng/ml NGF, 25 ng/ml BDNF, 25 ng/ml NT3 and 40 pM FGF-2. After two weeks a substantial number of cells present dendritic features as described by Sidverskaya *et al*., (2009).

Human Embryonic Kidney cells

Human Embryonic Kidney (HEK) cells transfected with TRPV1 channels (TRPV1-HEK-293) provided by Dr Uma Anand, were cultured in DMEM with 10% fetal calf and plated on collagen coated MatTek dishes (glass bottom plastic petri-dishes).

Sperm

Boar sperm cells were provided by JSR genetics. Sperms are diluted in PBS or HBSS prior to experiments and seeded onto polylysine coated dishes and allowed to settle down on the bottom of the dish for 30 minutes prior to experiments.

Drosophila eye

For imaging the eye of the fruit fly (*Drosophila Melanogaster*), wild Dahomey type female flies were used, which were kindly provided by Professor Linda Partridge's lab. Female flies were immobilised on ice and were decapitated. The head was placed on the petri-dish and fixed with silicon grease to expose the eye for the imaging. Experiments were performed in PBS solution.

PC12

PC12 cells were cultured in RPMI-1640 (GIBCO) with 10% heat-inactivated horse serum (GIBCO), 5% fetal calf serum (GIBCO), 100 µg⁄mL streptomycin and 100 µg ⁄mL penicillin (GIBCO). Neurotransmitter release experiments were performed in: 10 mM HEPES, 150 mM NaCl, 4.2 mM KCl, and 11.2 mM glucose; pH 7.4) buffer solutions.

Auditory Hair cells

Auditory hair fixed samples were provided by Professor Gregory I. Frolenkov (University of Kentucky, Lexington, KY).

Cardiac myocytes

Cardiac myocytes were isolated from adult rats, after digestion of intact perfused ventricles as described by Dr Julia Gorelik (Gorelik et al., 2006).

Materials for imaging neurons

Hank's Balanced Salt Solution (HBBS)

HEPES-buffered Hank's balanced salt solution (Invitrogen) is a phosphate buffered salt solution that maintains physiological pH at atmospheric conditions. It is used as bath solution for imaging neurons and HEK cells and for calcium imaging experiments, unless otherwise specified. Osmolarity and the pH of the prepared solutions were always checked to ensure to be close to physiological condition and to prevent movement of molecules and undesired stimulation, due to osmotic and Ph differences.

Calcium indicators

4 µM cell permeable Fluo-4 Acetoxymethyl (AM; Invitrogen) was used to monitor calcium fluctuations inside living cells and the activity of calcium permeable ion channels. For cell injection experiments 200 µM cell impermeable Alexa fluor 488 (Invitrogen) was used. 10 µM FM1-43 (Invitrogen) was used for hippocampal neuron experiments to label synaptic vesicles.

Calcium Imaging

HEK Cells and DRG neurons were incubated and loaded in DMEM solution + 4µM Fluo-4 for 15 minutes, and washed in HBSS solution in dark at room temperature for 20 minutes, before every experiment.

Medium for calcium imaging experiments

1.4 mM $CaCl_2$, 0.4 mM $MgSO_4$, 5.4 mM KCl, 135 mM NaCl, 5 mM D-Glucose, 10 mM HEPES adjust pH at 7.4, filter sterilise before adding 0.1% Bovine Serum Albumin (BSA).

Scanning Ion Conductance Microscopy's basic components

Head stage amplifier

Head stage cv 200B (Axon Instruments) is the current amplifier stage that is connected to the electrode. It is capable of recording currents through single channel. SICM and Scanning electrochemical Microscopy electrodes, were connected to the amplifier with a DigiData 1322A digitizer (Molecular Devices), and connected to PC with pClamp 10 software (Molecular Devices).

Positioning system

Three dimensional piezo electric system (Physik Instrumente) is used for mounting and positioning the pipette. In order to reduce mechanical vibration caused by the rapid vertical movements of z piezo, that carries the pipette, the sample is mounted on a separate x-y

piezo. The circuit driving the z piezo is adjusted to give a non-oscillation step response of 1 millisecond (ms).

PZT Servo Controller

PZT Servo Controller (Physik Instruments) is a closed loop controller for x y and z piezos.

Scanning head

Scanning head (Ionoscope, UK), provides housing for mounting of the holders, motors *piezos*, and also acts as faraday cage.

ScanIC Ion conductance scanner

SICM controller (Ionoscope, UK) is the data acquisition system, utilising a SBC6711 DSP board (innovative Integration, USA) at a sampling frequency of 20 kHz the z and x-y positioning is controlled. The DSP card provides the scan control, data acquisition and the digital feedback. The user control interface and image generation is done by the PC. The system was controlled by a program written in Delphi (Borland).

Anti-vibration table

Active anti-vibration isolation table (Halcyonics) was used to damp vibration that could cause noise in the SICM system operation.

Epifluorescent Microscope

Epifluorescent inverted Nikon microscope (ECLIPSE TE2000-U) used to mount the SICM scan head and for fluorescence and optical imaging of fixed or live cell work.

Pipettes and probes

Capillary borosilicate glass (O.D. 1 mm, I.D. 0.58; Intracel, UK) pipettes for the Ion Conductance imaging and delivery experiments, were pulled with a laser pipette puller (Model P-2000; Sutter Instruments, US). The pipettes were filled with a MicroFil™ syringe micro-pipettes (World Precision Instruments, US). Ion current was used pre and post experiments to ensure the resistance of the pipette remains close to 100 nm (a resistance of approximately 100 MΩ in PBS buffer).

Acrodisc Syringe Filters

Sterile Acrodisc Syringe Filters (0.2µm; Pall Corporation, USA) used to filter external and pipette solution to minimize pipette blockage.

Fluorescence experiments

Experiments on the HEK cells were performed with a laser aligned to the nano-pipette tip on the surface of HEK cell. For DRG cell body measurements, a mercury lamp with a blue filter (460-480 nm excitation) was used. The fluorescence response was recorded with a D104-814 photomultiplier (Photon Technology International, UK) and a 500-550 nm green light filter. The shutter was closed between the experiments to reduce photo-bleaching. A

photomultiplier with a pinhole (D-104-814, Photon Technology International, Surbiton, England), a 100X 1.3 NA oil immersion objective, and an epifluorescent filter block were used to collect the fluorescence signal.

Pressure application system to the pipette

Homebuilt Pressure application set up consisted of mercury direct current (DC) motor controller unit (Physik Instrumente) to control the positioning of a 20 ml syringe (Figure 2.1). A silicon tube connected the syringe to the pipette holder with side port (Harvard Apparatus). Pressure sensor (World Precision Instruments, country) was used for feedback control of pressure to keep the pressure constant (Jonsson et al., 2012).

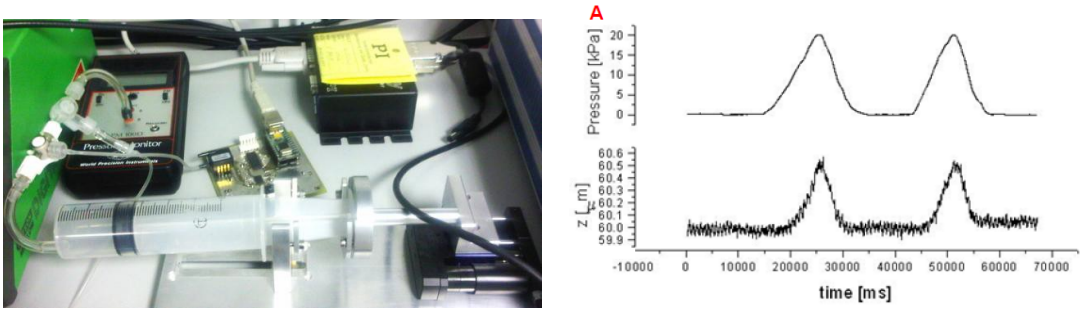

Figure 2.1. (A) Home built pressure application tool contains a Mercury DC motor controller (Physik Instrumente), a syringe, pressure monitor (World Precision Instruments) communicating port, pressure sensor (Sensor Techniques) and the pressure controller software. (B) Schematics of pressure application to the cantilever using SICM probe. Graph of z displacement of a cantilever under applied hydrostatic pressure ramp, over time. The system was calibrated using AFM cantilever with spring constant of 0.0054 Nm^{-1} using a 0.5 micron pipette immersed in PBS.

References

Anand, U., Otto, W., Facer, P., Zebda, N., Selmer, I., Gunthorpe, M., Chessell, I., Sinisi, M., Birch, R., & Anand, P. 2008, "TRPA1 receptor localisation in the human peripheral nervous system and functional studies in cultured human and rat sensory neurons", *Neuroscience Letters*, vol. 438, no. 2, pp. 221-227.

Gorelik, J., Yang, L. Q., Zhang, Y., Lab, M., Korchev, Y., & Harding, S. E. 2006, "A novel Z-groove index characterizing myocardial surface structure", *Cardiovasc.Res.*, vol. 72, no. 3, pp. 422-429.

Shah, M. & Haylett, D. G. 2000, "Ca2+ channels involved in the generation of the slow afterhyperpolarization in cultured rat hippocampal pyramidal neurons", *Journal of Neurophysiology*, vol. 83, no. 5, pp. 2554-2561.

Sviderskaya, E. V., Easty, D. J., Lawrence, M. A., Sanchez, D. P., Negulyaev, Y. A., Patel, R. H., Anand, P., Korchev, Y. E., & Bennett, D. C. 2009, "Functional neurons and melanocytes induced from immortal lines of postnatal neural crest-like stem cells", *FASEB J.*, vol. 23, no. 9, pp. 3179-3192.

Chapter 3

Scanning Ion Conductance Microscopy

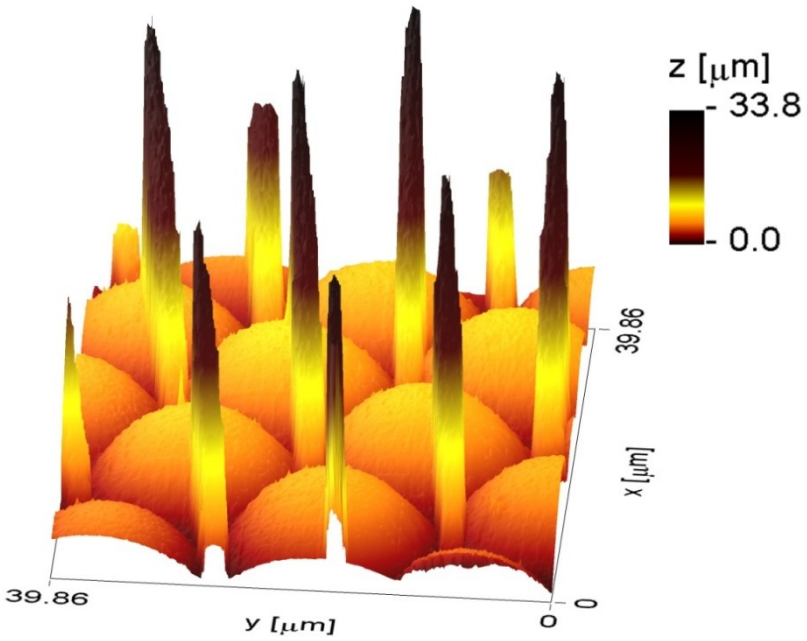

*Topographical image of *Drosophila* eye acquired with SICM.

In this chapter the principle of scanning ion conductance microscopy and its advantages compared to other scanning probe microscopes in studying biological samples is discussed. In particular, recent improvements in the setup for imaging elaborated cellular structures will be discussed.

Microscopy

Ever since Robert Hooke(Hooke, 1665) made observations under his microscope and named, 'cells' as the basic unit of biological organisms, the study of biological systems on a small scale has increased exponentially (Figure 3.1). The ability to image living cells, and to be able to monitor molecular events at precise cellular structures, is essential to comprehend biological processes. The resolution of an optical microscope is limited by the diffraction of light and this is usually around 200 nm (Schermelleh et al., 2008). In recent years novel illumination methods were developed to surpass this limit. PALM (Betzig et al., 2006), STORM(Rust et al., 2006) and STED microscopy (Willig et al., 2006), all belong to the class of super-resolution microscopy and they almost routinely achieve limit of resolution well below the diffraction limit. However, they either require specialized fluorophores tagged to the studied molecules, or they use very complicated algorithms, limiting their widespread application.

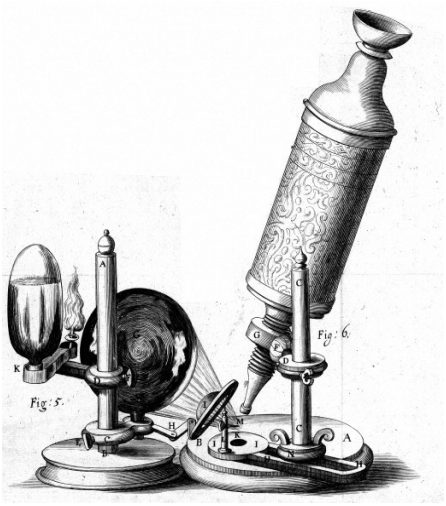

Figure 3.1. A drawing of a light microscope, by Robert Hooke (Credit: Wellcome Library, London). Imaging with light microscopes is limited by the diffraction of light and prevents the observation of nanostructures and nano-particles.

Scanning probe microscopy (SPM) is a method that examines the surface features, by the interaction between a sharp probe and the sample surface. The interaction is recorded as a signal for a feedback circuit to keep the amount of interaction constant. Topographical images can be reconstructed by scanning the probe over the surface under study. One of the advantages of SPMs over other high resolution imaging techniques such as electron microscopy is the possibility to scan live samples under physiological conditions.

Atomic Force Microscopy (AFM) (Binnig et al., 1986) is the most widely used SPM. AFM uses a cantilever with sharp tip as a probe (Figure 3.2). A laser beam is focused on the end of the cantilever and the interaction between the tip and the sample is recorded as changes in the reflected laser beam. AFM can record high resolution images, down to the level of single atoms on inorganic materials. AFM has been applied as well in biology (Figure 3.3), and it is extensively used in the field of virology, the study of DNA and chromosomes, imaging bacteria and mammalian cells, biological membrane studies, and research in mechanical properties of cell membranes (Chang et al., 2012).

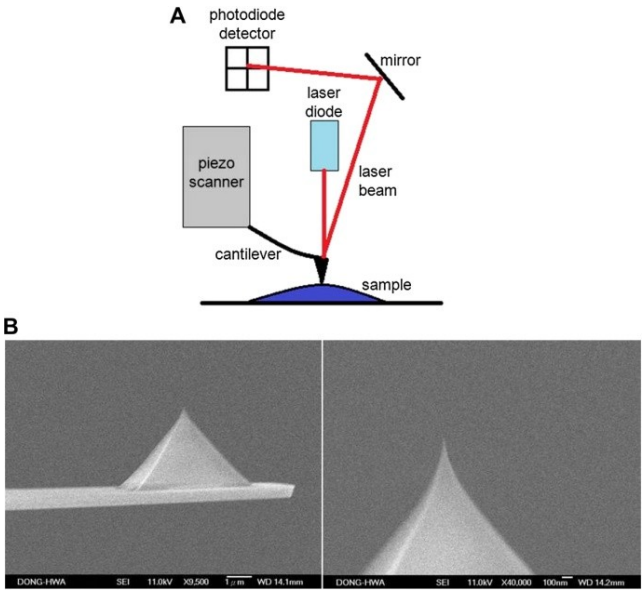

Figure 3.2. (A) Schematic of AFM probe interaction. The cantilever is controlled by the piezo scanner and is sensitive to force. A tip sample interaction deflects the cantilever that in turn results in deflecting the laser beam that is generated by the laser diode. The deflection is measured and is used to generate a topographical image. The AFM creates topographic images of sample surface by plotting the laser beam deflection, as the AFM tip moves over the surface. **(B)** Electron microscopy of a typical cantilever tip (Chang et al., 2012).

Despite the high resolution supremacy of AFM compared to other imaging methods, there are some disadvantages in using it on soft biological membranes. AFM cantilevers makes a physical contact with the substrate, and imaging of soft samples, such as cells, can result in imaging artifacts and eventually it may rupture the cell membrane (Rheinlaender et al., 2010).

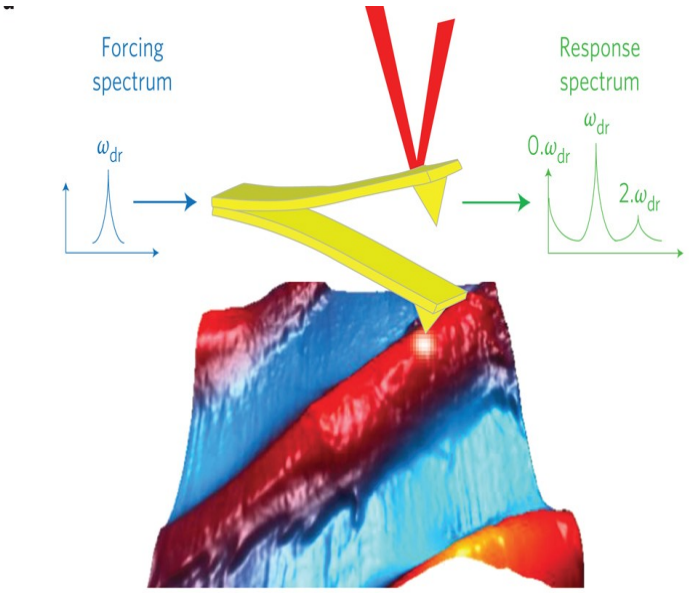

Figure 3.3. Schematic representation of an oscillating AFM cantilever interacting with a live cell in liquid (Raman et al., 2011).

Development of Scanning Ion Conductance Microscopy

Nano-scale imaging of living cells is the frontier in understanding fundament biological processes on the cell surface. The Scanning Ion Conductance Microscope (SICM) allows non-contact measurement of living cells with a resolution comparable to Scanning electron Microscopy (SEM). Figure 3.4 shows the SICM set-up used in the lab.

SICM was invented by Paul Hansma's group in 1989 (Hansma et al., 1989), but only 10 years later Yuri Korchev's group, demonstrated its great potential for live cell imaging (Korchev et al., 1997). SICM uses an electrolyte filled glass nano-pipette, which acts as a proximity sensor. A potential is applied between the electrode in the nano-pipette, and a ground electrode placed in the bath solution. When the nano-pipette approaches the surface, the

ion flow between the nano-pipette solution and the bath is reduced. This drop in ion current is used as the input in a feedback loop to control the vertical position of the nano-pipette. (Hansma et al., 1989; Korchev et al., 1997).

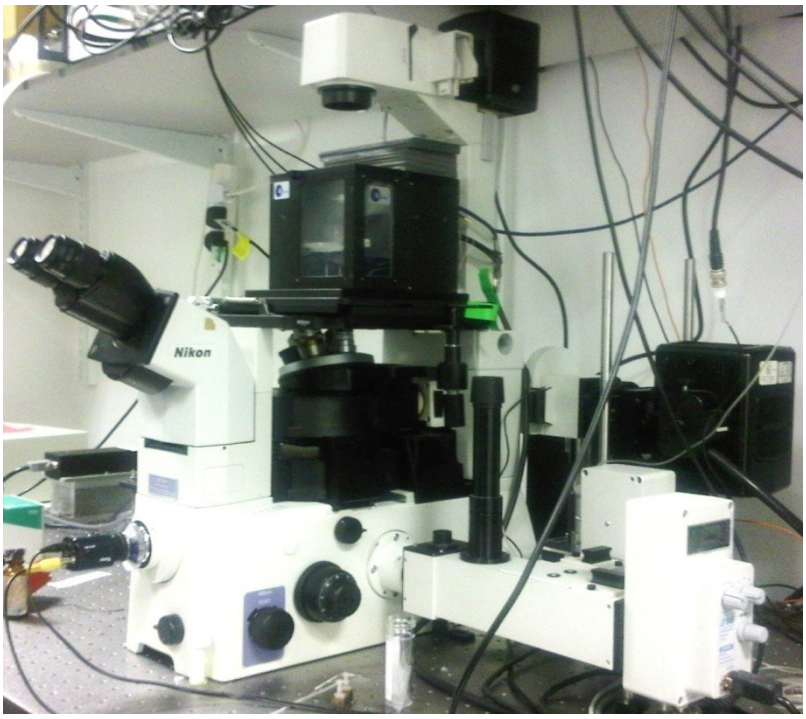

Figure 3.4. SICM setup mounted on inverted microscope.

The most important advantage of SICM to other SPMs is its non-contact character making it suitable tool for biological applications. There is no contact at all between the nano-pipette and the sample and this allows continuous imaging over long period of time for the observation of live (Lab et al., 2013; Chen et al., 2012; Korchev et al., 1997; Novak et al., 2009).

Rheinlaender and colleagues have made the first direct comparison of SICM and AFM images on the same fixed biological samples and demonstrated the superiority of SICM to

AFM in imaging soft biological membranes (Figure 3.5)(Rheinlaender et al., 2011). Recent improvements in SICM protocols have also allowed the study of biological processes in living cells with high spatial and temporal resolution (Bhargava et al., 2013; Novak et al., 2009; Shevchuk et al., 2012; Shevchuk et al., 2006).

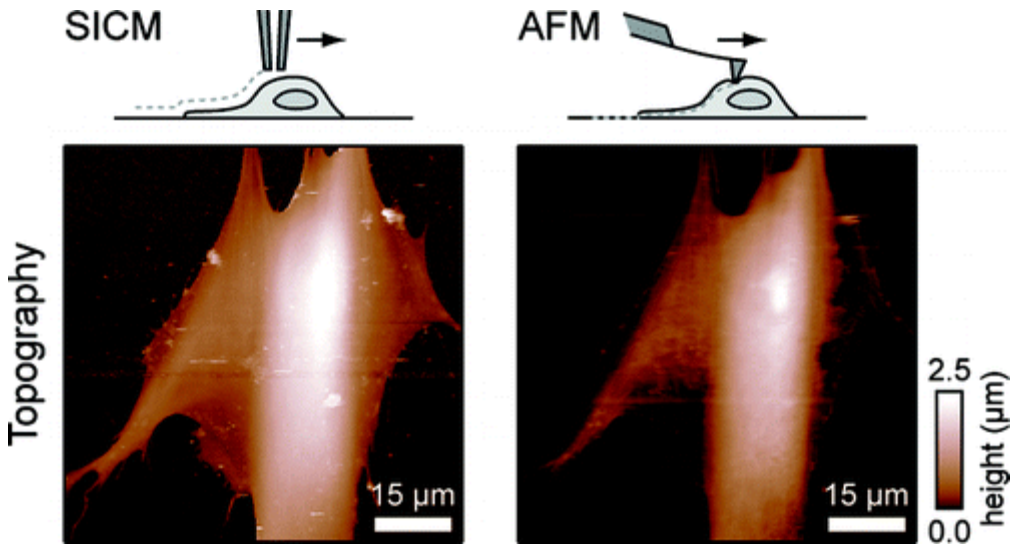

Figure 3.5. Direct comparison of SICM with AFM on the same fibroblast sample. As it is illustrated in AFM imaging, the finite imaging force exerted by the cantilever couples the mechanical sample properties to the topography and produces artefacts. However the non-contact nature of SICM, produces a true topographical image with a comparable resolution. Reprinted with permission from (Rheinlaender et al.) Copyright (2011) American Chemical Society.

Principle of operation

In the sample-scan configuration of SICM the nano-pipette is mounted on a z-axis piezo electric translation stage. The sample is scanned in x and y direction while the z-axis piezo (carrying nano-pipette) is responsible for keeping the sample-pipette distance constant. In the conventional implementation of the SICM technique the pipette sample separation distance is usually kept constant at a value equal to the inner radius of the pipette while raster-scanning the sample in x-y plane by means of a feedback mechanism monitoring the pipette current and adjusting the z-axis piezo to keep the current constant (Hansma et al., 1989). In particular, recent advances in imaging protocols, (i.e. hopping-probe SICM) allowed high resolution imaging of convoluted cellular structures such as neurons or hair cells.

In a hopping probe ion conductance microscopy (HPICM) (Novak et al., 2009), the nano-pipette approaches surface only at selected imaging points. As the pipette approaches the cell membrane, the current drops rapidly. When current drop reaches a predefined value, so called the “set-point value” ranging between 0.25 – 1 %, the z-axis position of the pipette is recorded, and the z piezo withdraws the pipette from the surface. Higher set point values results in the tip getting closer to the surface**.** At each imaging point a reference current is also measured when the pipette is further from the sample surface. The sample is then moved by the x y piezo to a different imaging point (Novak et al., 2009).

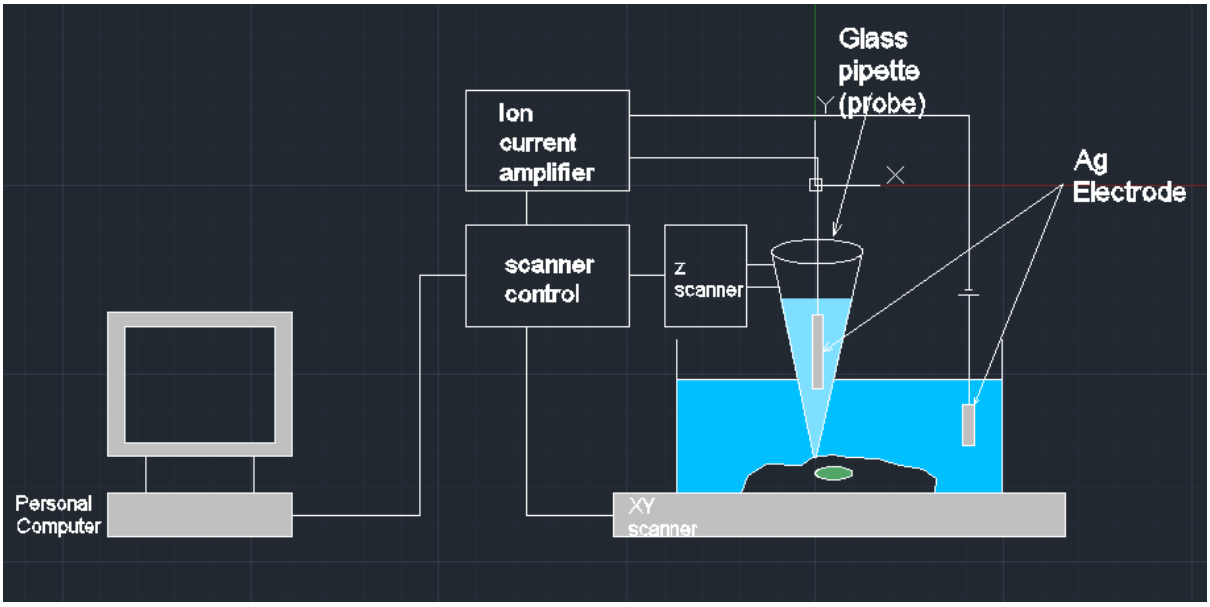

Figure 3.6. Cartoon, showing the SICM setup.

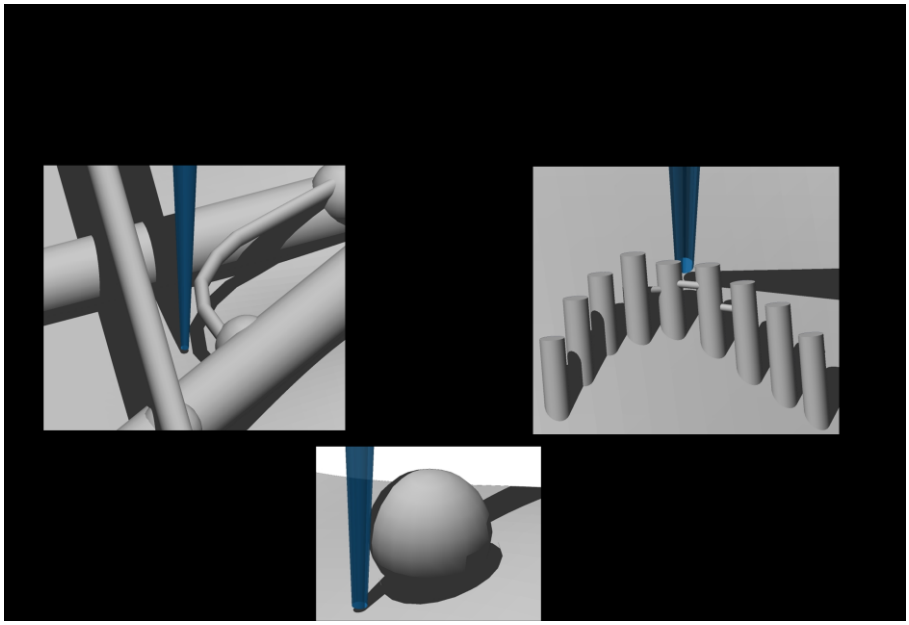

Figure 3.7. Challenges in high resolution imaging of biological samples. Cartoon is to demonstrate the necessity of hopping mode imaging.

Figures 3.6 and 3.7 show cartoons of a SICM set up and the challenges for nanopipette in imaging elaborated samples respectively. Imaging elaborated and complex samples in the standard SICM imaging configuration often results in generation of image artefacts and

crashing of the nano-pipette tip to the tall features of the sample. The hopping probe imaging mode, overcomes this limitation and limits any collision with the sample by withdrawing the pipette, further from the sample surface by a pre-set value of several µm before reapproaching to the next imaging point.

Imaging improvement

The rate at which a nano-pipette approaches the sample surface (fall rate) and the response of x-y piezo stage, determines the imaging speed. The delay in withdrawal response of z piezo after the command is sent (z axis latency), determines the maximum fall rate which can be used to preserve the non-contact scanning mode. This delay is detrimental for imaging of dynamic biological samples.

For hopping mode imaging to work effectively, the z y and x piezo need to be perfectly synchronised. Since the large travel range x-y piezos, holding the sample, are inherently slower than the shorter travel range z-axis piezo, the scanner controller has to wait for x-y piezos to finish their movement before the pipette can approach the surface to measure the height. Depending on the hardware configuration, following the withdrawal of the pipette the x-y waiting time varies between 5 to 20 ms.

PIHera x-y piezo (PIHera P-621.2 XY Nano-positioning Stage (Physik Instrumente, Germany) with 100 x 100 µm travel range), stages are mounted on top of each other. One piezo (x or y) is carrying the other one, which results in a slower response because it is carrying a higher mass than the other one. It takes about 10ms to finish the movement of x-y in a sample-scan setup configuration. Pipette scanning setup where pipette is mounted on 100x100x100

µm x-y-z piezo-actuator cube has 20 ms x-y delay due to additional load of z-axis piezo. The delay in x-y is related to the speed of the hardware.

Due to inherent z-axis piezo latency, the actual position of the pipette differs from the command send to z-axis piezo resulting in delayed recovery of the pipette current after pipette withdrawal. One can find out the time it takes for the current, to recover before accurate measurement is taken, by comparing the I-reference value and z piezo position. The delay of 2000 microseconds is usually required to ensure the z piezo has moved the pipette away from the surface for reference measurement (LISA piezo actuator P-753.21C (PI, Germany) with 25 µm travel range).

A further delay has to be added to this waiting time in order to take into account the delay time for the x-y piezos. For a sample-scan pipette the current is ignored for the first 2 ms, which is the time it usually take for the sample scan pipette to retract to the highest point further from the sample. For a pipette scan system this time needs to be higher (4-6ms) which decreases the imaging speed.

Hop amplitude needs to be adjusted according to the size of the pipette and the type of the system. The bigger the pipette the higher the hop amplitude is required. Selecting 2 micron hopping amplitude should be enough for 100 nm pipette. For a patch clamp pipette of ~ 1 µm in diameter, 6 µm hop amplitude is required for effective control of the pipette.

Modification of the scan head box

In hopping mode imaging z piezo speed should be set as fast as possible to decrease the imaging time. This rapid movement of the z piezo causes mechanical resonance in the system and cause vibrations on the soft x-y piezos that absorb the mechanical energy generated by z movement. To overcome this problem a 9 kg of steal block was added to the SICM scanning box. The increased load is to absorb the mechanical energy generated by the rapid rise and fall rate of the z piezo, and suppress the ringing effect. This is most effectively reduced by increasing the weight on the scanning system.

Topographical image

SICM uses the standard way of displaying topography using height-coded image. Colour of each pixel is determined by its z-coordinate (height). Figure 3.8 shows some images taken by ICM system on different samples.

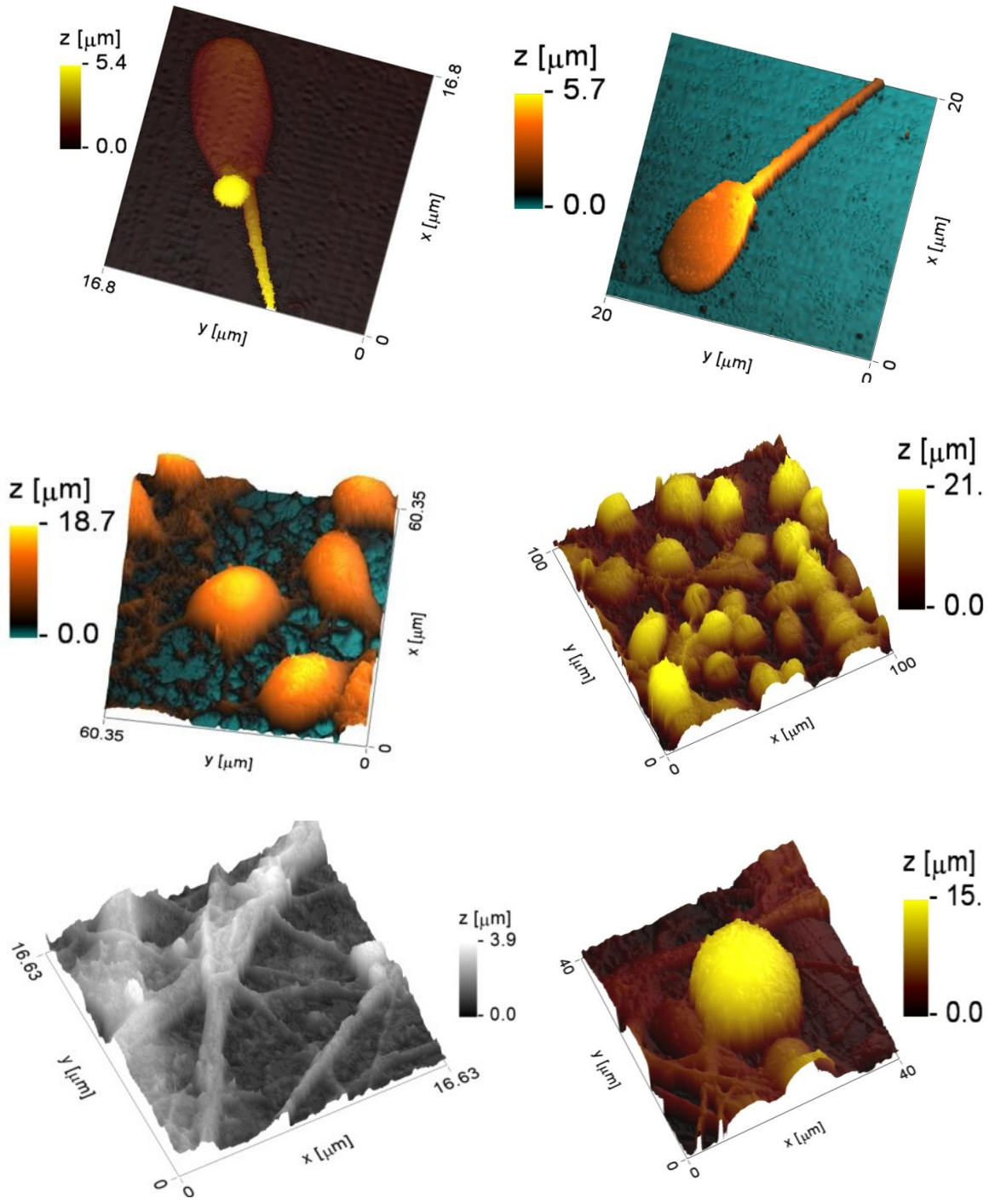

Figure 3.8. SICM topographical images. **(1,2)** Images of Sperm **(3,4)** Differentiated melanocytes **(5)** varicosities of sensory neurons **(6)** sensory neuron cell body.

Scanning range

In order to be able to image samples with features taller than 20 µm, such as tissue samples or elaborated neuronal cultures, the nano-pipette needs to travel deep with in the sample or climb to reach tall features. To achieve this, the scanning range of the SICM microscope has been increased, by changing the range of the z piezo to 100 µm.

The rate at which the nano-pipette approaches the sample surface (fall rate) and the response of x-y piezo stage determines the imaging speed. The delay in the withdrawal response of z piezo, after the command to withraw is sent (z axis latency) determines the maximum fall rate, which is taken into account in order to preserve the non-contact scanning mode. This delay is detrimental for imaging of dynamic biological samples.

In order to overcome this limitation and to preserve a reasonable scanning speed for tall samples, a small fast shear piezo-actuator (150 kHz resonance frequency) was added onto the z piezo. As the pipette approaches the surface and the set point value is reached, the fast shear piezo actuator quickly withdraws the pipette and hence prevents it from going any further down. This implementation allows an increase in the fall rate of the pipette of up to 10 times without the risk of pipette-sample collision. This modification enables a very rapid approach and withdrawal of the pipette from the surface. The *Drosophila* compound eye (Ommatidia) and other samples were used to demonstrate the practicality of this modification (Figures 3.9 & 3.10).

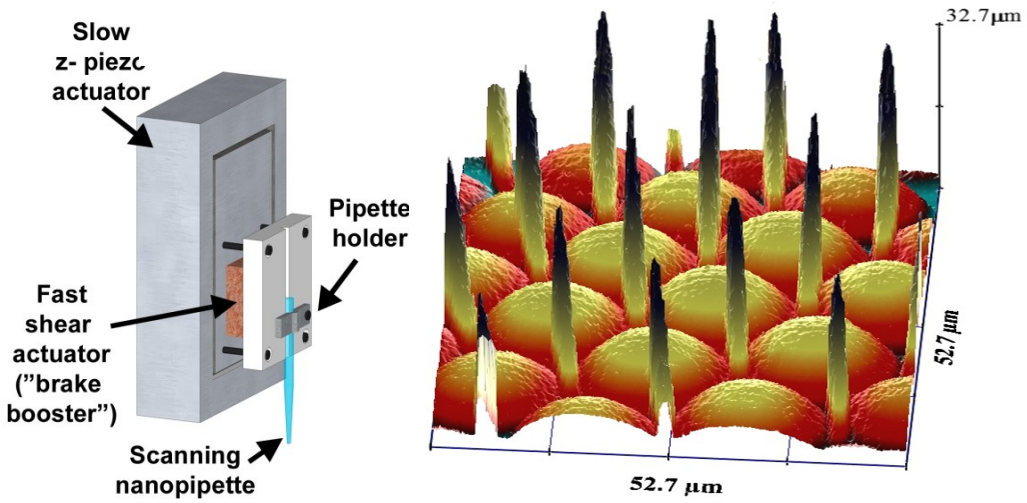

Figure 3.9. SICM for imaging large structures. **(A)** Schematic representation of piezo assembly for z movement of the pipette with addition of fast shear actuator. **(B)** Topographical image of *Drosophila* eye obtained with SICM. 30 µm required from vertical range of this particular sample with 100 z-axis PIHera piezo (PI, Germany) with resonance frequency of just 790 Hz. To speed up imaging Fast 5 µm shear actuator PICA (PI, Germany) with resonance frequency of 150 kHz was mounted on the 100 µm piezo as demonstrated on the left Scan duration was reduced from 2.5 hr to ~ 30 minutes.

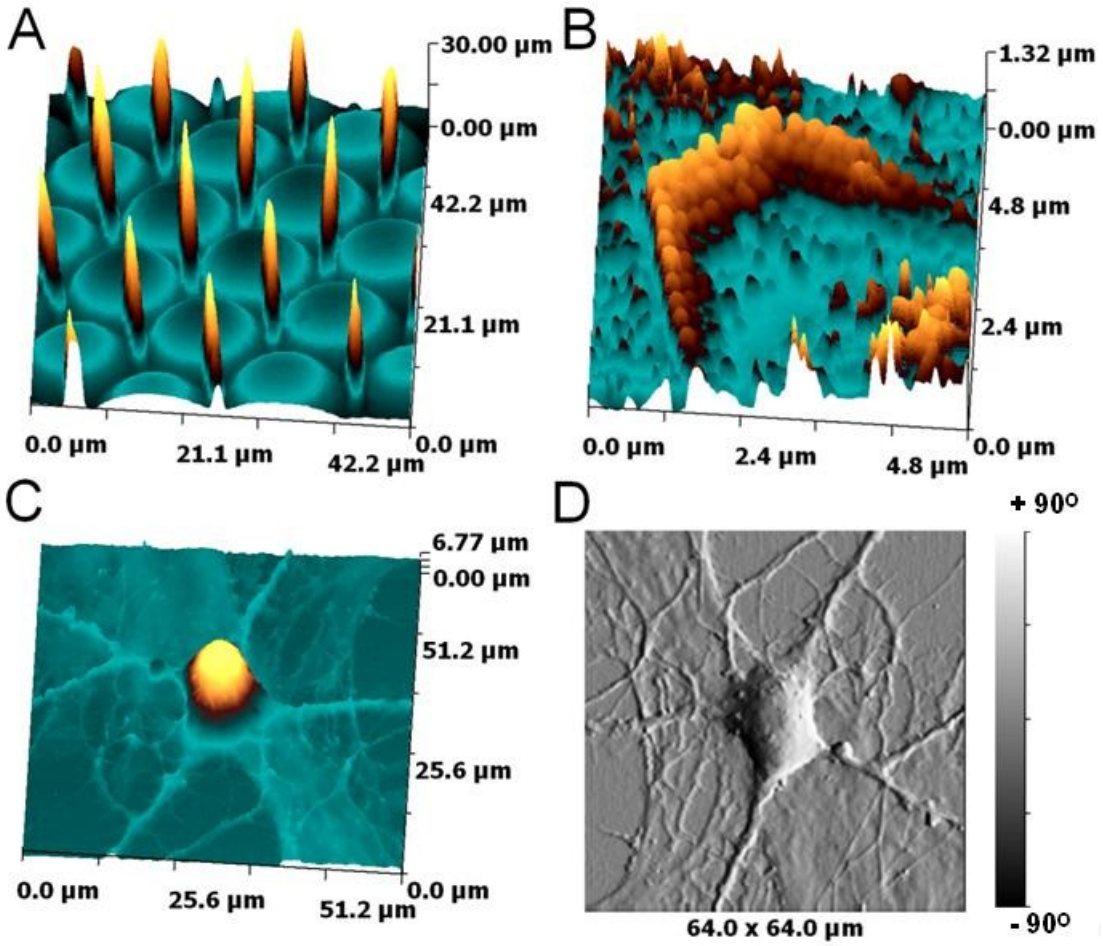

Figure 3.10. SICM imaging of complex biological surfaces. **(A)** Topographical image of Drosophila eye with sensory hairs projections **(B)** Stereocilia of outer hair cells in cultured organs of corti. **(C)** Hippocampal neuron and its dendritic network. **(D)** Same as in **(C)** presented as a first derivative image of hippocampal neuron, to better show the details in topography Zero slopes are set as grey, 90 degree angles are set to white and -90 degree angles are set to black (Shevchuk et al., 2011).

Slope image (Figure3.11 **(D)**), is generated for better visualisation of surface features i.e. to highlight small features on the surface. This is done by calculating the first derivative of topography from left to right. Zero slopes are set as grey, 90 degree angles are set to white

and -90 degree angles are set to black. When the neuron is scanned, the cell body of the neuron appears as greyish ball, but if there is a small feature on the cell body, the 90 degree edge of that feature stands out in the slope image, and the sharp edges becomes emphasized. Sharp edges appear either very black or very bright depending on their angle. A slope image is useful for selection of structures on the cell surface for precise chemical delivery and measurements, such as patch-clamp recording.

Functional experiments on neurons

In excitable living cells such as neurons, depolarizing electrical signals lead to activation of different types of voltage gated calcium channels, leading to influx of calcium. Calcium channels are expressed throughout the nervous system. Release of intracellular calcium stores, leads to further amplification of these signals. Furthermore calcium signalling is necessary for induction of learning and memory related forms of neuronal plasticity. Transient intracellular increase in calcium concentration occurs in various stages of development and can influence gene expression, neurite outgrowth and neuronal migration. Calcium signalling is a useful tool to study individual neurons and their sub-cellular compartments, in tissue culture and brain slices, in real time (Stosiek et al., 2003).

Formation of small blebs was observed during scanning of primary culture neurons. The size and number of blebs appeared to increase, over time. This indicated that neurons are not in a good condition. Calcium recording of cultured dish also indicates spontaneous calcium elevations in neurons and glial cells. This is probably due to neurotransmitter release and neuronal network communications. Since imaging is carried out in room temperature it is important to use a media that is pH and osmotically regulated throughout the experiment. A

perfusion system has been implemented to perfuse the solution in the culture dish to keep the cells in relatively silent state (Figure 3.11).

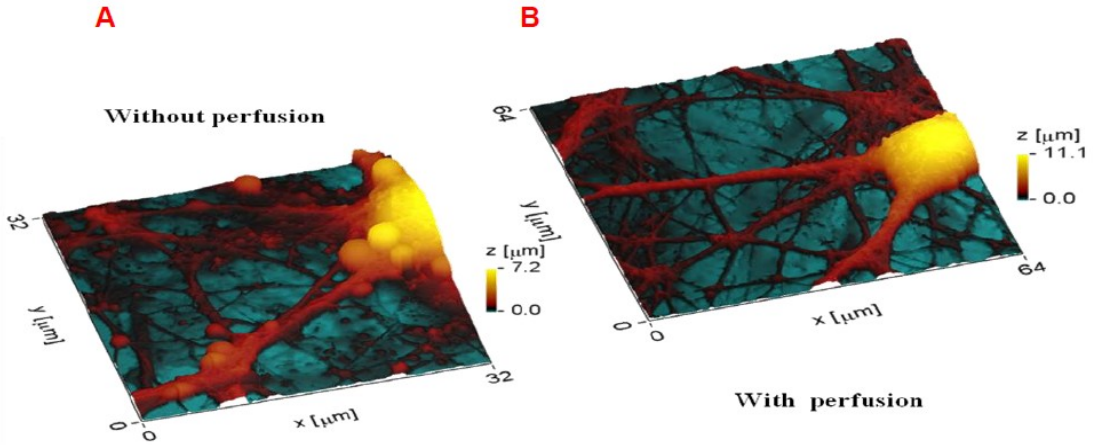

Figure 3.11. SICM images of primary cultures of hippocampal neurons. **(A)** Displays a neuron with blebs developed within one hour in media without perfusion, and **(B)** displays an apparently healthy neuron with no visible blebs in the topography which was perfused throughout imaging.

Multi-point delivery with Scanning Surface Confocal Microscopy

The Scanning Surface Confocal Microscopy (SSCM) was implemented for simultaneous local delivery and laser confocal fluorescence recording under the nano-pipette tip (Gorelik et al., 2002). For surface confocal measurements the objective was placed on a 20 µm travel range focusing piezo-actuator P-725 (PI, Germany). Since the laser and the nano-pipette tip are aligned, fluorescence can be measured at each time point right underneath the nano-pipette position.

A reference fluorescence signal is measured when the pipette is not delivering any chemicals and is far away from the sample surface. The fluorescence signal is then measured when local reagents are delivered. These two values can be subtracted from each other for highly sensitive detection of fluorescent change at the surface (see Figure 3.12). Calcium elevation can also be recorded continuously for the duration of the application.

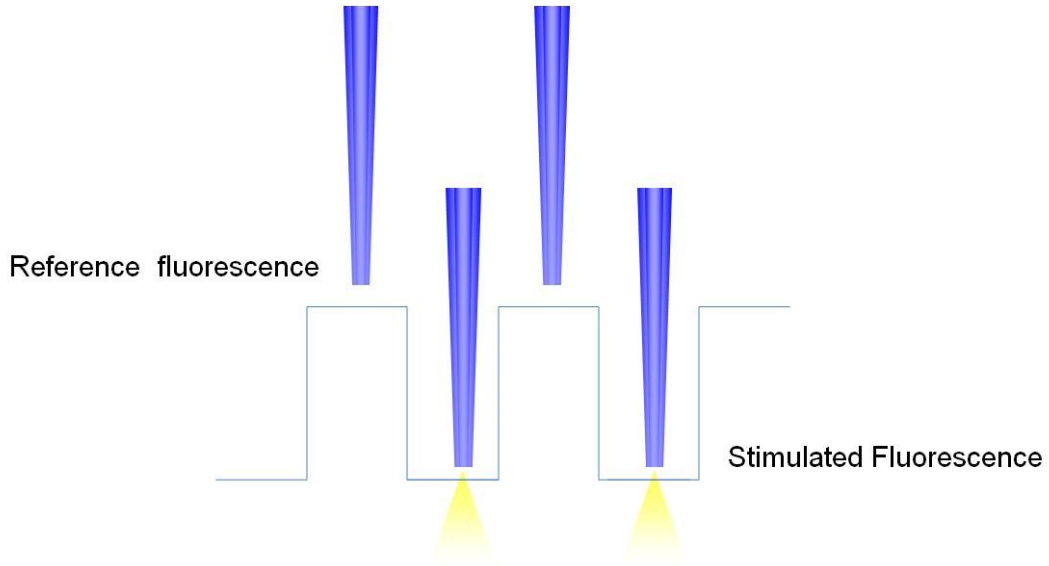

Figure 3.12. Schematic of Scanning Surface Confocal (SSCM) fluorescence measurement. Fluorescence is measured when the pipette is close to the surface (when the chemical is delivered). As the pipette jumps up to move to the next point, the reference fluorescence is measured. Subtraction of stimulated from reference fluorescence measurements, gives the functional fluorescence image of potential receptor activities on the cell surface.

References

Betzig,E., Patterson,G.H., Sougrat,R., Lindwasser,O.W., Olenych,S., Bonifacino,J.S., Davidson,M.W., Lippincott-Schwartz,J., and Hess,H.F. (2006). Imaging intracellular fluorescent proteins at nanometer resolution. Science *313*, 1642-1645.

Bhargava,A., Lin,X., Novak,P., Mehta,K., Korchev,Y., Delmar,M., and Gorelik,J. (2013). Super-resolution Scanning Patch Clamp Reveals Clustering of Functional Ion Channels in Adult Ventricular Myocyte. Circulation Research *112*.

Binnig,G., Quate,C.F., and Gerber,C. (1986). Atomic Force Microscope. Physical Review Letters *56*, 930-933.

Chang,K.C., Chiang,Y.W., Yang,C.H., and Liou,J.W. (2012). Atomic force microscopy in biology and biomedicine. Tzu Chi Medical Journal. *24,* 162 -169.

Chen,C.C., Zhou,Y., and Baker,L.A. (2012). Scanning Ion Conductance Microscopy. Annual Review of Analytical Chemistry *5*, 207-228.

Gorelik,J., Shevchuk,A., Ramalho,M., Elliott,M., Lei,C., Higgins,C.F., Lab,M.J., Klenerman,D., Krauzewicz,N., and Korchev,Y. (2002). Scanning surface confocal microscopy for simultaneous topographical and fluorescence imaging: application to single virus-like particle entry into a cell. Proc. Natl. Acad. Sci. U. S. A *99*, 16018-16023.

Hansma,P.K., Drake,B., Marti,O., Gould,S.A.C., and Prater,C.B. (1989). The Scanning Ion-Conductance Microscope. Science *243*, 641-643.

Hooke, R. Micrographia: or some physiological descriptions of minute bodies, made by magnifying glasses with observations and inquiries thereupon. 1665. John Martyn, Printer to the Royal Society, London.
Ref Type: Generic

Korchev,Y.E., Bashford,C.L., Milovanovic,M., Vodyanoy,I., and Lab,M.J. (1997). Scanning ion conductance microscopy of living cells. Biophysical Journal *73*, 653-658.

Lab,M.J., Bhargava,A., Wright,P.T., and Gorelik,J. (2013). The scanning ion conductance microscope for cellular physiology. Am. J. Physiol Heart Circ. Physiol *304*, H1-11.

Novak,P., Li,C., Shevchuk,A.I., Stepanyan,R., Caldwell,M., Hughes,S., Smart,T.G., Gorelik,J., Ostanin,V.P., Lab,M.J., Moss,G.W., Frolenkov,G.I., Klenerman,D., and Korchev,Y.E. (2009). Nanoscale live-cell imaging using hopping probe ion conductance microscopy. Nat. Methods *6*, 279-281.

Raman,A., Trigueros,S., Cartagena,A., Stevenson,A., Susilo,M., Nauman,E., and Contera,S.A. (2011). Mapping nanomechanical properties of live cells using multi-harmonic atomic force microscopy. Nature Nanotechnology *6*, 809-814.

Rheinlaender,J., Geisse,N.A., Proksch,R., and Schaeffer,T.E. (2011). Comparison of Scanning Ion Conductance Microscopy with Atomic Force Microscopy for Cell Imaging. Langmuir *27*, 697-704.

Rust,M.J., Bates,M., and Zhuang,X. (2006). Sub-diffraction-limit imaging by stochastic optical reconstruction microscopy (STORM). Nat. Methods *3*, 793-795.

Schermelleh,L., Carlton,P.M., Haase,S., Shao,L., Winoto,L., Kner,P., Burke,B., Cardoso,M., Agard,D.A., Gustafsson,M.G., Leonhardt,H., and Sedat,J.W. (2008). Subdiffraction multicolor imaging of the nuclear periphery with 3D structured illumination microscopy. Science *320*, 1332-1336.

Shevchuk,A.I., Frolenkov,G.I., Sanchez,D., James,P.S., Freedman,N., Lab,M.J., Jones,R., Klenerman,D., and Korchev,Y.E. (2006). Imaging proteins in membranes of living cells by high-resolution scanning ion conductance microscopy. Angew. Chem. Int. Ed Engl. *45*, 2212-2216.

Shevchuk,A.I., Novak,P., Takahashi,Y., Clarke,R., Miragoli,M., Babakinejad,B., Gorelik,J., Korchev,Y.E., and Klenerman,D. (2011). Realizing the biological and biomedical potential of nanoscale imaging using a pipette probe. Nanomedicine. (Lond) *6*, 565-575.

Shevchuk,A.I., Novak,P., Taylor,M., Diakonov,I.A., Ziyadeh-Isleem,A., Bitoun,M., Guicheney,P., Lab,M.J., Gorelik,J., Merrifield,C.J., Klenerman,D., and Korchev,Y.E. (2012). An alternative mechanism of clathrin-coated pit closure revealed by ion conductance microscopy. The Journal of Cell Biology *197*, 499-508.

Stosiek,C., Garaschuk,O., Holthoff,K., and Konnerth,A. (2003). In vivo two-photon calcium imaging of neuronal networks. Proceedings of the National Academy of Sciences of the United States of America *100*, 7319-7324.

Willig,K.I., Rizzoli,S.O., Westphal,V., Jahn,R., and Hell,S.W. (2006). STED microscopy reveals that synaptotagmin remains clustered after synaptic vesicle exocytosis. Nature *440*, 935-939.

CHAPTER 4

Carbon nano-probe

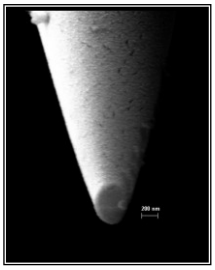

*An SEM image of a theta quartz nano-pipette filled with carbon.

Here the adaptation of the SICM platform to accommodate electrochemical experiments is demonstrated. In particular, the development of a novel electrochemical probe, fabricated by pyrolytic decomposition of carbon within a quartz nano-pipette will be discussed. This method is simple and carbon nano-electrodes of adaptable sizes can be fabricated in a few steps. Functionalisation of the carbon electrode will also be discussed. Simultaneous topographical and electrochemical experimental measurements with the electrochemical nano-probe, using voltage constant mode and voltage switching mode will also be demonstrated.

Some of the materials presented in this chapter have now been published in the journal of ACS Nano, under the title: "Electrochemical Nanoprobes for Single-Cell Analysis" (Actis et al., 2014).

*Voltage switching mode & neurotransmitter release detection experiments were performed by Dr. Yasufumi Takahashi.

Scanning Electrochemical Microscopy

Scanning electrochemical microscopy (SECM) (Bard et al., 2006), uses an ultramicro-electrode (UME), to detect redox currents of the oxidation/reduction of electro-active species at the electrode, and to map electrochemical activity of surfaces and interfaces (Figure 4.1). The tip of the SECM UME is generally immersed in a redox mediator solution. Application of a sufficent positive or negative potential between the SECM tip and the ground electrode results in oxiation or reduction of the mediator at the tip of the electorde. The rate of the redox reaction is dependent on the diffusibility of the mediator to the surface (Sun et al., 2007).

Ferrocenemethanol and hexaammineruthenium (III) chloride are two standard electrochemical mediators used in SECM experiments. Application of positive and ngative potential to the SECM probe results in oxidation and reduction of Ferrocenemethaol and Hexaammineruthenium(III) chloride respectively:

$$FcCH_2OH \quad \rightleftarrows \quad [FcCH_2OH]^+ + e^-$$

$$[Ru(NH_3)_6]^{3+} + e^- \quad \rightleftarrows \quad [Ru(NH_3)_6]^{2+}$$

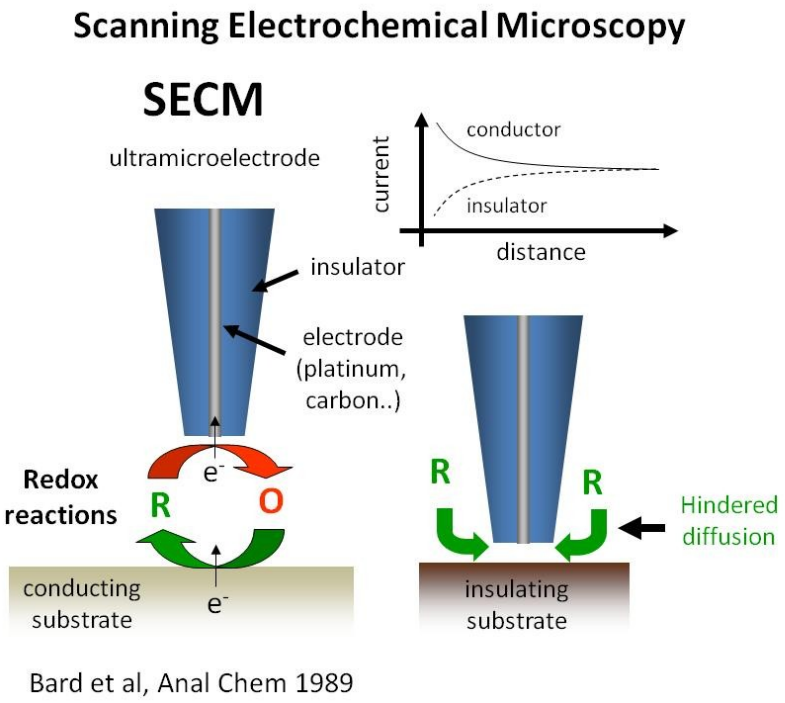

Figure 4.1. Schematic representation of SECM probe operation. The SECM probe tip uses a redox mediator as a way to detect surfaces. Current distance plot shows the approach curves of an SECM electrode to a conducting (solid line) and an insulating (Dashed line) substrate. When the electrode approaches a conducting substrate, the electrochemical species-that is either oxidised/reduced (Depending on the mediator) at the electrode's tip-undergoes the opposite reaction at the substrate, thus causing signal amplification, or in technical term a positive feedback. However in approaching an insulating substrate, the availability of the species (R) to the tip is hindered by the inert underlying substrate, that results in a reduction of the signal that can be used as a feedback to control the tip substrate distance.

SECM, similar to SICM requires a tip-sample distance of a few electrode radii, however the nature of the surface (conductor or insulator) and not just its distance to the probe, affects the signal measured at the micro-electrode and this limits the application of SECM probes

for simultaneous electrochemical measurement and feedback signal measurement for probe positioning. This is the reason that SECM imaging is normally performed at constant height from the sample surface and makes it suitable for only flat samples to obtain accurate spatial recordings. Electrochemical and topographical convolution in biological samples, create challenges in the interpretation of local changes in redox current.

The comibnation of SECM with AFM have contributed to the position improvement of the SECM probe feedback system (Macpherson et al., 1996). However due to the softness of the biological membranes, this method of measurement is not suitable for most biological samples, as the AFM system uses a shear force as a feedback signal. The force between AFM probe and cell has been proven to be high and detrimental to the biological membrane, preventing it from producing an artefact-free image (Shevchuk et al., 2011).

In order to obtain high spatial resolution data, small diameter UMEs and also small sample-tip distance is required. However the topographical imaging resolution cannot be improved using this method on its own, as the resistance signal for feedback control is degraded by miniaturisation of electrode (Kurulugama et al., 2005).

Small UME of one hundred nano-meter size has to be coated to provide insulation, that increases the size of the probe to micrometer range and therefore affects the aspect ratio of UME which as a result causes limitations in the spatial resolution.

Two groups have combined SICM and SECM to address the problems caused by UMEs (Comstock et al., 2010; Takahashi et al., 2010). In these experiments, insulated gold film coated nano-pipettes were exposed by focused ion beams to act as UME. The electrode inserted into the pipette provided an ion current measurement for distance feedback control thereby generating a robust feedback system for SECM imaging for simultaneous topographical and electrochemical imaging (Figure 4.1), (Shevchuk et al., 2011).

Carbon electrodes have wide applications and are cheap and easy to fabricate (Westerink and Ewing, 2008; Robinson et al., 2008; McCreery, 2008). Carbon electrodes have been shown to be capable of detecting neurotransmitter release (Robinson et al., 2008) and can also be used for detection and analysis of exocytic vesicle sizes and frequency of vesicle release (Westerink and Ewing, 2008). SICM membrane topography combined with electrochemical detections identify morphological changes on cell membranes associated with exocytosis event (Shin and Gillis, 2006). Here in the lab we attempt to produce other types of UMEs suitable for cell measurements.

Fabrication of carbon nano-electrodes

"Fabricating reproducible electrodes with defined size and geometries is essential for achieving high quality electrochemical measurements. Here the carbon nano-electrode fabrication method is discussed where a disk-shaped carbon is embedded into a quartz nano-pipette. The size of the probe is determined by the radius of the quartz nano-pipette

and therefore can be adjusted by changing the pulling parameters of the laser puller. nano-electrodes as small as 4 nm in radius are fabricated using this method.

The probe fabrication has been optimised and the final protocol consists of **two steps**:

1. A quartz capillary is pulled into a sharp nano-pipette using a laser puller. A P-2000 laser puller (Sutter Instrument) was used to pull quartz capillaries with an outer diameter of 1.2 mm and an inner diameter of 0.90 mm (Q120-90-7.5; Intracel). General pulling parameters used were: Heat 790, Filament 3, Velocity 45, Delay 130, and Pull 90. Final pull was manipulated to achieve different sizes (Takahashi et al., 2011; Ying et al., 2005). Double-barrel nano-pipette fabrication: Double-barrel nano-pipettes were fabricated from theta quartz capillaries (o.d. *1.2* mm, i.d. 0.9 mm, Sutter Instrument).

2. A tygon tubing is used to deliver high pressured mixed propane/butane gas to the nano-pipette from the back. The sharp end of the nano-pipette (taper), is then carefully inserted in to a quartz capillary (o.d. 1.0 mm, i.d. 0.7 mm; Sutter Instrument) that is connected via tygon tubing to Argon gas from its other end. Argon creates an inert environment to prevent excessive carbon release from the tip and to protect the deposited carbon layer from etching. Butane jet flame torch lighter is used for heating up the nano-pipette taper for carbon deposition (figure 4.2 & 4.3).

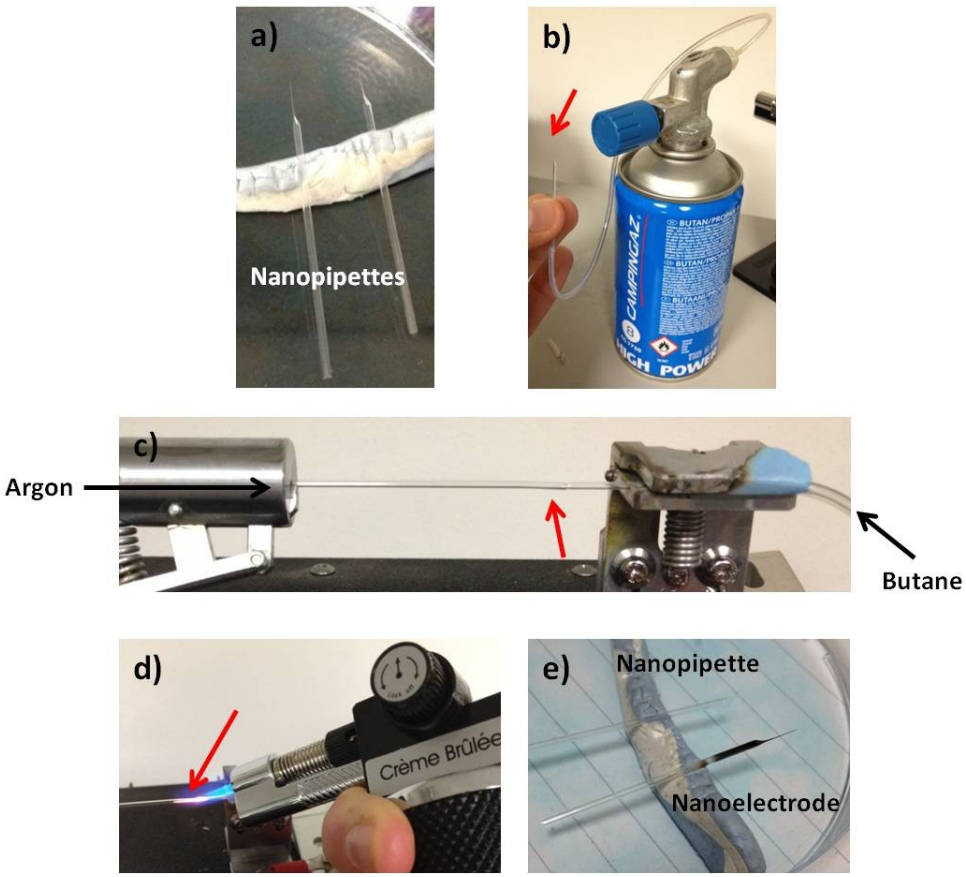

Figure 4.2. Photographic representations of carbon nano-electrode fabrication. **(A)** A pair of Nano-pipettes fabricated with a P-2000 laser puller (Sutter Instrument) from quartz capillaries. **(B)** nano-pipette is plugged to Campingas cartridge (mixed propane/butane), with a tygon tube in order to load with the gas. **(C)** nano-pipette is clamped inserted into a quartz capillary, which is connected with a tube to an argon tank. The nozzle of the tank is opened briefly to create a flow of Argon. This is done in order to prevent the tip from melting and oxidation of deposited carbon because of the high temperature. **(D)** "crème brûlée" jet flame torch heats the pipette tip to create a pyrolytic carbon layer deposition between 15-20 seconds. **(E)** demonstrates a dark carbon layer covering the inside of the nano-pipette where the deposition took place. Red arrows point to the nano-pipette tip.

SEM imaging, Raman spectroscopy, energy dispersive X-ray spectroscopy and electrochemical recordings are performed to show successful deposition and assess the quality of carbon layer deposition. These nano-electrodes are most suitable for SECM imaging experiments and to study electrochemical processes at nano-scale (Figure 4.3).

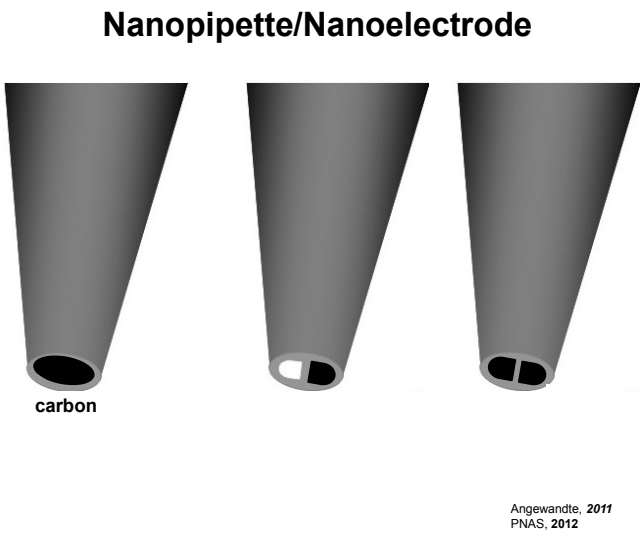

Figure 4.3. Schematic of carbon nano-probes. Carbon probes are fabricated from a single barrel and theta glass quartz pipettes. It is possible to fabricate a double barrel probe with one barrel for SICM & the second barrel for electrochemical measurements by using blue-tack to block one barrel before the carbon deposition step. Adapted from (Takahashi et al., 2011).

SEM imaging

Figure 4.4 shows the SEM micrograph of a carbon nano-electrode showing the active electrode area of about 25 nano-meters in diameter Zeiss Auriga equipped with a field emission gun was used for SEM imaging. Accelerating voltage was set to 5 kV. A ~5 nm layer of Cr sputter coating was deposited on the nano-electrode before imaging.

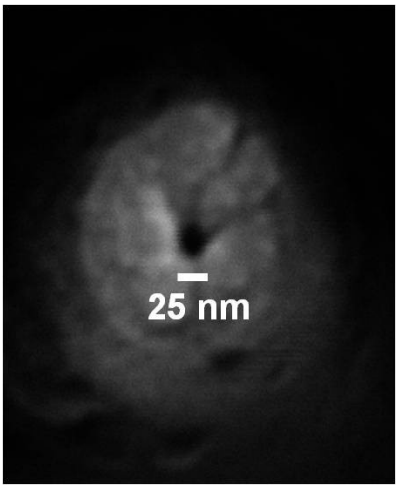

Figure 4.4 SEM micrograph of a nano-electrode tip. Top view of a carbon filled quartz probe.

The presence of a well adherent carbon layer to the quartz glass was confirmed with Energy-dispersive X-ray (EDX) spectroscopy that shows ~ 300 nm carbon layer thickness extending several millimeters away from the nano-pipette opening tip (Figure 4.5 & 4.6). Mirkin's lab have shown the surface of the nano-electrodes with AFM imaging (Nogala et al., 2012).

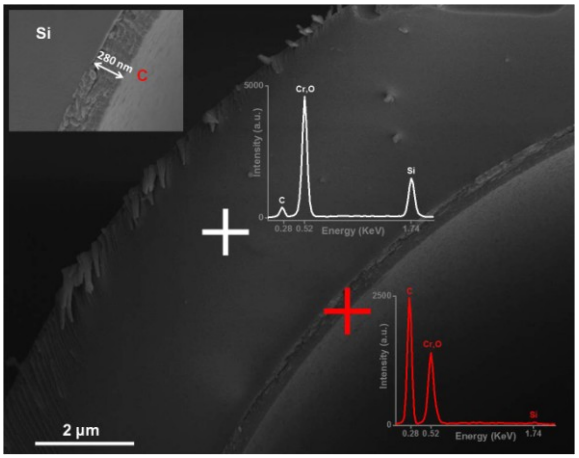

Figure 4.5. SEM micrograph and EDX analysis of a broken electrode. Red and white crosses indicate the EDX analysis positions. A carbon layer with ~280 nm thickness can be seen between quartz/carbon interface. Samples were sputter coated with a 10nm Cr layer before SEM imaging.

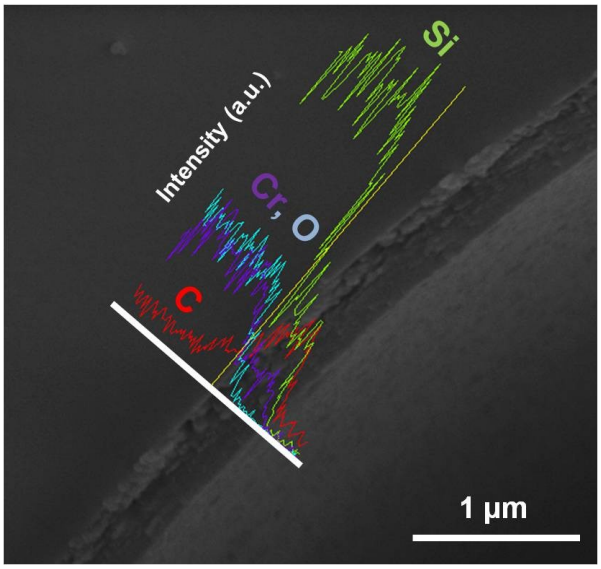

Figure 4.6. SEM micrograph and EDX line analysis of a broken nano-electrode. Graphic lines are to show the intensity of x ray emission for Si (green line), Cr (purple line), O (blue line), and C (red line) along the white line. Lines show that the signal for Si and O decrease at the interface quartz/carbon while the signal for C increases. Samples were sputter coated with a 10nm Cr layer before SEM imaging.

Raman spectroscopy of Carbon Nano-electrodes

Raman spectroscopy is generally used to characterize carbon materials. Here nano-electrodes were fixed to a glass substrate to acquire Raman spectra close to the tip of the nano-electrode. A typical Raman spectrum with resolved *D* and *G* bands at 1367 cm^{-1} and 1576 cm^{-1} respectively is shown in Figure 4.7. Since no highly ordered graphite from the extended spectrum regions (not shown) of the *G'* (or *2D*) band in the region ~ 2500-2800 cm^{-1} were seen, it seems that the deposition step of carbon in here produces a highly disordered graphitic network.

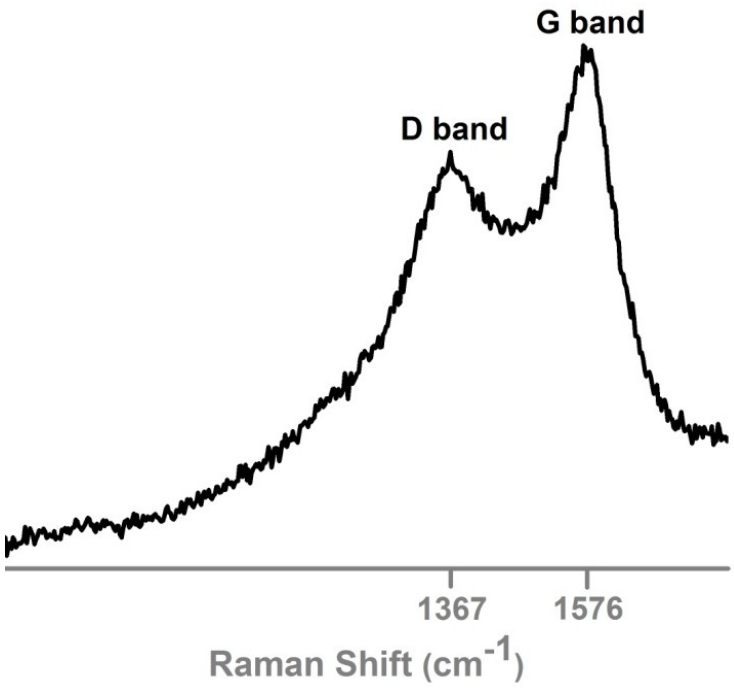

Figure 4.7. Representative Raman spectrum of a carbon nano-electrode (λ_{ex} = 514 nm, 50 × obj., NA = 0.75, 1 s × 100 accumulations, 20 mW (max)) at the tip.

Renishaw 1000 confocal Raman micro-spectrometer with an Ar-ion laser, 514 nm, via a 50 × objective (NA = 0.75) and Peltier-cooled CCD detector were used for Raman spectroscopy. 1 s × 100 accumulations with a maximum output laser power of 20 mW was used to get the spectra (Figure 4.7).

Electrochemical characterisation

Electrical contact was established by inserting a conductive wire (Ag or Cu) into the carbon barrel to make contact with the carbon. In double barrel experiments, a silver chloride electrode is inserted in the second barrel. A silver chloride electrode pellet is placed in 2 ml

solution to act as reference electrode for both electrochemical and ion conductance measurements.

The size of the carbon electrode is measured by measuring the half cone angle from imaging. Size and aspect ratio of the carbon electrode can also be estimated from the steady state current generated by immersion of the probe in bulk electrochemical solution and recording the voltammogram. Generally 10 mM hexaammineruthenium (III) chloride or 1mM ferrocenemethanol in PBS were used as electrochemical mediators.

Cyclic voltammemetry (CV) is performed to assess the size and quality of the electrochemical electrodes. The probe is immersed in a solution containing electrochemical mediator. The potential at the electrochemical electrode vs Ag/AgCl, is ramped to a specified value in a linear fashion, over a certain time period. As the potential value is reached, the voltage is rammed in the opposite direction. As the voltage is linearly ramped redox mediator is oxidised or reduced depending on the type of the mediator. The current during the voltage ramp at the working electrode is measured and ploted against time. In Micro-nano electrodes the current changes in a sigmoidal manner, reaching a plateu at the maximum potential. The small size of the electrode limits the amount of redox reaction taking place at its tip (Diffusion limited), therefore the plateu value indicates the radial diffusion limit of redox reaction, taking place at the tip of the micro-nano electrode. Cyclic voltammetry measurements were performed by sweeping the potential from +/- 500 mV to 0, depending on the type and concentration of the mediator used.

The ratio (Rg) of the quartz capillary's outer and inner diameters of 1.2 mm and 0.9 inner respectively is roughly maintained after the puling. Therefore a final RG of ~ 1.5 is expected following the pulling procedure. Using this value, the radius r of the nano-pipette can be

calculated from steady-state current reduction (I_{ss}) value. This is done by employing the expression for disk micro-electrodes with a RG (Glass radius to electrode radius) value of 1.5 (Lefrou and Cornut, 2010):

Equation 1:

$$r = \frac{I_{ss}}{4.64nFCD}$$

Where n represent the number of electrons transferred in the tip reaction, F the Faraday constant, D the diffusion coefficient of $Ru(NH_3)_6Cl_3$, and C the concentration of the mediator in solution (Figure 4.8).

SECM with Carbon Nano-electrodes

The tip radius value from the Equation above can be further confirmed by recording approach curves of the SECM probe on substrates. Bard's group have pioneered the use of SECM for geometric characterisation of nano-electrodes (Mirkin et al., 1992). This is done by comparing approach curves of nano-electrodes with simulated curves of defined geometry. The carbon filled nano-pipette was integrated into the SECM system (Takahashi et al., 2012). SICM-SECM set up and parameters for electrochemical experiments are as described previously (Takahashi et al., 2010; Novak et al., 2009; Takahashi et al., 2012).

A Petri-dish was used as the substrate, the dish was filled with 2 ml solution of 10 mM $Ru(NH_3)_6Cl_3$ in PBS. The nano-electrode was then mounted on to the piezo and allowed to approach the surface. The recorded approach curve was then compared to the simulated data and it fitted well with the prediction for disc micro-elecrode with a value of 1.5 Rg , (Figure 4.8).

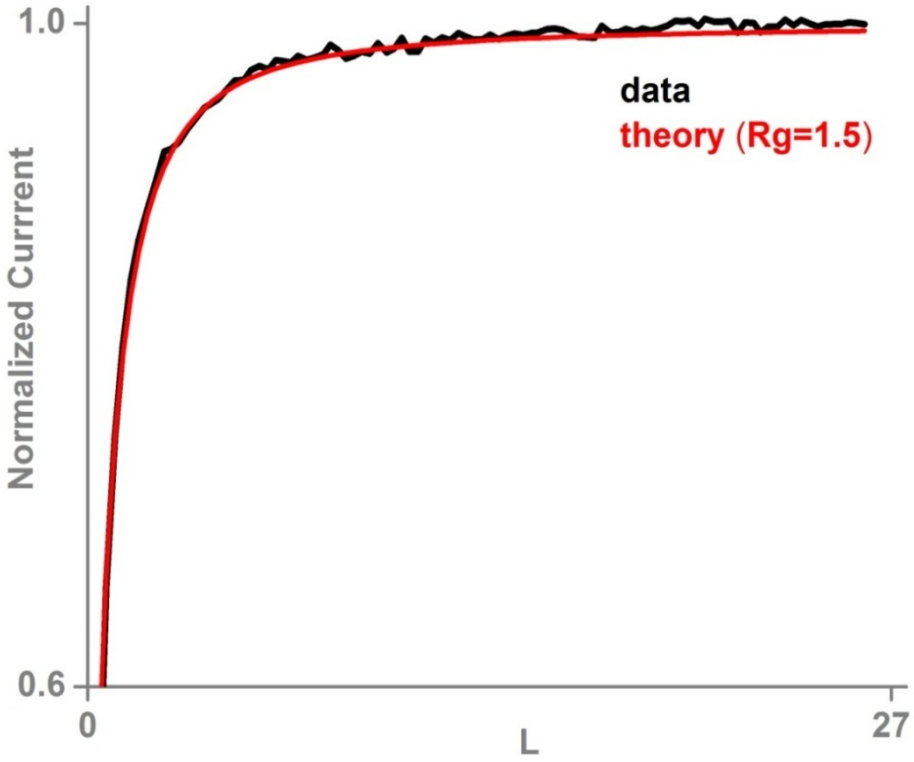

Figure 4.8. Represents a graph of nano-electrode approaching insulating substrate. Black line represents experimental data and red line is the theoretical approach curve for a disk shaped electrode with Rg=1.5. L is distance divided by the nano-electrode radius. Nano-pipette fabrication protocol: Heat 790, Filament 3, Velocity 45, Delay 130, and Pull 90. Solution: 10 mM $Ru(NH_3)_6Cl_3$ in PBS. Applied Voltage: -400 mV vs Ag/AgCl.

Nano-electrodes of controllable sizes

The nano-electrode radius can be reliably controlled by varying the pulling parameters for nano-pipette fabrication. Laser pullers have five parameters that can be adjusted to obtain nano-pipettes with desired shapes and sizes (heat, filament, velocity, delay, and pull). The apparent nano-electrode radius decreases with increasing heat power (Figure 4.9). This effect is well known for nano-pipette fabrication, where higher heat power generates a smaller sized nano-pipette (Sutter Manual). The same trend is observed after filling of the nano-pipette opening with carbon which indicates the confinement of the carbon layer to the inner area of the nano-pipette and the minimal variability introduced by the carbon filling process. Furthermore, nano-electrode radius can be controlled in the range 7-150 nm by simply adjusting laser puller's heat. Adjustment of the other four parameters (filament, velocity, delay, and pull) may provide an even finer control of nano-electrode radius. The laser pulling process generates a pair of virtually identical nano-pipettes.

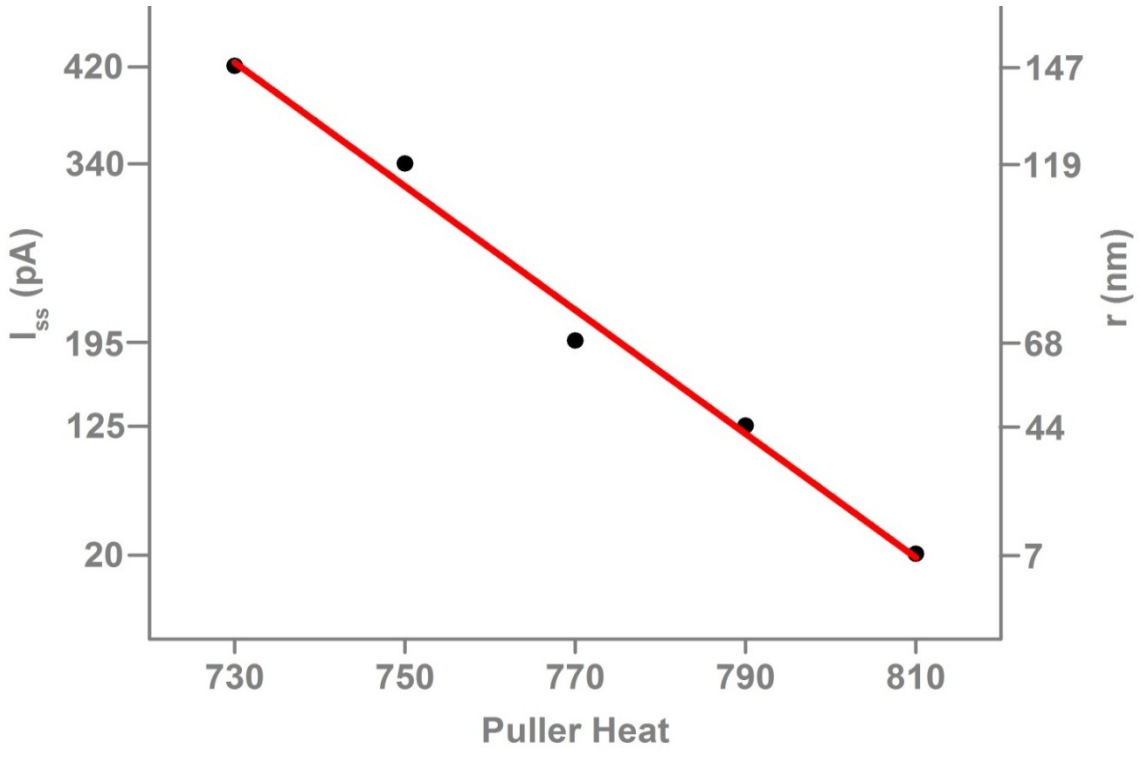

Figure 4.9. Graph represents cyclic voltammetry vs heating pull parameters. Black dots are experimental data taken from the steady state current value, red line is the linear fit to experimental data (R^2=0.986). Solution: 10 mM $Ru(NH_3)_6Cl_3$ in PBS. Sweep rate 50 mV s^{-1}.

Cyclic voltammograms after carbon filling of the nano-pipette pairs were compared to show the minimal variability introduced by the carbon filling step (Figure 4.10). The CVs overlap reasonably well for the 4 pairs studied. The variability of nano-electrode fabrication thus relies mostly on the variability of the nano-pipette pulling step. However, it has to be said that experimental parameters during the carbon filling step, such as butane and Ar pressure, have to be carefully monitored to ensure a highly reproducible nano-electrode.

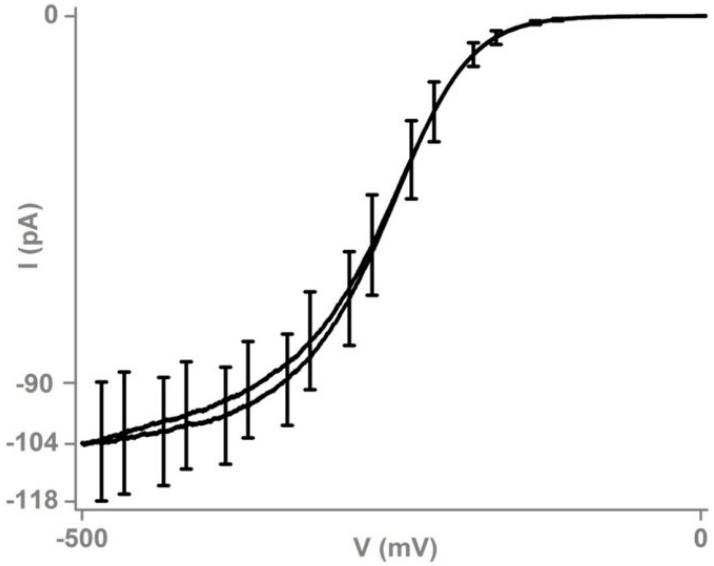

Figure 4.10. Reproducibility of nano-electrode fabrication at a set pulling protocol. Nano-pipette fabrication protocol: Heat 790, Filament 3, Velocity 45, Delay 130, and Pull 90. Average steady state current (104±14) pA corresponding to an apparent radius of (30 ± 4) nm (N=7). Solution: 10 mM $Ru(NH_3)_6Cl_3$ in PBS. Sweep rate 50 mV s^{-1}.

When cyclic votammograms of the pair of carbon probes fabricated form a single pull are compared minimal variability is observed which also indicates minimum effect of deposition step (Figure 4.11).

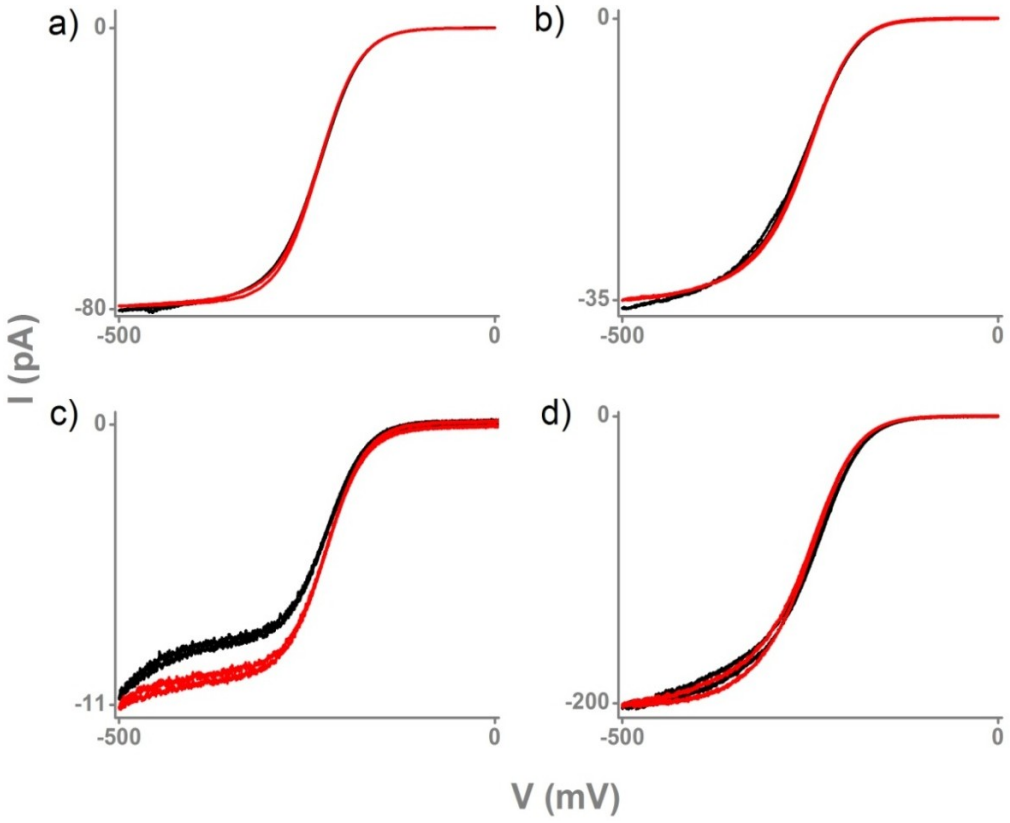

Figure 4.11. Four graphs to represent reproducibility of nano-electrode fabrication. Each graph show cyclic voltammograms (red and black curves) examples of a pair of nano-electrodes fabricated from a single laser pull, to produce two relatively identical pipettes. The overlap of cyclic votammograms signifies minimal variability introduced during fabrication steps. Solution: 1mM $Ru(NH_3)_6Cl_3$ in PBS. Sweep rate 50 mV s^{-1}.

Here CVs for 4 pairs of carbon nano-pipettes are overlapped to demonstrate the variability is mostly introduced in the pulling stage (Figure 4.12). These experiments show methodical examination of nano-electrode geometry that reveals the reliability and reproducibility of carbon deposition on a nano-pipette (Figures 4.11, 4.12, 4.13). L=0 is just above the

substrate surface. In order to achieve a zero current at L=0, the probe has to make a contact with the surface for the current to reach zero. This can be achieved by using a higher set point values. However the probe is highly likely to collide with the surface, that is not completely flat or approach the surface at an angle. Therefore approach curves to the substrate is recorded at lower set point to avoid crashing and damaging the electrode.

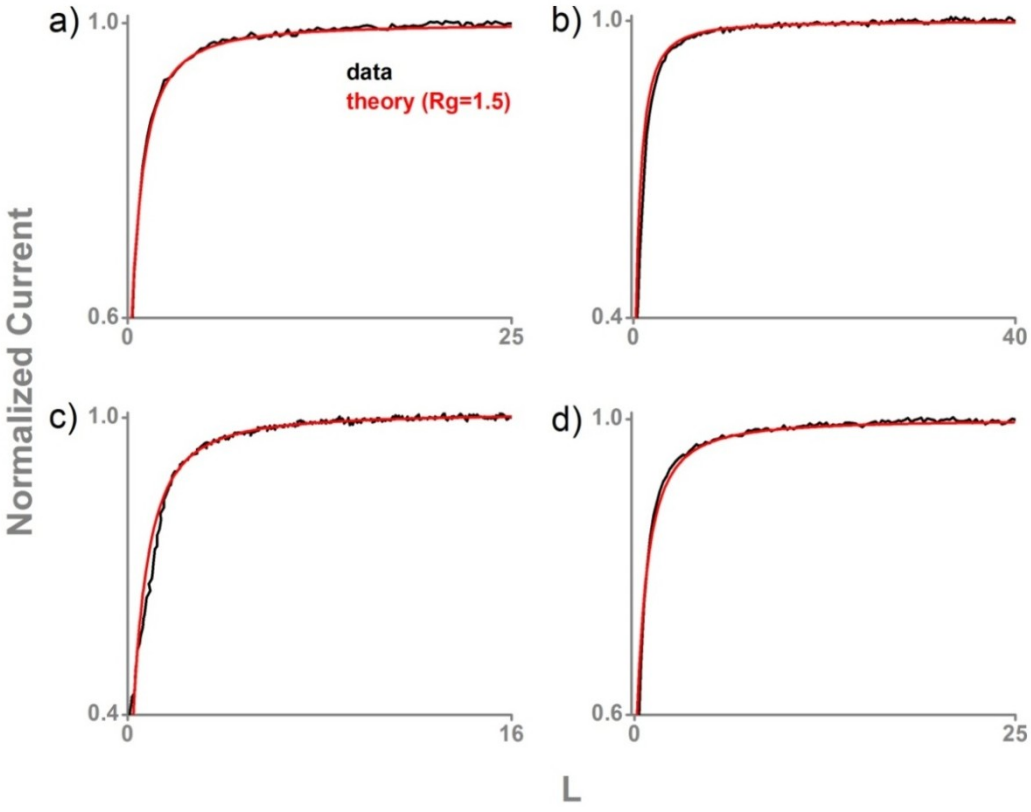

Figure 4.12. Four nano-electrode approach curves, to demonstrate the reproducibility of fabrication procedure. Black line is the actual experimental data. Red line is the theoretical approach curve, for a disk shaped electrode of Rg=1.5. L represents distance normalised by the nanoelectrode radius **(a)** r=64nm, **(b)** r= 73nm, **(c)** r= 48nm, **(d)** r= 81nm. **L** is the distance normalized by the radius of the nano-electrode. Solution: 1mM $Ru(NH_3)_6Cl_3$ in PBS.

-Applied Voltage -400 mV vs Ag/AgCl. The formula used to obtain the simulation curve can be found in; Cornut & Lefrou, 2010.

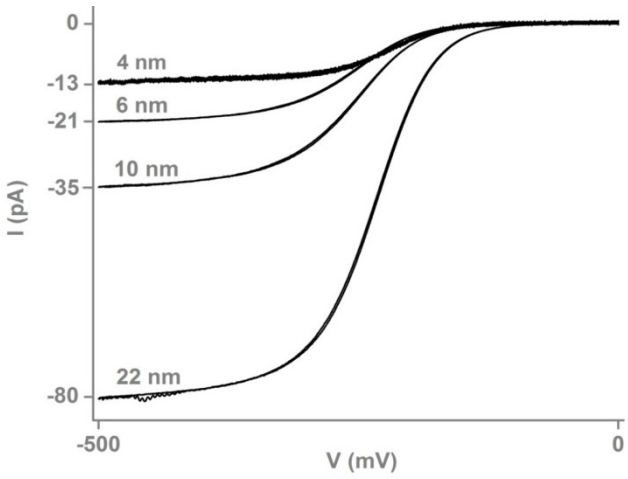

Figure 4.13. Cyclic voltammetry of 4 carbon-filled nano-pipettes. A sigmoidal shape with minimal hysteresis is observed down to 4nm nano-electrodes. Bath solution contained 10 mM $Ru(NH_3)_6Cl_3$ in PBS. Sweep rate was performed at 50 mV s^{-1}.

Platinisation of carbon nano-electrodes

Nano-electrodes made of carbon are relatively inert. They are suitable as probes for high resolution electrochemical imaging but they are not useful as sensors. To overcome this limitation, I electrodeposited platinum on the carbon electrode. Carbon nano-electrodes can be platinised by the reduction of Pt at the carbon nano-electrode, induced by cyclic voltammetry ramp from 0 V to -800 mV while the nano-pipette was immersed into chloroplatinic acid H_2PtCl_6 (2 mM) in 0.1 sulfuric acid medium (figure 4.14). The Pt deposition only slightly increases the nano-electrode area but dramatically affects its catalytical properties. In particular oxygen reduction is enhanced on the platinised nano-

electrode resulting in higher cathodic current (figure 4.15). At concentrations higher that 300 µM of hydrogen peroxide, the platinum can get modified or its absorbtion on the surface may be influenced by production of gas.

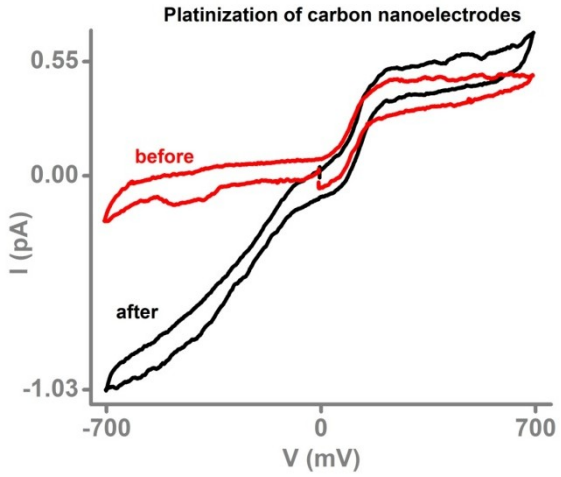

Figure 4.14. Platinisation of carbon nano-electrodes. Cyclic voltammograms in 1mM Ferrocenemethanol in PBS, of a carbon nano-electrodes (apparent radius ~2 nm), before (red curve) and after (black curve) platinisation. The catalytic activity for oxygen reduction is increased in platinised nano-electrodes.

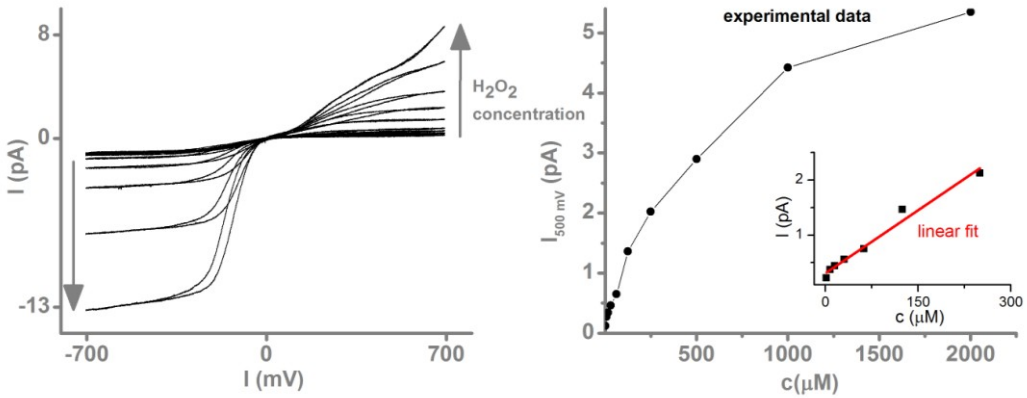

Figure 4.15. Analytical detection of hydrogen peroxide at a platinised carbon nano-electrode. **(A)** Detection of the oxidation of hydrogen peroxide by the platinised carbon nano-electrode and **(B)** its dose response curve. Showing a linear reylationship beween the concentration of analyte and the measured current at lower concentrations of H_2O_2 (The insert is the initial part of the curve). The increase in the oxygen current is due to the instability of the hydrogen peroxide solution in 1X PBS.

The deposition of carbon in quartz nano-pipettes is not limited to single barrel nano-pipette. A method was developped to fabricate “multifunctional nano-probes”. Starting from a double barrel quartz nano-pipette, one barrel can be selectively filled with carbon while leaving the other one unchanged. The same platinisation procedure described earlier can be applied to these probes as shown in figure 4.16. Here the potential sweep is applied only to the barrel desired barrel for selected deposition of platinum.

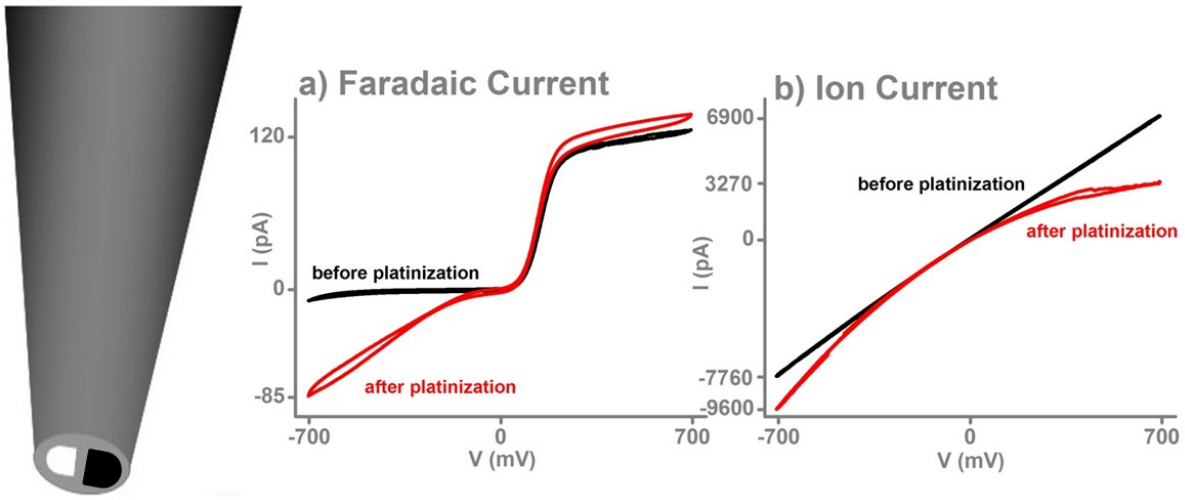

Figure 4.16. Cartoon showing a "multifunctional nano-probe". **(A)** Cyclic voltammograms in 1mM Ferrocene Methanol in PBS of the carbon nano-electrode before (black curve) and after (red curve) platinisation. **(B)** I-V curve of the nano-pipette "barrel" before (black curve) and after (red curve) platinisation of the nano-electrode barrel, showing a slight change in the current rectification that is a possible indication of platinum overgrowth.

These multifunctional probes are currently used in our lab to monitor intra- and extracellular concentrations of reactive oxygen species (ROS) as well as oxygen consumption by cancer cells and neurons.

Our group already showed the potential of these nano-electrodes for cell imaging at the nano-scale, and the functionalisation of the nano-electrode could lead to a probe capable of combined topographical and intracellular sensing" Adapted with permission from (Actis et al.) Copyright (2014) American Chemical Society.

Electrochemical imaging with carbon nano-electrodes

Constant current SECM imaging mode allows noncontact topographical measurements of living cells, without causing physical damage to the cell. One drawback to conventional constant current mode imaging has been caused by the large size of the probe, that by making its feedback control less sensitive to steep slopes and cell protrusions where the imaging constant current (hindered diffusion) feedback SECM system is challenged (Kwak and Bard, 1989).

The following experiment utilises the carbon nano-electrodes described earlier in this chapter, in order to achieve a high resolution electrochemical and topographical images of live cells. Constant current hopping mode was used to obtain reliable distance control using the reduction current of -1mM $Ru(NH_3)_6Cl_3$ dissolved in PBS- at the nano-electrode as a distance feedback control. $Ru(NH_3)_6Cl_3$ is a cell membrane impermeable hydrophilic mediator, making it suitable for SECM topographical imaging experiment of biological membrane (Wong and Xu, 1995; Kurulugama et al., 2005).

Boar spermatozoon, A431 cells, differentiated rat adrenal pheochromocytona cells (PC12), cardiac myocytes and auditory hair cells were imaged using the carbon nano-electrodes integrated in the hopping probe scanning electrochemical microscope (Figure 4.17). Cell topography experiments were conducted at a constant height and constant distance in relation to the surface as done in SICM imaging. The diffusion-limited faradaic current drop is recorded and used to control distance from the underlying surface (Kwak and Bard, 1989). Figure 17 represents highly resolved SECM images, that shows a significant improvement compared with the conventional SECM methods (Kurulugama et al., 2005). The resolution of

SECM image has not yet achieved the SICM topographical resolution (Takahashi et al., 2011; Shevchuk et al., 2006; Takahashi et al., 2012).

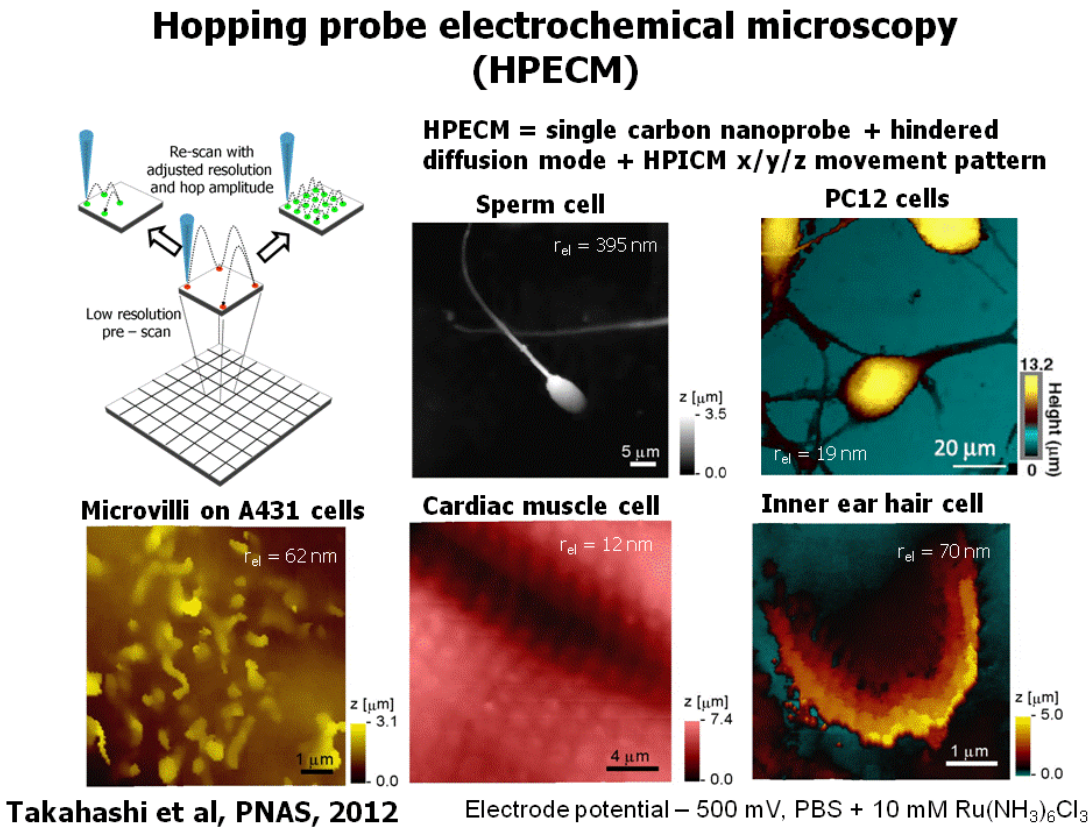

Figure 4.17. SECM (Constant-current) images of a boar sperm cell, differentiated PC12, A431 cell, **(**cardiac myocyte, and hair cells). The carbon electrode was held at −500 mV ground electrode, in PBS containing 10 mM $Ru(NH_3)_6Cl_3$. Top left image shows the prescan measurement that is madeto adjust the resolution according to the roughness of the sample, in order to improve the imaging speed as done in the SICM (Takahashi et al., 2012).

Voltage switching mode SECM

Previous SECM studies have demonstrated that it is possible to employ two redox mediators, whereby one is used to record topography and one to record tissue permeability activity (Gonsalves et al., 2000). Here a description of a recent SECM imaging mode will follow: This innovative mode is called voltage switching, where topographical and electrochemical measurements are recorded at different potentials by rapidly switching the voltage applied to the tip. The distinction here from other reports is the use of nano-scale probes for high resolution electrochemical imaging and detection of electro-active species on cell surface.

Voltage switching mode SECM configuration, enables the same SECM probe to be used for topographical imagng as well as for local functional recordings (for instance neurotransmitter release detection). The surface topographical information enables the positioning of the probe to specific sites (for example synaptic vesicles), to make functional measurements.

Topographical images were taken using constant current mode by $Ru(NH_3)_6Cl_3$ reduction as described above, while electrochemical current were measured ot the same tip with a different potential, from a constant height from the underlying surface (Takahashi et al., 2012).

xyz position of the carbon nano-electrode in this experiment were controlled as described for SICM at a sampling frequency of 20 kHz. The nano-pipette approaches the surface with 30 nm/ms fall rate. As soon as the current drops below the set point value, the pipette is stopped as described for SICM measurements. The Z position of the nano-pipette is saved

into the software as an image pixel for topography. Voltage is then switched from a hindered diffusion detection mode (negative), to surface flux measurement mode (positive) for 20 ms, where the steady state current is measured. Following this measurement the pipette is quickly withdrawn from the surface and the current was switched back to negative and a steady state current is measured as a reference measurement. The sample is then moved laterally on XY to a next imaging point and the pipette is approached to the surface (Novak et al., 2009; Takahashi et al., 2012). VSM-SECM was used by Dr Yasufumi Takahashi in Japan to evaluate the Epidermal Growth Factor Receptor expression levels on cell surface (Takahashi et al., 2012). Figure 4.18 shows the position at which VSM measurement is taking place. -500mV was applied to the electrode to detect the reduction current of $Ru(NH_3)_6Cl_3$ (diffusion limited). As the electrode reaches the set point the voltage is switched to 350mV to measure oxidation.

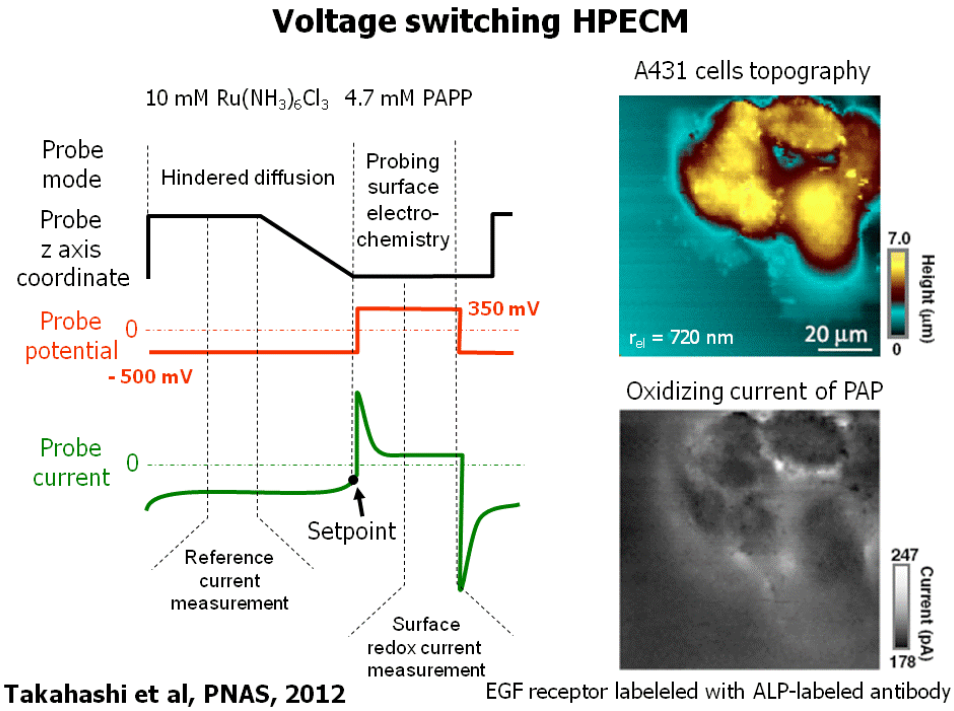

Figure 4.18. Represents the voltage switching mode SECM. Hindered diffusion signal is implemented in the hopping mode to detect the surface. At a certain set point value, where the pipette is close to the surface, the voltage is switched to the opposite direction in order to measure the redox current of a functional mediator. Figure 4.18 shows the topographical and electrochemical images of A431 cells, taken by Dr Yasufumi Takahashi. Probe current was kept at -500 mV to approach the sample surface, where the z position was recorded to produce the topographical image. Before withdrawal of the pipette from each point, the potential was switched to 350 mV in order to to measure the oxidising current. The current was then switched back to the imaging mode for controlled feedback, where the pipette was withdrawn to measure the reference current and approaching the next imaging point. Measurements were conducted in HEPES buffer containing 10mM $Ru(NH_3)_6Cl_3$ and 4.7 mM PAPP. Electrode radius 721 nm (Takahashi et al., 2012).

Neurotransmitter Detection Using Faraday Current Feedback

It is possible to deposit an additional carbon on the outside surface of the pipette to achieve a so called smoked electrode to get a larger surface area to achieve a higher sensitivity. To fabricate a smoked electrode, a larger quartz nanopipettes (over 200 nm in radius) is required. An increased flow of Argon causes the carbon to be deposited inside as well outside the tip of the nanopipette, generating a "smoked" nanoelectrode.

Smoked electrodes have been used to measure neurotransmitter release from PC12 cells. Oxygen reduction at -1.0 V was selected for feedback by optically aligning the electrode to land on the cell. 75% drop in the current was used as a set-point for distance control. After

the set-point value was reached and the pipette is at a specified distance from the surface, voltage was switched to 650 mV for the detection of neurotransmitter release. PC12 cells were stimulated by addition of 105 mM K^+ with a second micro-pipette (3 µm diameter) (Amatore et al., 2008; Isik and Schuhmann, 2006). Figure 4.19 shows several neurotransmitter release related current spikes detected by the carbon electrode.

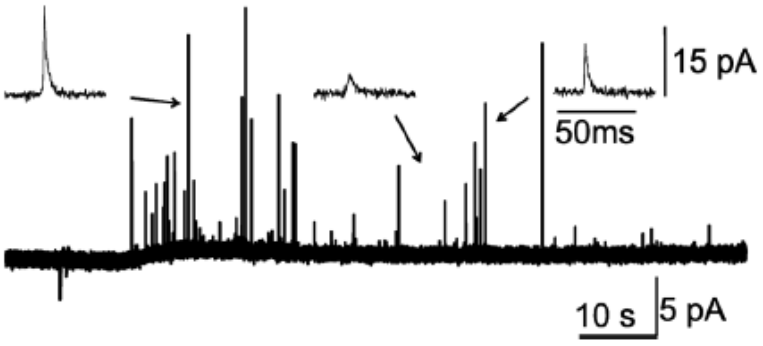

Figure 4.19. Represents neurotransmitter release current spikes following whole cell stimulation of neurons with 105 mM K^+ using a second pipette. For Neurotransmitter release detection the current was held at 650 mV, where an electrode with a radius of 6 µm was used (The steady state current measurements performed in 1mM $FcCH_2OH$ and PBS was 2.0 nA which indicates an electrode size of 6.0 µm. Experiment for neurotransmitter release detection was carried out by Dr Yasufumi Takahashi (Takahashi et al., 2012).

Reference

Actis,P., Tokar,S., Clausmeyer,J., Babakinejad,B., Mikhaleva,S., Cornut,R., Takahashi,Y., Lopez,C.A., Novak,P., Shevchuck,A.I., Dougan,J.A., Kazarian,S.G., Gorelkin,P.V., Erofeev,A.S., Yaminsky,I.V., Unwin,P.R., Schuhmann,W., Klenerman,D., Rusakov,D.A., Sviderskaya,E.V., and Korchev,Y.E. (2014). Electrochemical Nanoprobes for Single-Cell Analysis. Acs Nano *8*, 875–884.

Amatore,C., Arbault,S., Guille,M., and Lemaitre,F. (2008). Electrochemical monitoring of single cell secretion: Vesicular exocytosis and oxidative stress. Chemical Reviews *108*, 2585-2621.

Bard,A.J., Li,X., and Zhan,W. (2006). Chemically imaging living cells by scanning electrochemical microscopy. Biosensors & Bioelectronics *22*, 461-472.

Comstock,D.J., Elam,J.W., Pellin,M.J., and Hersam,M.C. (2010). Integrated Ultramicroelectrode-Nanopipet Probe for Concurrent Scanning Electrochemical Microscopy and Scanning Ion Conductance Microscopy. Analytical Chemistry *82*, 1270-1276.

Gonsalves,M., Barker,A.L., Macpherson,J.V., Unwin,P.R., O'Hare,D., and Winlove,C.P. (2000). Scanning electrochemical microscopy as a local probe of oxygen permeability in cartilage. Biophysical Journal *78*, 1578-1588.

Isik,S. and Schuhmann,W. (2006). Detection of nitric oxide release from single cells by using constant-distance-mode scanning electrochemical microscopy. Angewandte Chemie-International Edition *45*, 7451-7454.

Kurulugama,R.T., Wipf,D.O., Takacs,S.A., Pongmayteegul,S., Garris,P.A., and Baur,J.E. (2005). Scanning electrochemical microscopy of model neurons: Constant distance imaging. Analytical Chemistry *77*, 1111-1117.

Kwak,J. and Bard,A.J. (1989). Scanning Electrochemical Microscopy - Theory of the Feedback Mode. Analytical Chemistry *61*, 1221-1227.

Lefrou,C. and Cornut,R. (2010). Analytical Expressions for Quantitative Scanning Electrochemical Microscopy (SECM). Chemphyschem *11*, 547-556.

Macpherson,J.V., Unwin,P.R., Hillier,A.C., and Bard,A.J. (1996). In-situ imaging of ionic crystal dissolution using an integrated electrochemical/AFM probe. Journal of the American Chemical Society *118*, 6445-6452.

McCreery,R.L. (2008). Advanced carbon electrode materials for molecular electrochemistry. Chemical Reviews *108*, 2646-2687.

Mirkin,M.V., Fan,F.R.F., and Bard,A.J. (1992). Scanning Electrochemical Microscopy .13. Evaluation of the Tip Shapes of Nanometer Size Microelectrodes. Journal of Electroanalytical Chemistry *328*, 47-62.

Nogala,W., Velmurugan,J., and Mirkin,M.V. (2012). Atomic Force Microscopy of Electrochemical Nanoelectrodes. Analytical Chemistry *84*, 5192-5197.

Novak,P., Li,C., Shevchuk,A.I., Stepanyan,R., Caldwell,M., Hughes,S., Smart,T.G., Gorelik,J., Ostanin,V.P., Lab,M.J., Moss,G.W., Frolenkov,G.I., Klenerman,D., and Korchev,Y.E. (2009). Nanoscale live-cell imaging using hopping probe ion conductance microscopy. Nature Methods *6*, 279-281.

Robinson,D.L., Hermans,A., Seipel,A.T., and Wightman,R. (2008). Monitoring rapid chemical communication in the brain. Chemical Reviews *108*, 2554-2584.

Shevchuk,A.I., Frolenkov,G.I., Sanchez,D., James,P.S., Freedman,N., Lab,M.J., Jones,R., Klenerman,D., and Korchev,Y.E. (2006). Imaging proteins in membranes of living cells by high-resolution scanning ion conductance microscopy. Angew. Chem. Int. Ed Engl. *45*, 2212-2216.

Shevchuk,A.I., Novak,P., Takahashi,Y., Clarke,R., Miragoli,M., Babakinejad,B., Gorelik,J., Korchev,Y.E., and Klenerman,D. (2011). Realizing the biological and biomedical potential of nanoscale imaging using a pipette probe. Nanomedicine. (Lond) *6*, 565-575.

Shin,W. and Gillis,K.D. (2006). Measurement of changes in membrane surface morphology associated with exocytosis using scanning ion conductance microscopy. Biophysical Journal *91*, L63-L65.

Sun,P., Laforge,F.O., and Mirkin,M.V. (2007). Scanning electrochemical microscopy in the 21st century. Phys. Chem. Chem. Phys. 9, 802-823.

Takahashi,Y., Shevchuk,A.I., Novak,P., Babakinejad,B., Macpherson,J., Unwin,P.R., Shiku,H., Gorelik,J., Klenerman,D., Korchev,Y.E., and Matsue,T. (2012). Topographical and electrochemical nanoscale imaging of living cells using voltage-switching mode scanning electrochemical microscopy. Proc. Natl. Acad. Sci. U. S. A *109*, 11540-11545.

Takahashi,Y., Shevchuk,A.I., Novak,P., Murakami,Y., Shiku,H., Korchev,Y.E., and Matsue,T. (2010). Simultaneous noncontact topography and electrochemical imaging by SECM/SICM featuring ion current feedback regulation. J. Am. Chem. Soc. *132*, 10118-10126.

Takahashi,Y., Shevchuk,A.I., Novak,P., Zhang,Y., Ebejer,N., Macpherson,J.V., Unwin,P.R., Pollard,A.J., Roy,D., Clifford,C.A., Shiku,H., Matsue,T., Klenerman,D., and Korchev,Y.E. (2011). Multifunctional nanoprobes for nanoscale chemical imaging and localized chemical delivery at surfaces and interfaces. Angew. Chem. Int. Ed Engl. *50*, 9638-9642.

Takahashi,Y., Shiku,H., Murata,T., Yasukawa,T., and Matsue,T. (2009). Transfected Single-Cell Imaging by Scanning Electrochemical Optical Microscopy with Shear Force Feedback Regulation. Analytical Chemistry *81*, 9674-9681.

Westerink,R. and Ewing,A. (2008). The PC12 cell as model for neurosecretion. Acta Physiologica *192*, 273-285.

Wong,D.K.Y. and Xu,L.Y.F. (1995). Voltammetric Studies of Carbon Disk Electrodes with Submicrometer-Sized Structural Diameters. Analytical Chemistry *67*, 4086-4090.

Ying,L.M., Bruckbauer,A., Zhou,D.J., Gorelik,J., Shevehuk,A., Lab,M., Korchev,Y., and Klenerman,D. (2005). The scanned nanopipette: A new tool for high resolution bioimaging and controlled deposition of biomolecules. Physical Chemistry Chemical Physics *7*, 2859-2866.

Chapter 5

Chemical Delivery

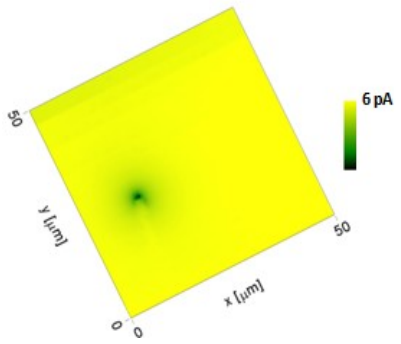

*An SECM image of chemical mediator release around the tip of a carbon nano-electrode glued to a petri-dish.

In this chapter the delivery of molecules from the nano-pipette tip under applied pressure and voltage gradients over the pipette will be discussed. Experimental and theoretical data are compared in order to calculate the concentration of molecules at the tip of the nano-pipette as a function of the driving force (voltage or pressure) and distance. Finally the fabrication and characterization of double barrel nano-pipettes, where one barrel is selectively filled with pyrolytic carbon will is discussed.

Some of the materials presented in the following chapter have now been published in the journal of Analytical Chemistry under the title: “Local delivery of molecules from a nanopipette for quantitative receptor mapping on live cells” (Babakinejad et al., 2013).

*Theoretical simulations in this chapter were performed in collaboration with Dr Peter Jonsson.

SICM for chemical delivery

"There are a number of useful applications for the local delivery of molecules, to specific regions on surfaces. There are many motivations to develop local delivery methods, these include the ability to achieve local stimulation of receptors, to map molecular structures on cell surfaces (Piper et al., 2008; Bruckbauer et al., 2007), or to create molecular arrays (Rodolfa et al., 2005; Bruckbauer et al., 2004). Some of the methods devised to achieve this include micro-fluidic based methods (Meister et al., 2009; Juncker et al., 2005; Qasaimeh et al., 2013; Ainla et al., 2010), hollow atomic force microscopy cantilevers (Meister et al., 2009), electro-phoretic delivery with organic electronic devices (Simon et al., 2009), and voltage driven delivery using nano- to micrometer pipettes (Bruckbauer et al., 2007; Takahashi et al., 2011; Ying et al., 2002; Ying et al., 2005).

For chemical delivery with a nano-pipette, the amount of molecules released from the tip depends on: the concentration inside the pipette, the size of the nano-pipette tip and the magnitude of the outward flow. The latter can be regulated by applying voltage or pressure over the pipette. A higher flow rate generates a higher flux of molecules at the tip of the nano-pipette, up to a point that the concentration outside of the pipette is equal to the concentration inside. Higher flow rates also release and expose molecules to a larger area outside of the nano-pipette, thus for local delivery experiments it is important to keep the flow rate as small as possible.

For quantitative delivery of molecule, the separation between the nano-pipette and the surface is a crucial parameter that has to be precisely controlled. When the pipette is far from surface, the concentration profile is broad, and covers a larger area. Conversely as the pipette gets closer to the surface the concentration profile becomes more localised. It is

necessary to know the concentration profile at different voltages and pressures as well as at different distances from the surface, in order to be able to estimate the concentration experienced by the targeted structure, and hence to achieve a quantifiable delivery and measurement system. The SICM distance controlled feedback system, provides the distance control, which is necessary for quantitative local delivery experiments, to attain meaningful and reproducible data on biological samples.

Using electrochemical probes to study delivery from pipettes

In this section, approximate expressions are derived to estimate how different parameters involved relate to each other and influence the rate of the flow and concentration profile in particular. Finite element simulations are used to describe in detail the concentration profile outside the pipette. Later the combined SICM-SECM system is used for distance controlled delivery of chemicals by changing the applied voltage and by voltage independent pressure application (Sanchez et al., 2008).

The concentration profile of molecules delivered from a nano-pipette tip can be described as a function of (i) nano-pipette radius, (ii) applied force (by external voltage or pressure), and (iii) distance to the surface. Having an estimate of the local concentration profile at the tip of a nano-pipette opens the possibility for accurate delivery of specific molecules to nano-meter-sized regions and for controlled stimulation of receptors on cell surfaces.

Theoretical description of delivery from a pipette

The flux of molecules, ***J***, in any part of the system is given by:

$$\boldsymbol{J} = -D\nabla c + \left(\boldsymbol{u}_{\mathrm{p}} + \boldsymbol{u}_{\mathrm{ep}} + \boldsymbol{u}_{\mathrm{eo}}\right)c \tag{1}$$

Where D is the diffusivity and c the concentration of molecules and $\boldsymbol{u}_{\mathrm{p}}$, $\boldsymbol{u}_{\mathrm{ep}}$ and $\boldsymbol{u}_{\mathrm{eo}}$ is the velocity field due to pressure-driven flow, electro-phoresis and electro-osmosis, respectively. Integrating Equation 1 over a spherical shell, radius R, with its center at the tip of the pipette and making the simplifying approximation that c is only a function of R yields:

$$c_0 Q_{\mathrm{tot}} = -D\frac{dc(R)}{dR}4\pi R^2 + c(R)Q_{\mathrm{tot}} \tag{2}$$

Where Q_{tot} is the integral of $\boldsymbol{u}_{\mathrm{p}} + \boldsymbol{u}_{\mathrm{ep}} + \boldsymbol{u}_{\mathrm{eo}}$ over any cross-section of the pipette (the total flow leaving the pipette due to pressure and electric fields) and c_0 is the concentration of molecules in the bulk of the pipette. It should be mentioned that the true concentration profile will also contain angular dependent terms, which close to the aperture of the pipette may have a significant contribution to concentration profile. However, to estimate the influence of the different parameters on the concentration profile at $R > R_0$, where R_0 is the radius of the pipette tip, the expression in Equation 2 can be used as a first approximation. Equation 2 has the following solution:

$$c(R) = c_0\left(1 - \exp\left(-Q_{\mathrm{tot}}/4\pi DR\right)\right) \tag{3}$$

According to Equation 3 there is no difference in the concentration profile for pressure and voltage-induced delivery as long as the total amount of molecules being delivered is the same. A series expansion of Equation 3 gives that when $R >> R_0$ the concentration drops as $1/R$. When a voltage difference, $\Delta\Psi$, is applied over the pipette, the magnitude of the electric field, E, inside the pipette can approximately be written (Ying et al., 2004):

$$E(z) = \frac{R_0 \tan(\theta)}{R_p(z)^2} \Delta\Psi \tag{4}$$

Where R_p is the radius of the pipette a distance z above the tip of the pipette. The total flow Q_{tot} out of the pipette due to electrophoresis and electro-osmosis is then:

$$Q_{tot,\Delta\Psi} = (\mu_{ep} + \mu_{eo})\pi R_0 \tan(\theta)\Delta\Psi \tag{5}$$

Where ϑ is the inner half-cone angle of the pipette and μ_{ep} and μ_{eo} are the electro-phoretic and electro-osmotic mobility of the molecules, respectively. The electro-phoretic mobility is related to the diffusivity of the molecule by:

$$\mu_{ep} = \frac{qD}{k_B T} \tag{6}$$

where q is the charge of the molecule, k_B is the Boltzmann factor and T is the temperature. The electro-osmotic mobility can be determined from the expression:

$$\mu_{eo} = -\varepsilon_0 \varepsilon_r \zeta / \eta \tag{7}$$

where ε_0 is the permittivity of vacuum, ζ is the zeta potential of the pipette wall, ε_r the relative permittivity of the electrolyte solution and η the viscosity of the bulk solution. With $\zeta = -20$ mV for a glass surface in a ~150 mM Na^+ electrolyte(Kirby and Hasselbrink, Jr., 2004), $\varepsilon_r = 80$ and $\eta = 1$ mPa s this gives $\mu_{eo} = 1.4\times10^{-8}$ m^2/V s.

When a pressure drop Δp is applied over the pipette Q_{tot} can be shown to be approximately given by (Sanchez et al., 2008):

$$Q_{tot,\Delta p} = \frac{3\pi R_0^3 \tan(\theta)\Delta p}{8\eta} \tag{8}$$

Where η is the viscosity of the liquid ($\eta = 1$ mPa s in this work).

Since the theoretical concentration profile for both pressure- and voltage-induced delivery only depends on Q_{tot} (see Equation 3) it is possible to estimate the voltage difference that needs to be applied to obtain the same concentration profile as when a pressure drop of Δp is applied over the pipette. From Eqs. 5 and 8 this gives:

$$\Delta\Psi = \frac{3R_0^2\Delta p}{8\eta(\mu_{ep} + \mu_{eo})} \tag{9}$$

If there is a surface a distance h below the tip of the pipette the concentration profile will change. As a first approximation we can estimate the effect of the surface by adding to Equation 3 the concentration profile that would arise from an imaginary pipette positioned

at a distance *h* below the surface. This has the effect of setting the flux at the surface equal to zero resulting in the following concentration profile:

$$c(R_+, R_-) = c_0\left(2 - \exp\left(-Q_{\text{tot}}/4\pi DR_+\right) - \exp\left(-Q_{\text{tot}}/4\pi DR_-\right)\right) \tag{10}$$

Where R_+ is the distance from the tip of the real pipette and R_- is the distance from the tip of the imaginary pipette to the position where the concentration is evaluated. At the surface the concentration varies with the radial position, *r*, as:

$$c(r) = 2c_0\left(1 - \exp\left(-Q_{\text{tot}}\Big/4\pi D\sqrt{r^2 + h^2}\right)\right) \tag{11}$$

Where *r* = 0 is the position on the surface that is directly below the center of the pipette. By moving the pipette closer to the underlying surface the concentration profile will be focused to a smaller area. From Equation 11 it is possible to derive that the radial distance where the concentration has dropped to half the value at *r* = 0 is approximately given by:

$$r_{1/2} \approx \sqrt{3}h_0 \tag{12}$$

Under the assumption that $c << c_0$. It should also be noted that the expression in Equation 9 only approximates the concentration outside the pipette for low to moderate flow rates Q_{tot} where $c << c_0$. In fact, the expression in Equation 11 approaches the value $2c_0$ when Q_{tot} is large instead of c_0. For a more accurate model of the concentration at higher values of the applied pressure/voltage the concentration can be set equal to c_0 when:

$$\frac{Q_{\text{tot}}}{4\pi D\sqrt{r^2+h^2}} > \ln(2) \tag{13}$$

Numerical Simulations

COMSOL Multiphysics® 4.3 (COMSOL AB, Stockholm, Sweden) was used to simultaneously solve for the concentration, flow velocity and electric field in the studied system. The geometry used for the simulations is shown in Figure 5.1, utilizing the cylindrical symmetry to transform the three-dimensional problem to a set of partial differential Equations in two dimensions. The following values for the pipette parameters were assumed: $\theta = 3°$, $R_0 = 50$ nm and $R_0/R_1 = 0.58$.

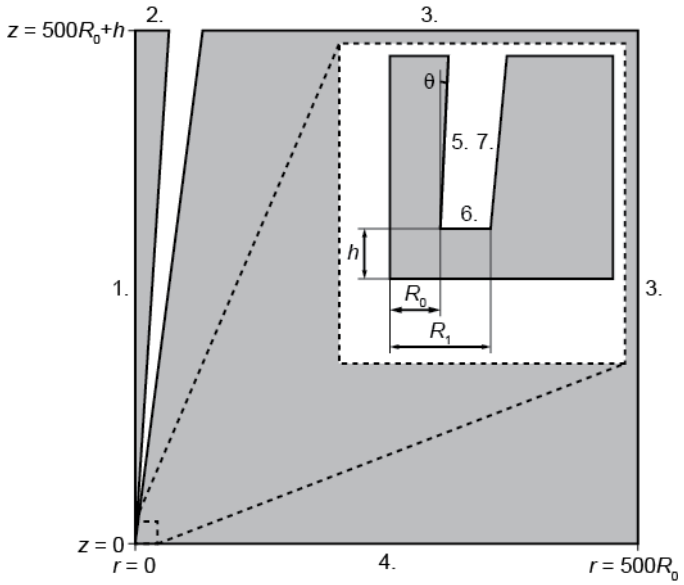

Figure 5.1. The geometry used in the finite element simulations, corresponding to the radial cross section of a pipette (white). R_0 is the inner tip radius of the pipette. Pipette is immersed in the bath solution. Grey indicates liquid phase.

The electrical potential, Ψ was determined using the *Electrostatics module* for the 2D axisymmetric case. The following boundary conditions were used (see Figure 5.1 for the numbering of boundaries): **1.** axial symmetry, **2.** the electric field in the *z*-direction given by $E_z = E_{\text{top}}$, **3.** $\Psi = 0$ and **4.-7.** the "zero charge" condition ($\boldsymbol{n}\cdot\nabla\Psi = 0$, where $\boldsymbol{n}$ is a unit normal to the boundary). The electric field E_{top} is related to the total voltage drop, $\Delta\Psi$, over the pipette by (Ying et al., 2004):

$$\Delta\Psi = \Psi_{\text{top}} + \frac{E_{\text{top}} R_{\text{top}}}{\tan(\theta)} \tag{14}$$

Where Ψ_{top} is the average value of the voltage at boundary 2 in Figure 5.1.

To determine the liquid flow, ***u***, in the system Navier-Stokes Equations for creeping flow were solved using the 2D symmetric, *Creeping flow module*. The following boundary conditions were used (see Figure 5.1 for numbering of the boundaries): **1.** axial symmetry, **2.** a velocity given by:

$$\boldsymbol{u} = -\left(\frac{2\left(R_{\text{top}}^2 - r^2\right)Q_{\text{tot},\Delta\text{p}}}{\pi R_{\text{top}}^4} + \mu_{\text{eo}} E_{\text{top}} \right) \boldsymbol{e}_z \tag{15}$$

Where $Q_{\text{tot},\Delta\text{p}}$ is the flow rate through the pipette due to pressure-driven flow (Jonsson et al., 2012), μ_{eo} the electro-osmotic mobility and $\boldsymbol{e}_z$ is a unit vector in the z-direction, **3.** $p = 0$ and no viscous stress, **4.** no-slip and **5-6.** a velocity given by:

$$\boldsymbol{u} = \mu_{\text{eo}} \boldsymbol{E}_{\text{t}} \tag{16}$$

Where $\boldsymbol{E}_{\text{t}}$ is the electric field tangential to the wall ($\boldsymbol{E}$ = -$\nabla\Psi$) and **7.** no-slip. The flow rate $Q_{\text{tot},\Delta\text{p}}$ is related to the total pressure drop over the pipette, Δp, by (Sanchez et al., 2008):

$$\Delta p = p_{\text{top}} + \frac{8\eta Q_{\text{tot},\Delta\text{p}}}{3\pi R_{\text{top}}^3 \tan(\theta)} \tag{17}$$

Where p_{top} is the average value of the pressure at boundary 2 in Figure 5.1.

The *Transport of diluted species* module in 2D symmetry was used to calculate the concentration of molecules in- and outside the pipette with a convective flow velocity:

$$\boldsymbol{u} = \mu_{\mathrm{ep}} \boldsymbol{E} + \boldsymbol{u}_{\mathrm{p}} \tag{18}$$

Where μ_{ep} is the electro-phoretic mobility, $\boldsymbol{E}$ the electric field determined from the electrostatic stimulations and $\boldsymbol{u}_{\mathrm{p}}$ the velocity field from the creeping flow simulations. The boundary conditions used were (see Figure 5.1 for numbering of the boundaries): **1.** axial symmetry, **2.** $c = c_0$, **3.** $c = c(R_+, R_-)$ from Equation 10 and **4.-7.** no flux ($\boldsymbol{J} \cdot \boldsymbol{n} = 0$).

The simulations were performed such that first the electric field was modeled, then the liquid flow using the values of the electric field as input for the electro-osmotic flow and finally the concentration profile using both the electric field and the simulated flow velocities. The mesh of the simulations was chosen sufficiently fine such that no significant change in the results was obtained using a finer mesh.

The analytical formulas derived in the Theory, are simplifications of how the concentration looks like outside the pipette. The formula in Equation 10 (describing the concentration on the surface) is a good approximation when the pipette tip is more than one pipette radius from the surface at a low to moderate flow rates of delivery (See formula 13). The numerical simulations were used to check the validity of the simplifed formulas to get a better understanding of in which regime these approximations are valid. Checking all conditions with experiments would have taken a very long time and would thus not be practically

feasable. However, some experiments were also conducted to see if the approximate expressions also could describe the experimental results.

Results

In deriving the analytical expression in Equation 3 it was assumed that the concentration profile roughly varies as a function of the radial distance to the center of the pipette tip, $c(R)$. We found that this is approximately true when $R >> R_0$, but is less accurate close to the tip of the nano-pipette (see Figure 5.2 **(A)**), where the height h in the simulation was set to $5000R_0$, to mimic the situation of a non-bounded pipette, and $D = 2\times10^{-10}\ \mathrm{m^2/s}$). This is also confirmed by Figure 5.2 **(B)** which shows a line profile of the concentration at an applied pressure of 20 kPa. The line profile is given as a function of r at a distance z = 0.5 µm below the tip of the pipette. The solid black curve is the approximate analytical expression for the concentration given by Equation 3, with the same parameter values as used in the simulations (Q_{tot} was calculated using Equation 8 for pressure and Equation 5 for voltage delivery. Not unexpectedly, the theoretical curve deviates from the simulated values at small r, but is in better agreement at larger r. The reason for the discrepancy is that the non-radially symmetric convective contribution to the molecular flux is significant close to the tip of the pipette. Nevertheless, at larger distances diffusion dominates the molecular flux which gives the radial dependence assumed in Equation 3. Figure 5.2 **(B)** also shows the line profile when instead of pressure a voltage $\Delta\Psi = 660\ \mathrm{mV}$ is applied. With $\mu_{ep} = \mu_{eo} = 1.4\times10^{-8}\ \mathrm{m^2/V\ s}$ this gives the same value of Q_{tot} as for the case when dosing with 20 kPa pressure; $Q_{tot} = 1.54\times10^{-16}\ \mathrm{m^3/s}$ (see Eqs. 5 and 8).

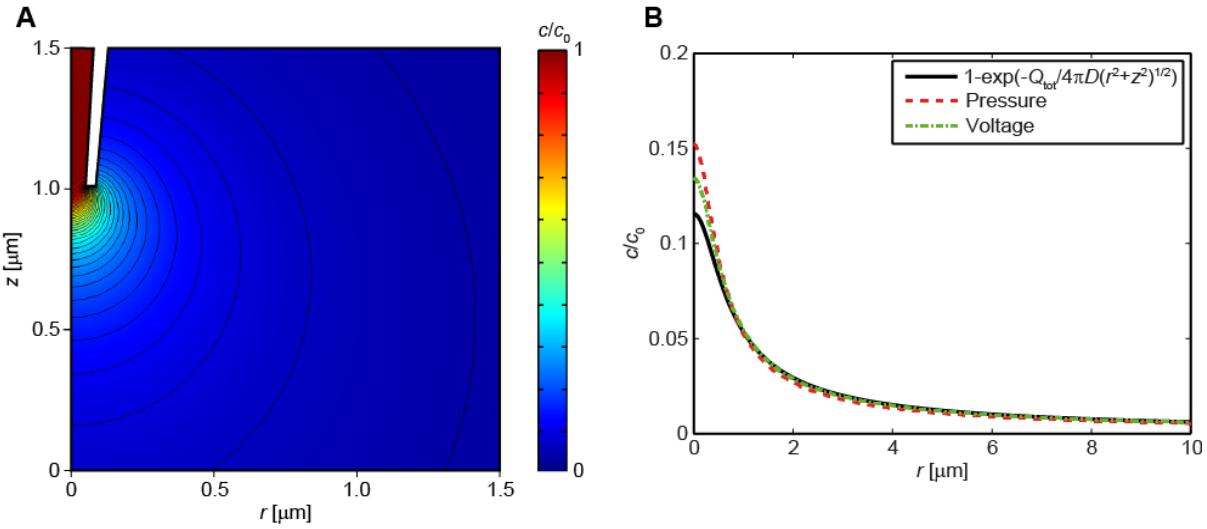

Figure 5.2. (A) The magnitude of the concentration and contour profiles when a pressure difference of 20 kPa is applied at the top of the nano-pipette. **(B)** A comparison between simulated values for voltage and pressure-induced delivery and the analytical expression in Equation 3 a distance z = 0.5 µm below the tip of the pipette.

If there is a surface below the pipette the concentration profile changes as can be seen in Figure 5.3 **(A)**, where the pipette is positioned 250 nm ($5R_0$) above the surface. The diffusivity of the studied molecules was again $D = 2\times10^{-10}$ m^2/s. The solid black line corresponds to the expression in Equation 11, with the same parameter values as used in the simulations (Q_{tot} was calculated using Equation 8 for pressure and Equation 5 for voltage delivery).

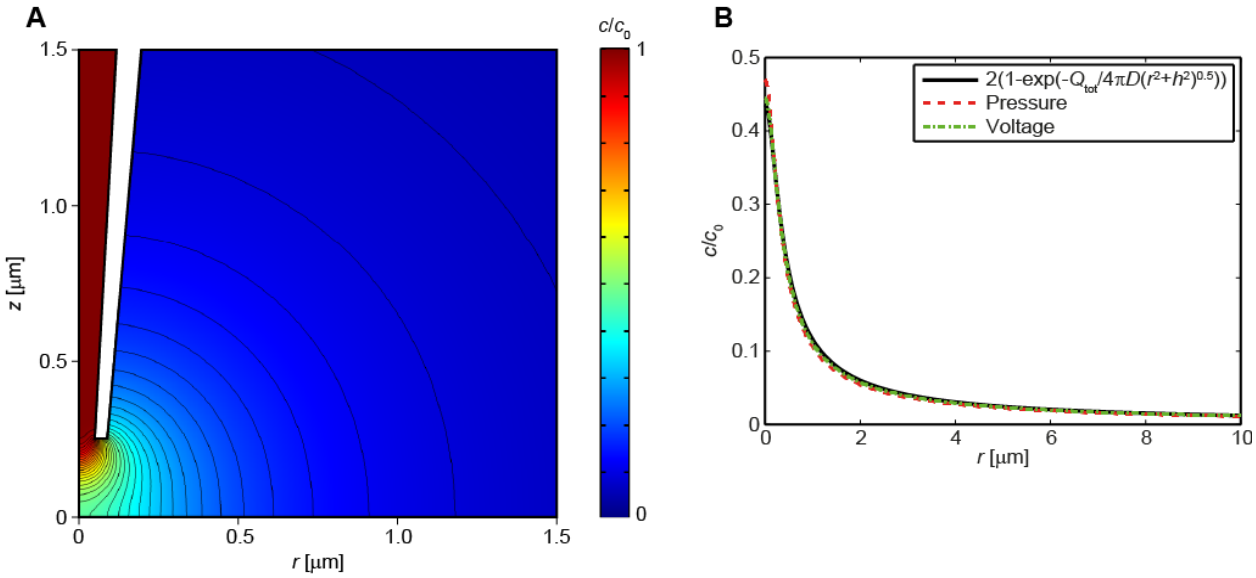

Figure 5.3. (A) Surface plot and contour lines of the relative concentration of molecules due to pressure-induced dosing at an applied pressure of 20 kPa when there is a surface a $5R_0$ below the pipette. **(B)** Comparison of the theoretical expression in Equation 11 with the simulated concentration profile on the surface (z = 0) for pressure- and voltage-induced delivery.

The contour lines in Figure 5.3 **(A)** are similar to the ones in Figure 5.2 **(A)** but change close to the surface to account for the zero flux condition. The concentration profile along the surface at z = 0 is given in Figure 5.3 **(B)** together with the theoretical expression from Equation 11, using Equation 5 to get $Q_{\text{tot}} = 1.54\times10^{-16}$ m^3/s. In addition, the concentration profile from a simulation with voltage-induced dosing was also included in Figure 5.3 **(B)**. The applied voltage was here chosen to $\Delta\Psi = 660$ mV, which with $\mu_{\text{ep}} = \mu_{\text{eo}} = 1.42\times10^{-8}$ m^2/V s gives $Q_{\text{tot},\Delta\Psi} = 1.54\times10^{-16}$ m^3/s (see Equation 5), the same total flow rate as in the pressure-induced dosing. However, it should be noted that even though the theoretical curve in Figure 5.3 **(B)** well describes the simulated concentration profiles for both

pressure- and voltage-induced dosing this will not be the case for all situations (see Figure 5.4).

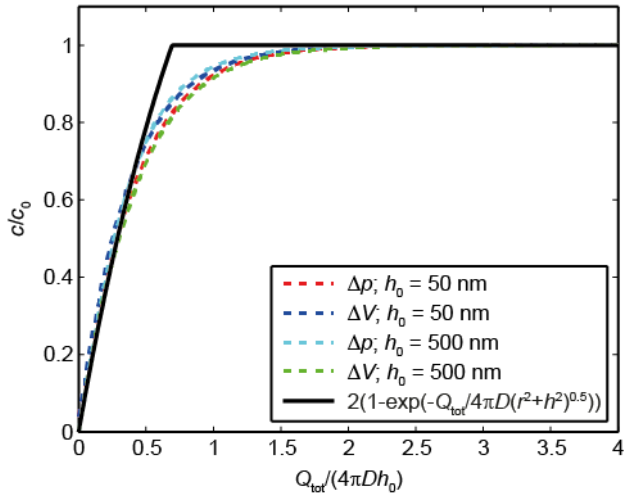

Figure 5.4. Simulated values of the concentration on the surface (r = 0) for pressure- and voltage-induced dosing (dashed lines). The solid line is the theoretical expression given by Equation 11, set to c_0 when $Q_{tot}/(4\pi Dh) > \ln(2)$.

Figure 5.4 shows the simulated values of the concentration on the surface (r = 0) for some different applied pressures and voltages. The distance between the nano-pipette and the surface was either equal to R_0 or $10R_0$ (50 or 500 nm) and both pressure- and voltage induced delivery was investigated, where in the latter case $\mu_{ep} = \mu_{eo} = 1.42\times10^{-8}$ m^2/V s was again assumed. The diffusivity of the studied molecules was set to 2×10^{-10} m^2/s. Equations 5 and 8 were used to convert the applied pressure/voltage into values of Q_{tot}. From Figure 5.4 it can be observed that the expression from Equation 11 is in good agreement with the simulated curves up to $c/c_0 \approx 0.7$ after which the simulated values are lower than the expression in Equation 11. We can conclude from information in Figs. 5.2 to 5.4 that to accurately obtain the concentration profile for high pressures/voltages, or for distances smaller than R_0, numerical simulations need to be used" (Babakinejad et al., 2013).

Mapping the concentration profile of an electrochemical mediator

Local delivery of molecules was achieved with a nano-pipette by dosing redox-active molecules, over an electrochemical probe electrode. Experiments were generally performed in PBS solution with the SICM probe containing 1 mM electrochemical mediator similar to what described in chapter 4. Here +/- 500 mV were applied to the electrochemical probes depending on the mediator, while +/- 200 mV was applied to the SICM probe, both vs. the ground electrode, unless otherwise specified.

Electrochemical disc sensor

In order to demonstrate that chemicals are delivered from the SICM nano-pipette to the surfaces below the nano-pipette tip, initially I used a 25 µm diameter disc shape Pt substrate as a sensor, kindly provided by Dr. Yasufumi Takahashi. The electrochemical substrate was selected with a size similar to that of a single cell, in order to demonstrate how a cell membrane sense the release of chemicals from the nano-pipette.

The nano-pipette was filled with 1 mM ferrocenemethanol in PBS as the electrochemical mediator, and the substrate was placed in PBS solution without any mediator. The electrochemical substrate measures Faraday current resulting from oxidation/reduction of the redox mediator, delivered by the SICM nano-pipette. The SICM probe approached the surface of the dish to scan the substrate disc at +200 mV at 3 different pressures. Topographical images were taken, jointly with electrochemical recordings of the substrate. Simultaneous measurements at each points makes it possible to superimpose the

topographical and electrochemical data and thus to compare every electrochemical recording event with the corresponding position of the SICM nano-pipette. Figure 5.5 represents a 3D topographical image of the electrochemical substrate and, corresponding 2D electrochemical images at different pressures. As the pressure gets bigger the flow rate of molecules is increased, and consequently the electrochemical signal detection is enhanced.

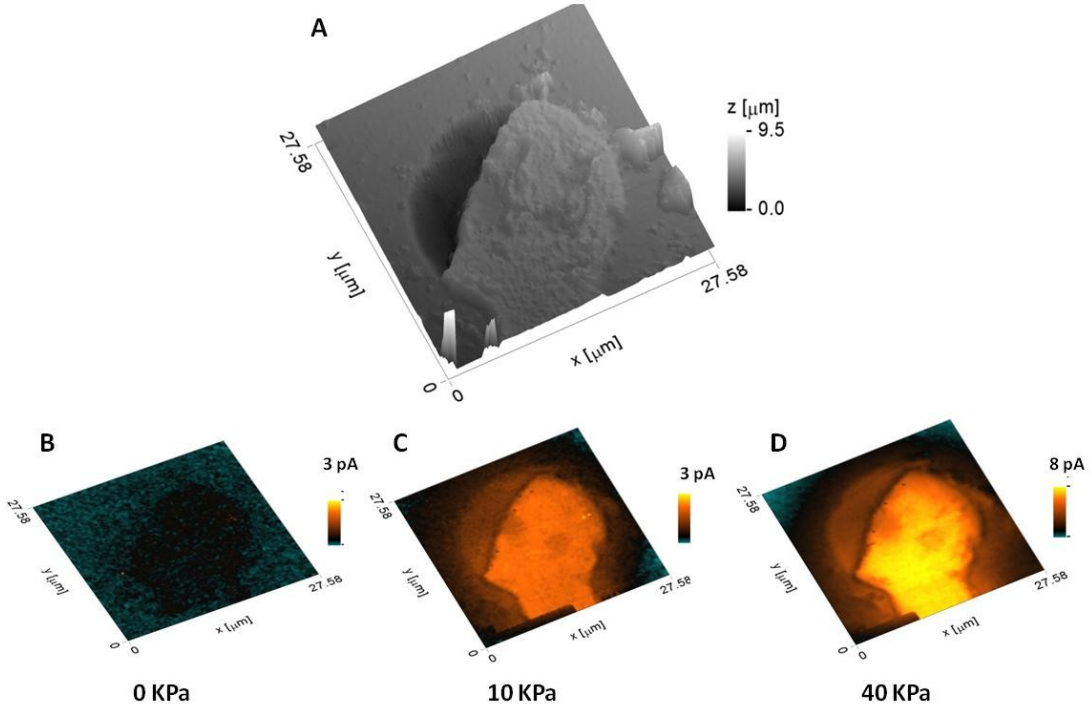

Figure 5.5. Topographical and electrochemical images of the electrochemical substrate disc. (**A)** The height-coded topographical image of the electrochemical substrate. **(B)**, **(C)** & **(D)** refer to three separate electrochemical measurements performed over the surface of the substrate, taken at different pressures over the SICM nano-pipette. The bath solution contained PBS.

Next, the nano-pipette was positioned to approach the centre of the electrochemical substrate and to maintain a constant distance from the substrate surface. When the pipette approaches the surface at a set distance, the feedback system is switched off to keep the pipette stationary, at a constant height from the surface. Figure 5.6 **(A)** & **(B)** illustrates the manner in which the electrochemical substrate responded to the increasing magnitude of pressure (more mediator being released). The nano-pipette was subsequently withdrawn and moved away from the substrate, and chopped on an empty area without debris, to attain a larger size of the nano-pipette, explained on the next page. Same process as explained before was carried out from the same position and distance relative to the substrate, to demonstrate the relationship between the probe size and the increase in electrochemical signal detection (Figure 5.6).

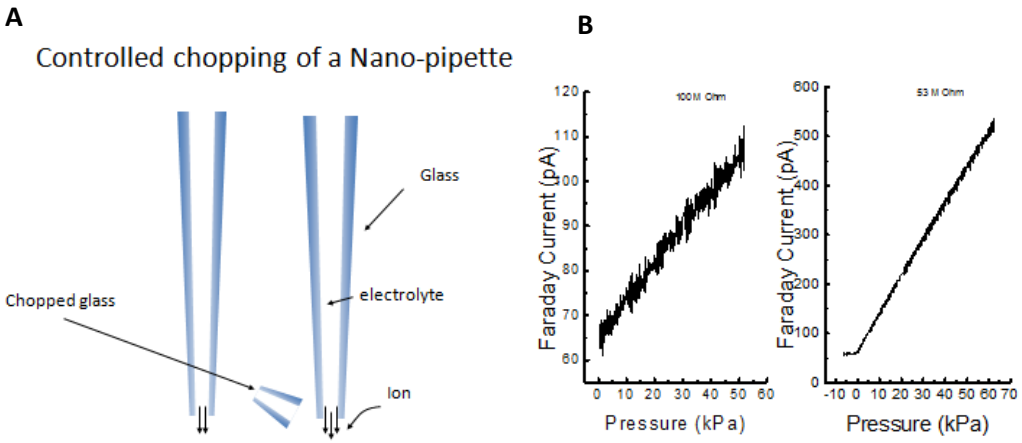

Figure 5.6. Single point molecule detection, by the disc substrate. **(A)** Schematic image of a chopped pipette. **(B)** A pressure ramp is applied to the SICM pipette to deliver the mediator to the substrate disc, with the pipette kept at a constant height from the disc surface. Experiments performed with two different sizes of pipette. The two recordings are measured from the sample point with probes of 100 MΩ and 53 MΩ sizes respectively.

The nano-pipette tip size can be increased by controlled chopping of the tip. For this the pipette is positioned in a clear area of a petri-dish. The fall rate of a nano- pipette of ~ 100 nm inner diameter, is increased to 500 nm/ms. The fast fall rate causes the pipette to overshoot and hit the dish. The resistance of the pipette is monitored to control the amount of chopping and the size of the pipette (Bhargava et al., 2013).

Inroder to be able to replicate how receptors sense local delivery of chemicals small electro-chemical nano-probes are needed. The electrochemical carbon nano-electrodes described in the previous chapter have been utilised as a sensor to detect local release of chemicals from a SICM nano-pipette.

The experimental set up for dosing to a nano-electrode

The carbon nano-electrode (described in the previous chapter) was placed in the dish with glue, and connected with a wire to the amplifier. The SICM probe containing 1 mM mediator dissolved in PBS was immersed to the bath solution (PBS) and positioned to approach the carbon nano-probe tip (Figure 5.7). The carbon nano-electrode was held at +500 mV vs the ground electrode and the SICM nano-pipette was biased at +200 mV to generate the ion current required for the topographical imaging experiment.

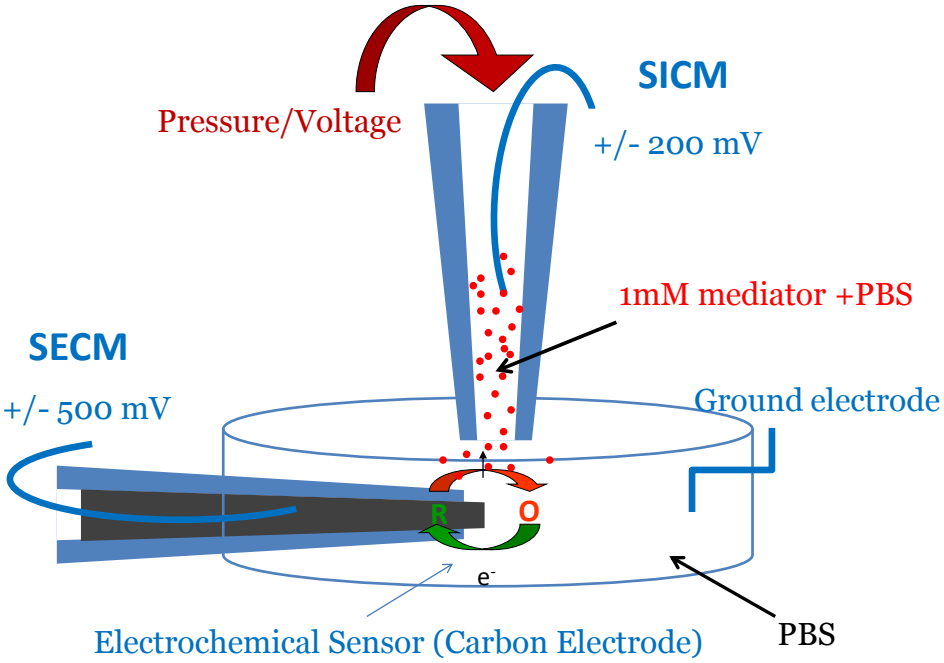

Figure 5.7. The principle of dosing. Schematic representation of chemical delivery to the electrochemical nano-sensor with the SICM nano-pipette.

Figure 5.8 illustrates how the distance between a nano-pipette probe tip, releasing chemicals, and the target structure, influences the concentration that the target structure experiences. The SICM nano-pipette, filled with 1 mM hexaammineruthenium (III) chloride in PBS, was immersed and positioned to approach the carbon electrode with distance feedback on. 20 kPa was subsequently applied over the nano-pipette and the mediator is delivered out of the pipette. Figure 5.8 shows how the Faraday current measured by the carbon electrode varies with changes in distance of the SICM nano-pipette from the carbon electrode.

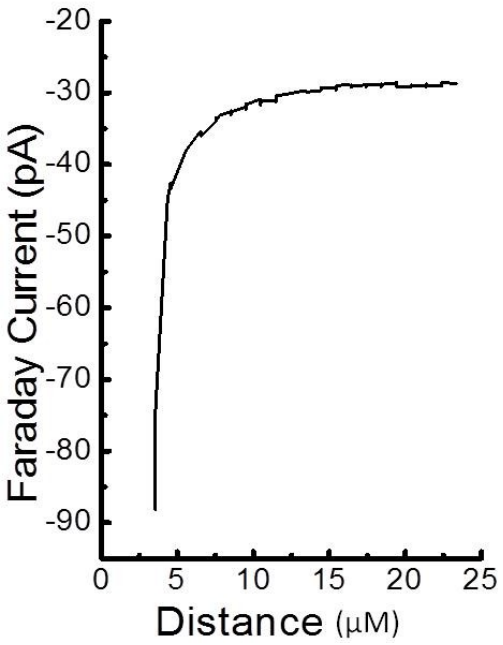

Figure 5.8. The relationship between distance and chemical delivery. Delivery of hexaammineruthenium (III) chloride from a 93 MΩ SICM nano-pipette (at 20 kPa pressure applied over the nano-pipette). The graph shows the faraday current measured by the electrochemically active carbon as a function of SICM nano-pipette tip distance to its surface.

Imaging an electrochemical nano-sensor

To demonstrate experimentally, how the released molecules from a nano-pipette is sensed at a point in space and how the concentration profile changes outside a nano-pipette, simultaneous electrochemical and topographical measurements were performed with the SICM and carbon nano-electrode, in a similar way to the substrate disc experiment. Chemical release of both charged and uncharged molecules from a nano-pipette were investigated. Experments were performd under a constant hydrostatic pressure applied to the pipette to map the spatial distribution of chemicals in relation to the tip of the carbon

nano-electrode sensor, where the maximum signal was detected over the tip of electrochemical probe and expected to drop in distance in accordance with Equation 3.

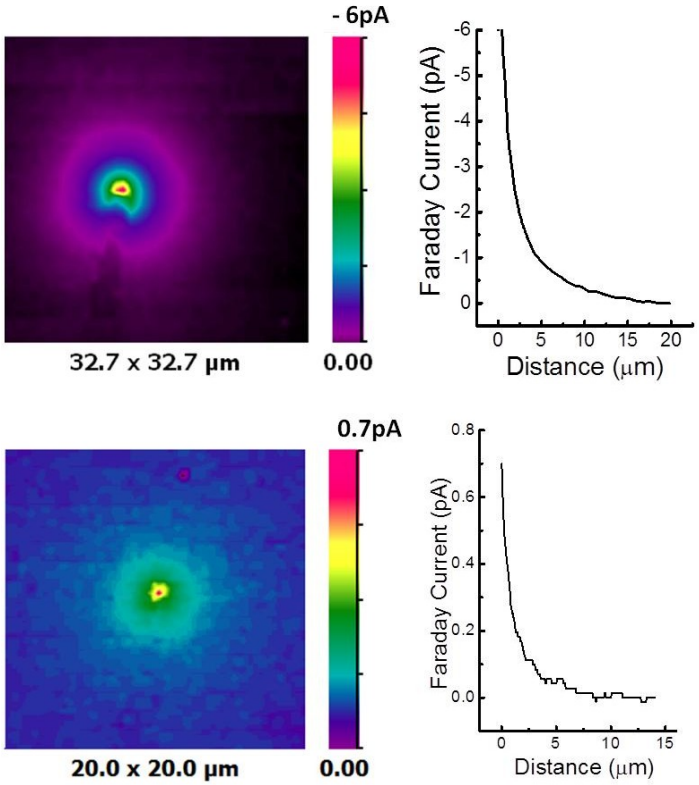

Figure 5.9. Measurement of local concentration changes produced by delivery from a pipette. (Top) picture shows the application of 1 mM hexaammineruthenium(III) chloride + PBS through a 137 MΩ scanning pipette, while measuring the topography of the SECM probe sensor immersed in PBS solution. The SICM electrode voltage was held at +200 mV. +10 kPa pressure was applied to the nano-pipette. The SECM electrode was held at -500 mV. (Bottom) picture is the application of 1 mM $FcCH_2OH$ + PBS through a 105 MΩ scanning pipette, while measuring the topography of the SECM probe sensor detecting the mediator release. The SICM electrode voltage was held at 200 mV. +20 kPa pressure was applied to the pipette. The SECM electrode was held at +500 mV. The line profiles of the Faraday current illustrates how the concentration drops with the distance away from the probe tip.

Comparison with the theoretical expressions

"The theoretical expressions mentioned earlier were compared with the experimental data recorded from local delivery of mediator via a SICM nano-pipette to the carbon nano-electrode. During scanning, a constant hydrostatic pressure of 20 kPa was applied to the SICM nano-pipette for the outward flow of electrochemical mediator from the nano-pipette opening. The Faraday current was also measured when having 1 mM ferrocenemethanol in the bath solution yielding a value of 16 pA to normalise the measured Faraday current obtained during dosing. When the pipette approached the surface at a set distance, the feedback system was switched off to keep the pipette at a stationary distance from the sample.

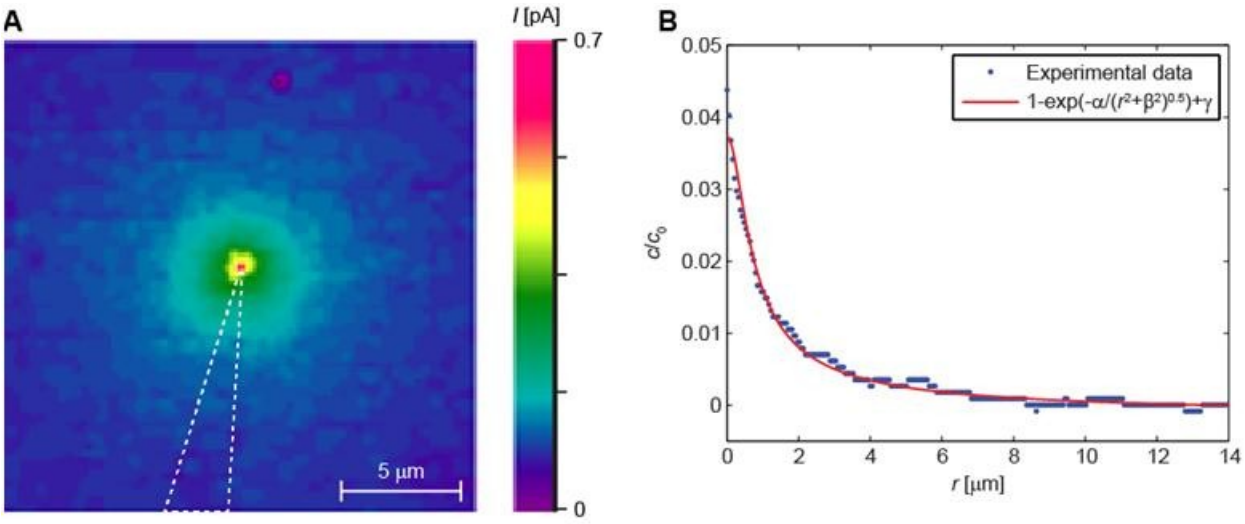

Figure 5.10. (A) Faraday current measured by a carbon nano-electrode when scanning the delivery pipette laterally above the electrode. The delivery was done by applying a pressure of 20 kPa and a voltage of 200 mV to the nano-pipette. The dashed line shows the outline of the electrode. **(B)** The line profile of the Faraday current converted into relative concentration of $FcCH_2OH$. The solid line is a curve fit to Equation 19.

The dashed lines in Figure 5.10 **(A)** outline the contour of the carbon nano-electrode as the topography of the nano-electrode was acquired simultaneously to the dosing of ferrocenemethanol (see also Figure 5.9). Figure 5.10 **(B)** shows the line profile of the Faraday current converted into relative concentration of $FcCH_2OH$. The solid line is a fit of the radial data to the expression:

$$c(r)/c_0 = 1 - \exp\left(-\alpha/\sqrt{r^2 + \beta^2}\right) + \gamma \qquad (19)$$

Where α, β and γ are parameters to be fitted resulting in: $\alpha = 0.020$ μm, $\beta = 0.50$ μm and $\gamma = -0.0015$. Equation 19 corresponds to the approximate expression in Equation 3 where $\alpha = Q_{tot}/4\pi D$, β is the *z*-offset of the scanning plane from the carbon electrode and γ an offset in the Faraday current. With $D = 8\times10^{-10}$ m^2/s for $FcCH_2OH$ (Miao et al., 2002), the fitted value of α gives $Q_{tot} = 2.0\times10^{-16}$ m^3/s. This value is of comparable magnitude to the value 1.8×10^{-16} m^3/s obtained from Eqs. 5 and 8 assuming: $R_0 = 50$ nm, $\theta = 3°$, $\eta = 1$ mPa s, $\mu_{ep} = 0$, $\mu_{eo} = 1.42\times10^{-8}$ m^2/V s, $\Delta p = 20$ kPa and $\Delta\Psi = 200$ mV Thus Equation 3 provides a reasonably good description of the radial concentration profile and the absolute number of molecules being delivered in this situation" Adapted with permission from (Babakinejad et al.) Copyright (2013) American Chemical Society.

Voltage vs pressure delivery

Pressure and voltage mediated applications are both useful methods to apply molecules from a nano-pipette tip. Voltage delivery seems to be a more robust method as it will allow rapid and accurate switching between applications. Moreover voltage mediated deliveryis

less dependent on the size of the nano-probe and permits use of much sharper probes for very localised application. Pressure application would be useful to compare the amount of molecule released for molecules of unknown charges, under pressure and voltage to be able to be able to select an appropriate value for voltage delivery.

Concentration at the tip

Double barrel probes (see Figure 5.11) have previously been used for simultaneous chemical delivery and voltammetry measurements in *in vitro* and *in vivo* experiments (Herr et al., 2008; Spaine and Baur, 2001; Hu et al., 2006).

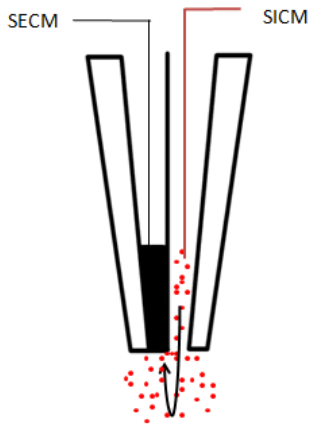

Figure 5.11. Cartoon illustration of a double barrel SICM-SECM nano-pipette. Red dots indicate chemical mediators released at the tip and being sensed by the carbon SECM sensor.

The development of multi-barrel nano-probes, have useful applications for chemical delivery and detection experiments. In double barrel experiments one barrel is coated with carbon to make it electrochemically active, while the other barrel is used for ICM imaging and chemical delivery. Each barrel is independently connected to the amplifier for recording of electrochemical and ion conductance signals. In order to avoid intra-barrel coupling between the two electrodes a minimal amount of electrolyte was added to the SICM barrel, to avoid contamination of signal with the electrochemical wire. The double barrel probe was then immersed into a dish containing PBS.

Application of a constant pressure to the SICM barrel generates a fix rate of mediator release at the tip of the nano-pipette. As a result a constant amount of Faraday current is expected to be sensed at the electrochemical section (the carbon-filled barrel).

The chhemical release at the tip of SICM nano-pipette was measured at different pressures with the SECM barrel for both charged (see Figure 5.12 **(A)**) and uncharged (see Figure 5.12**(B)**) molecules. Figure 5.12 illustrates experimentally, that charge of the molecules have an insignificant effect on pressure mediated delivery.

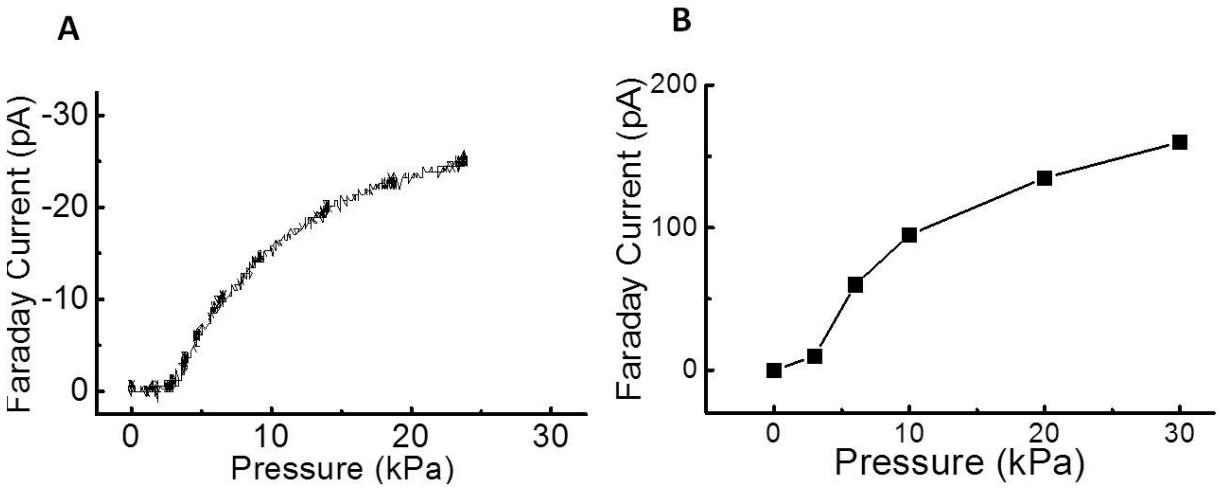

Figure 5.12. Pressure mediated local delivery. Application of 1 mM mediator **(A)** charged "1 mM hexxaammineruthenium (III) chloride" and **(B)** uncharged (1 mM ferrocenemethanol), from the pipette and detection of the electrochemical signal via the second barrel (carbon electrode), with the pipette immersed in PBS solution.

In order to demonstrate the effect of iontophoresis on chemical delivery, two different mediators were used; charged hexxaammineruthenium (III) chloride and uncharged ferrocenemethanol in PBS solution. Voltammetric measurements were performed at a constant pressure of 10 kPa, applied over the SICM nano-pipette in order to to drive out the molecule. The variable in this experiment was the voltage applied to the SICM probe to release charged or uncharged molecules. Figure 5.13 represents how difference in voltage is more effective in driving the charged molecules, compared to the uncharged redox mediator.

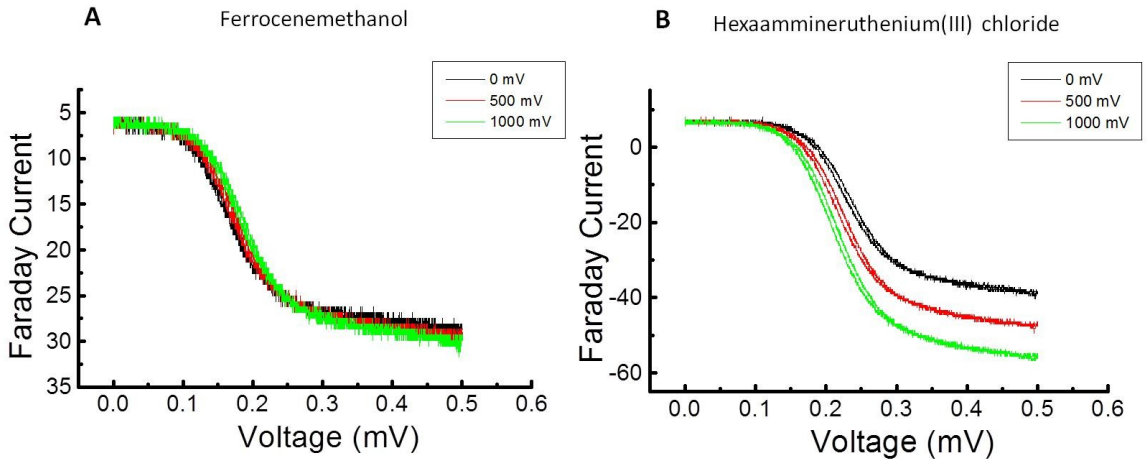

Figure 5.13. The effect of voltage on delivery of chemicals at the tip of a double barrel pipette. Voltamograms for the uncharged (Ferrocenemethanol) **(A)** and charged (Hexxaminеruthenium(III) Chloride) **(B)** mediator are given as a function of the voltage applied to the carbon electrode.

The double barrel nano-probes can be very powerful tool for chemical delivery and simultaneous measurement of the amount of substance released at the tip on cell membrane and also for intracellular recordings. It is also useful to monitor and detect any unanticipated blockage in intracellular or extracellular delivery of chemicals.

References

Ainla,A., Jansson,E.T., Stepanyants,N., Orwar,O., and Jesorka,A. (2010). A microfluidic pipette for single-cell pharmacology. Anal. Chem. *82*, 4529-4536.

Amatore,C., Arbault,S., Guille,M., and Lemaitre,F. (2008). Electrochemical monitoring of single cell secretion: Vesicular exocytosis and oxidative stress. Chemical Reviews *108*, 2585-2621.

Babakinejad,B., Jonsson,P., Lopez,C.A., Actis,P., Novak,P., Takahashi,Y., Shevchuk,A., Anand,U., Anand,P., Drews,A., Ferrer-Montiel,A., Klenerman,D., and Korchev,Y.E. (2013). Local delivery of molecules from a nanopipette for quantitative receptor mapping on live cells. Anal. Chem. *85*, 9333-9342.

Bard,A.J., Li,X., and Zhan,W. (2006). Chemically imaging living cells by scanning electrochemical microscopy. Biosensors & Bioelectronics *22*, 461-472.

Bhargava,A., Lin,X., Novak,P., Mehta,K., Korchev,Y., Delmar,M., and Gorelik,J. (2013). Super-resolution Scanning Patch Clamp Reveals Clustering of Functional Ion Channels in Adult Ventricular Myocyte. Circulation Research *112*, 1112-+.

Bruckbauer,A., James,P., Zhou,D., Yoon,J.W., Excell,D., Korchev,Y., Jones,R., and Klenerman,D. (2007). Nanopipette delivery of individual molecules to cellular compartments for single-molecule fluorescence tracking. Biophys. J. *93*, 3120-3131.

Bruckbauer,A., Zhou,D., Kang,D.J., Korchev,Y.E., Abell,C., and Klenerman,D. (2004). An addressable antibody nanoarray produced on a nanostructured surface. J. Am. Chem. Soc. *126*, 6508-6509.

Comstock,D.J., Elam,J.W., Pellin,M.J., and Hersam,M.C. (2010). Integrated Ultramicroelectrode-Nanopipet Probe for Concurrent Scanning Electrochemical Microscopy and Scanning Ion Conductance Microscopy. Analytical Chemistry *82*, 1270-1276.

Gonsalves,M., Barker,A.L., Macpherson,J.V., Unwin,P.R., O'Hare,D., and Winlove,C.P. (2000). Scanning electrochemical microscopy as a local probe of oxygen permeability in cartilage. Biophysical Journal *78*, 1578-1588.

Herr,N.R., Kile,B.M., Carelli,R.M., and Wightman,R. (2008). Electroosmotic Flow and Its Contribution to Iontophoretic Delivery. Analytical Chemistry *80*, 8635-8641.

Hu,H., Xie,S., Meng,X., Jing,P., Zhang,M., Shen,L., Zhu,Z., Li,M., Zhuang,Q., and Shao,Y. (2006). Fabrication and characterization of submicrometer- and nanometer-sized double-barrel pipets. Analytical Chemistry *78*, 7034-7039.

Isik,S. and Schuhmann,W. (2006). Detection of nitric oxide release from single cells by using constant-distance-mode scanning electrochemical microscopy. Angewandte Chemie-International Edition *45*, 7451-7454.

Jonsson,P., McColl,J., Clarke,R.W., Ostanin,V.P., Jonsson,B., and Klenerman,D. (2012). Hydrodynamic trapping of molecules in lipid bilayers. Proc. Natl. Acad. Sci. U. S. A *109*, 10328-10333.

Juncker,D., Schmid,H., and Delamarche,E. (2005). Multipurpose microfluidic probe. Nat. Mater. *4*, 622-628.

Kirby,B.J. and Hasselbrink,E.F., Jr. (2004). Zeta potential of microfluidic substrates: 1. Theory, experimental techniques, and effects on separations. Electrophoresis *25*, 187-202.

Kurulugama,R.T., Wipf,D.O., Takacs,S.A., Pongmayteegul,S., Garris,P.A., and Baur,J.E. (2005). Scanning electrochemical microscopy of model neurons: Constant distance imaging. Analytical Chemistry *77*, 1111-1117.

Kwak,J. and Bard,A.J. (1989). Scanning Electrochemical Microscopy - Theory of the Feedback Mode. Analytical Chemistry *61*, 1221-1227.

Lefrou,C. and Cornut,R. (2010). Analytical Expressions for Quantitative Scanning Electrochemical Microscopy (SECM). Chemphyschem *11*, 547-556.

Macpherson,J.V., Unwin,P.R., Hillier,A.C., and Bard,A.J. (1996). In-situ imaging of ionic crystal dissolution using an integrated electrochemical/AFM probe. Journal of the American Chemical Society *118*, 6445-6452.

McCreery,R.L. (2008). Advanced carbon electrode materials for molecular electrochemistry. Chemical Reviews *108*, 2646-2687.

Meister,A., Gabi,M., Behr,P., Studer,P., Voros,J., Niedermann,P., Bitterli,J., Polesel-Maris,J., Liley,M., Heinzelmann,H., and Zambelli,T. (2009). FluidFM: combining atomic force microscopy and nanofluidics in a universal liquid delivery system for single cell applications and beyond. Nano Lett. *9*, 2501-2507.

Miao,W.J., Ding,Z.F., and Bard,A.J. (2002). Solution viscosity effects on the heterogeneous electron transfer kinetics of ferrocenemethanol in dimethyl sulfoxide-water mixtures. Journal of Physical Chemistry B *106*, 1392-1398.

Mirkin,M.V., Fan,F.R.F., and Bard,A.J. (1992). Scanning Electrochemical Microscopy .13. Evaluation of the Tip Shapes of Nanometer Size Microelectrodes. Journal of Electroanalytical Chemistry *328*, 47-62.

Nogala,W., Velmurugan,J., and Mirkin,M.V. (2012). Atomic Force Microscopy of Electrochemical Nanoelectrodes. Analytical Chemistry *84*, 5192-5197.

Novak,P., Li,C., Shevchuk,A.I., Stepanyan,R., Caldwell,M., Hughes,S., Smart,T.G., Gorelik,J., Ostanin,V.P., Lab,M.J., Moss,G.W., Frolenkov,G.I., Klenerman,D., and Korchev,Y.E. (2009). Nanoscale live-cell imaging using hopping probe ion conductance microscopy. Nature Methods *6*, 279-281.

Piper,J.D., Li,C., Lo,C.J., Berry,R., Korchev,Y., Ying,L., and Klenerman,D. (2008). Characterization and application of controllable local chemical changes produced by reagent delivery from a nanopipet. Journal of the American Chemical Society *130*, 10386-10393.

Qasaimeh,M.A., Ricoult,S.G., and Juncker,D. (2013). Microfluidic probes for use in life sciences and medicine. Lab Chip *13*, 40-50.

Robinson,D.L., Hermans,A., Seipel,A.T., and Wightman,R. (2008). Monitoring rapid chemical communication in the brain. Chemical Reviews *108*, 2554-2584.

Rodolfa,K.T., Bruckbauer,A., Zhou,D., Korchev,Y.E., and Klenerman,D. (2005). Two-component graded deposition of biomolecules with a double-barreled nanopipette. Angew. Chem. Int. Ed Engl. *44*, 6854-6859.

Sanchez,D., Johnson,N., Li,C., Novak,P., Rheinlaender,J., Zhang,Y., Anand,U., Anand,P., Gorelik,J., Frolenkov,G.I., Benham,C., Lab,M., Ostanin,V.P., Schaffer,T.E., Klenerman,D., and Korchev,Y.E. (2008). Noncontact measurement of the local mechanical properties of living cells using pressure applied via a pipette. Biophys. J. *95*, 3017-3027.

Shevchuk,A.I., Frolenkov,G.I., Sanchez,D., James,P.S., Freedman,N., Lab,M.J., Jones,R., Klenerman,D., and Korchev,Y.E. (2006). Imaging proteins in membranes of living cells by high-resolution scanning ion conductance microscopy. Angew. Chem. Int. Ed Engl. *45*, 2212-2216.

Shevchuk,A.I., Novak,P., Takahashi,Y., Clarke,R., Miragoli,M., Babakinejad,B., Gorelik,J., Korchev,Y.E., and Klenerman,D. (2011). Realizing the biological and biomedical potential of nanoscale imaging using a pipette probe. Nanomedicine. (Lond) *6*, 565-575.

Shin,W. and Gillis,K.D. (2006). Measurement of changes in membrane surface morphology associated with exocytosis using scanning ion conductance microscopy. Biophysical Journal *91*, L63-L65.

Simon,D.T., Kurup,S., Larsson,K.C., Hori,R., Tybrandt,K., Goiny,M., Jager,E.W., Berggren,M., Canlon,B., and Richter-Dahlfors,A. (2009). Organic electronics for precise delivery of neurotransmitters to modulate mammalian sensory function. Nat. Mater. *8*, 742-746.

Spaine,T.W. and Baur,J.E. (2001). A positionable microcell for electrochemistry and scanning electrochemical microscopy in subnanoliter volumes. Analytical Chemistry *73*, 930-938.

Takahashi,Y., Shevchuk,A.I., Novak,P., Babakinejad,B., Macpherson,J., Unwin,P.R., Shiku,H., Gorelik,J., Klenerman,D., Korchev,Y.E., and Matsue,T. (2012). Topographical and electrochemical nanoscale imaging of living cells using voltage-switching mode scanning electrochemical microscopy. Proc. Natl. Acad. Sci. U. S. A *109*, 11540-11545.

Takahashi,Y., Shevchuk,A.I., Novak,P., Murakami,Y., Shiku,H., Korchev,Y.E., and Matsue,T. (2010). Simultaneous noncontact topography and electrochemical imaging by SECM/SICM featuring ion current feedback regulation. J. Am. Chem. Soc. *132*, 10118-10126.

Takahashi,Y., Shevchuk,A.I., Novak,P., Zhang,Y., Ebejer,N., Macpherson,J.V., Unwin,P.R., Pollard,A.J., Roy,D., Clifford,C.A., Shiku,H., Matsue,T., Klenerman,D., and Korchev,Y.E. (2011). Multifunctional nanoprobes for nanoscale chemical imaging and localized chemical delivery at surfaces and interfaces. Angew. Chem. Int. Ed Engl. *50*, 9638-9642.

Takahashi,Y., Shiku,H., Murata,T., Yasukawa,T., and Matsue,T. (2009). Transfected Single-Cell Imaging by Scanning Electrochemical Optical Microscopy with Shear Force Feedback Regulation. Analytical Chemistry *81*, 9674-9681.

Westerink,R. and Ewing,A. (2008). The PC12 cell as model for neurosecretion. Acta Physiologica *192*, 273-285.

Wong,D.K.Y. and Xu,L.Y.F. (1995). Voltammetric Studies of Carbon Disk Electrodes with Submicrometer-Sized Structural Diameters. Analytical Chemistry *67*, 4086-4090.

Ying,L., Bruckbauer,A., Rothery,A.M., Korchev,Y.E., and Klenerman,D. (2002). Programmable delivery of DNA through a nanopipet. Anal. Chem. *74*, 1380-1385.

Ying,L., Bruckbauer,A., Zhou,D., Gorelik,J., Shevchuk,A., Lab,M., Korchev,Y., and Klenerman,D. (2005). The scanned nanopipette: a new tool for high resolution bioimaging and controlled deposition of biomolecules. Phys. Chem. Chem. Phys. *7*, 2859-2866.

Ying,L., White,S.S., Bruckbauer,A., Meadows,L., Korchev,Y.E., and Klenerman,D. (2004). Frequency and voltage dependence of the dielectrophoretic trapping of short lengths of DNA and dCTP in a nanopipette. Biophys. J. *86*, 1018-1027.

CHAPTER 6

Application to cells

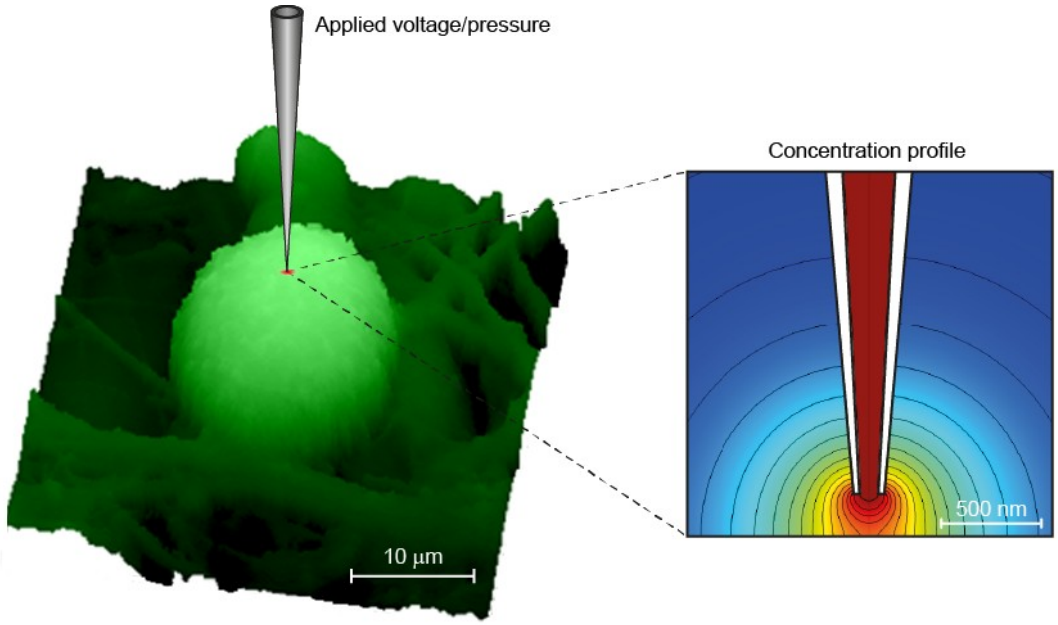

* Topographical image of a DRG neuron and a concentration profile of reagents being delivered through a nano-pipette.

In this chapter I describe the quantitative delivery of molecules from a 100 nm nano-pipette. In particular a capsaicin-filled nano-pipette to trigger capsaicin-sensitive TRPV1 receptors in sensory neurons and transfected cells as well as the experimental protocols for multi-point delivery of capsaicin to different regions of neurons, is discussed.

Introduction

I have applied the nano-pipette dosing platform to stimulate TRPV1 transfected HEK cells and dorsal root ganglia (DRG) sensory neurons with capsaicin, an activator of Transient Receptor Potential Vanilloid subfamily member 1 (TRPV1) channels. The function of TRPV1 channels is to sense and regulate temperature but they are also used as a model system to study pain transduction since TRPV1 channels are involed in noxious heat detection and pain sensation as well as pathophysiological condictions relatd to inflamatory or neuropathic pain (Caterina et al., 1997; Tominaga et al., 1998, Szallasi Arpad et al., 2007).

Activation of TRPV1 channels lead to the influx of cations into the cell (Caterina et al., 1997), that can be monitored by measuring changes in the fluorescence of the calcium-sensitive dye Fluo-4 (Camprubi-Robles et al., 2009). Cells were loaded with calcium sensitive dye. More channel opening leads to a larger influx of calcium and therefore a higher fluorescence signal, which is used as an indirect method to measure TRPV1 channel opening.

Different magnitudes of voltage or pressure mediated delivery of capsaicin are compared, to illustrate the triggering of TRPV1 channels in transfected HEK cells. Using Equation 9 in Chapter 5 it is possible to compare the cellular response to dosing with pressure and voltage. To illustrate this capsaicin was applied to TRPV1 transfected HEK cells using either pressure or voltage. Figure 6.2 shows a representative response of a cell (after testing tens of different cells) to the dosing of capsaicin using either pressure (see Figure 6.1 **(A)**) or voltage (see Figure 6.1 **(B)**). The distance between the tip of the pipette and the cell surface was 300 nm in both cases.

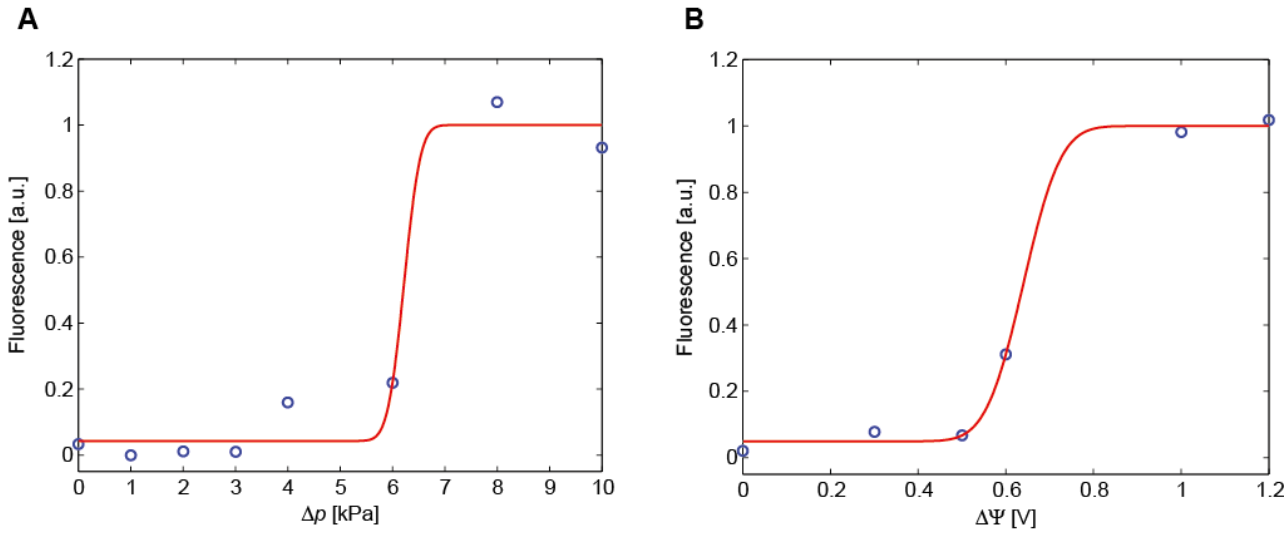

Figure 6.1. Representative fluorescence response when dosing capsaicin to TRPV1 transfected HEK cells loaded with the calcium sensitive dye Fluo-4 using **(A)** pressure and **(B)** voltage. The solid lines are curve fits of the data to an error function.

The solid lines in Figure 6.1 are curve fits of the data to an error function yielding that the applied pressure and voltage at which the fluorescence response reaches half the maximum value is 6.2 kPa and 0.64 V, respectively. Inserting R_0 = 50 nm, μ_{ep} = 0, $\mu_{eo} = 1.42\times10^{-8}$ $m^2/V\ s$ and $\eta = 1$ mPa s into Equation 9 in Chapter 5 gives that a pressure of $\Delta p = 6.2$ kPa would correspond to an applied voltage of $\Delta\Psi = 0.42$ V, comparable in magnitude to the experimental value obtained in Figure 6.1 (B). How the fluorescence increases from zero to a saturated level is not known and very complicated. The data is fitted in to an error function to emphasise the transition from a low to a saturated response.

Local delivery of molecules to a DRG cell body

"The delivery system was next tested in a biological pain model by studying the response of DRG neurons from neonatal rats upon local stimulation with capsaicin (see Figure 6.2). In these cultures, around 60% of neurons express the TRPV1 channels. Capsaicin was delivered under the application of a positive voltage to the nano-pipette, and changes in calcium concentration were recorded integrating the fluorescent signal over the cell body. In active cells (cells expressing TRPV1 channels), the response to different doses of capsaicin delivered from a nano-pipette was measured by plotting the slope of the fluorescence increase resulting from the opening of the channels (see Figure 6.2 **(B1)**).

The opening probability of TRPV1 channels depends on the concentration of capsaicin, given that the higher the capsaicin concentration, the higher the opening probability. However, there is a threshold concentration below which the channels remain essentially closed, and a maximum concentration from which all the channels are essentially open (Studer and McNaughton, 2010). Therefore, a typical dose-response curve has a sigmoidal shape, similar to the one that is shown in Figure 6.2 **(B2)** (Ralevic et al., 2003). In contrast to the widely used bath-dosing experiments, in the experiments being conducted here it has to be taken into account that as the applied voltage increases not only the amount of capsaicin being delivered increase, but also the area being exposed to the molecules. This means that increasing the voltage not only give rise to a higher probability of channel opening below the tip of the pipette (for below-saturation concentrations) but also to an increase in the number of channels that have access to an over-threshold capsaicin concentration.

Using Equation 5 and 11 in Chapter 5 it is possible to estimate the concentration of capsaicin delivered at different parts of the cell surface. As an illustration of this the concentration profile when a voltage of 0.44 V is applied over the pipette was investigated (the value of 0.44 V corresponds to the voltage in 6.2 **(B2)** where the fitted curve has reached 90% of its maximum value). With R_0 = 50 nm, $\theta = 3°$, η = 1 mPa s, μ_{ep} = 0 (assuming that capsaicin is uncharged at the pH used in the experiments (McLatchie and Bevan, 2001), μ_{eo} = 1.42×10^{-8} m^2/V s and $\Delta\Psi$ = 0.44 V inserted into Equation 5 in Chapter 5, a value of $Q_{tot,\Delta\Psi}$ = 5.14×10^{-17} m^3/s is obtained. To describe the delivery of capsaicin to different positions on the cell body, we modeled the DRG neuron as a hemisphere with radius R_{cell} = 10 μm. The concentration on different positions on the surface is then calculated using Equation 11 in Chapter 5 with $r = R_{cell}\phi$, where ϕ is the angle from the top of the sphere. With Q_{tot} = 5.14×10^{-17} m^3/s, D = 2×10^{10} m^2/s (Lambert and Sum, 2006), R_{cell} = 10 μm and h = 300 nm this gives the concentration curve shown in Figure 6.2 **(C)**. To convert from angle, ϕ, to fractional surface area, $A/A_{hemisphere}$, Equation 1 was used:

$$A/A_{hemisphere} = 1 - \cos\phi \qquad (1)$$

It can be observed from figure 6.2 **(C)** that the concentration of capsaicin is highest at the top of the hemisphere (just below the pipette) where it is 26 μM (not shown in the figure for scaling reasons) and is lowest at the base of the hemisphere where it is 520 nM. The TRPV1 channels will start to open at the top of the cell already at much lower voltages than 0.44 V, whereas the channels at the base of the cell open at higher voltages due to the extended distance to the pipette. Since the curve in Figure 6.2 **(B2)**, is the integrated response from the entire cell, the value of 520 nM can be seen as an estimate of the

concentration of capsaicin needed to saturate the response of a single TRPV1 channel in this cell. This value is comparable in magnitude to the saturation concentration of capsaicin obtained previously by others (Ralevic et al., 2003; Biro et al., 1998; Wood et al., 1988). In the future, further adaptations of the model including for example opening probability of TRPV1 channels at different capsaicin concentration and intracellular diffusion might be used in order to obtain more precise values of the saturation concentration.

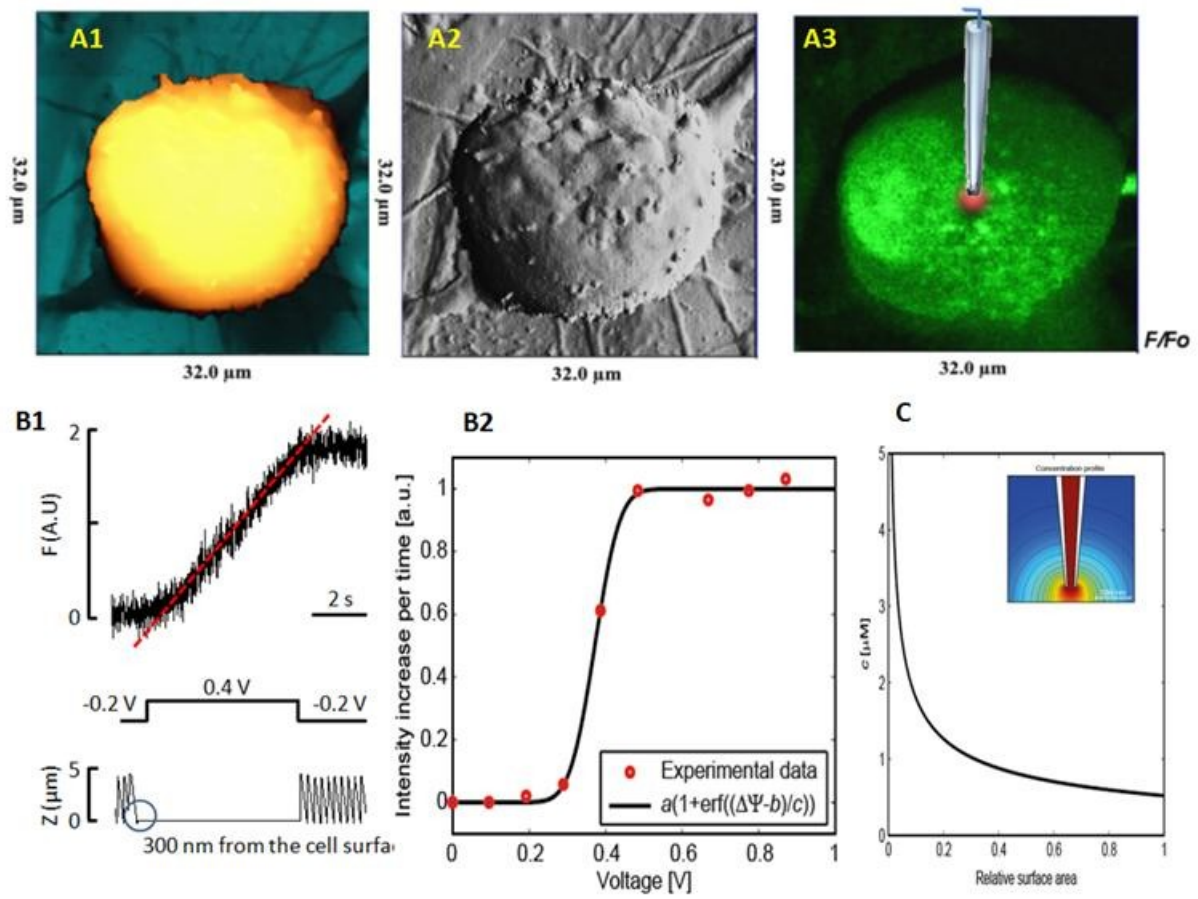

Figure 6.2. Capsaicin delivery to a DRG neuron. **(A1)** Topographical image of a DRG acquired with SICM. **(A2)** Image showing the derivative of the topography and **(A3)** the fluorescence image of the cell body. **(B1)** Representative recording from local stimulation with capsaicin of a DRG neuron. The bottom trace shows the vertical position of the nano-pipette; middle trace, the applied voltage via a nano-pipette and the top trace is the integrated fluorescence response from the cell body. **(B2)** The fluorescence response at different delivery voltages when dosing capsaicin to a cell loaded with the calcium sensitive dye Fluo4 AM. The solid line is a curve fit of the data to an error function. Error function is used to emphasise the transition from a low fluorescence value to a saturated response. **(C)** Theoretical concentration profile on the surface of a hemisphere with radius 10 µm at $\Delta\Psi$ = 0.44 V, showing the fraction of the surface where the concentration is above the concentration given on the y-axis.

It should be taken into consideration that the concentration generated locally can be very high but it drops rapidly away from the tip of the nano-pipette. Activation of only a few receptors and opening of a few channels, do not create enough calcium influx, for a measurable fluorescence signal. Therefore more channels need to open up in a wider area. For this a higher concentration in the nano-pipette is required or by applying a higher voltage or pressure. Since there are limitations in the system for the application of higher pressure/voltage, the concentration in the nano-pipette has been increased. From the discussion about the delivery to the cell body we actually estimate the concentration to saturate a TRPV1 channel to ~500 nM.

Local delivery of molecules to the surface of cellular structures with nano-meter resolution, makes it theoretically possibly to do functional mapping of individual ion channels and receptors in cells. Since delivery with the SICM system is localised and fast, the impact on the cells is minimised and this technique can therefore potentially allow multiple application on the same region to achieve multi dose-response curves from sub-cellular structures" Adapted with permission from (Babakinejad et al.) Copyright (2013) American Chemical Society.

Multi-point delivery with Scanning Surface Confocal Microscopy

The SICM imaging software has been modified to incorporate the multi dosing application. The time it takes to finish the movement from one point to another in the multipoint delivery depends on the distance between the two points. The speed of movement in x-y plane was set to be limited to 100 nm/ms. The reason for this speed limit is prevent any sliding of the Petri-dish. That means movement between two points 100 micrometers apart

will take 1 second. So in most of cases on a 100X100 micron frame it should take less than a second for the pipette to reach the next delivery point. For multi delivery experiments, the scanning surface confocal system is used by aligning the laser light to the tip of the nano-pipette (Described in Chapter 2 & 3). A topographical and fluorescence image is acquired simultaneously. With the help of the SICM software, several points are selected from a 100x100 μM frame and the duration of delivery, distance of pipette from the surface at the time of delivery and magnitude of voltage application is specified.

The application starts by x-y piezo (Sample holder) moving the sample to each pre-specified targets from the acquired image, to position the nano-pipette to approach the specified position on the neurite, under the feedback control. This procedure was implemented in a standard hopping probe configuration to prevent any mechanical interaction with cell structures.

After each delivery, the voltage is switched back to its prior setting, and the pipette withdraws from the surface in hopping mode. The sample holder then moves the dish to the next delivery point.

Different neuronal nano-structures are expected to have different distribution of channels (Nusser, 2012) and inputs from other related axonal and dendritic branches, can affect the shape of the calcium entry. Figure 6.3 **(A)** shows the topography of a DRG neuron and 3B shows the fluorescence response after voltage mediated capsaicin delivery to 4 different points. The rate and shape of calcium response in the different regions is heterogeneous. Figure 6.3 **(C2)**, **(3)** and **(4)** show fluorescence responses from three positions twice (red and black curves) to show the reproducibility. In these experiments the application lasted 6 seconds.

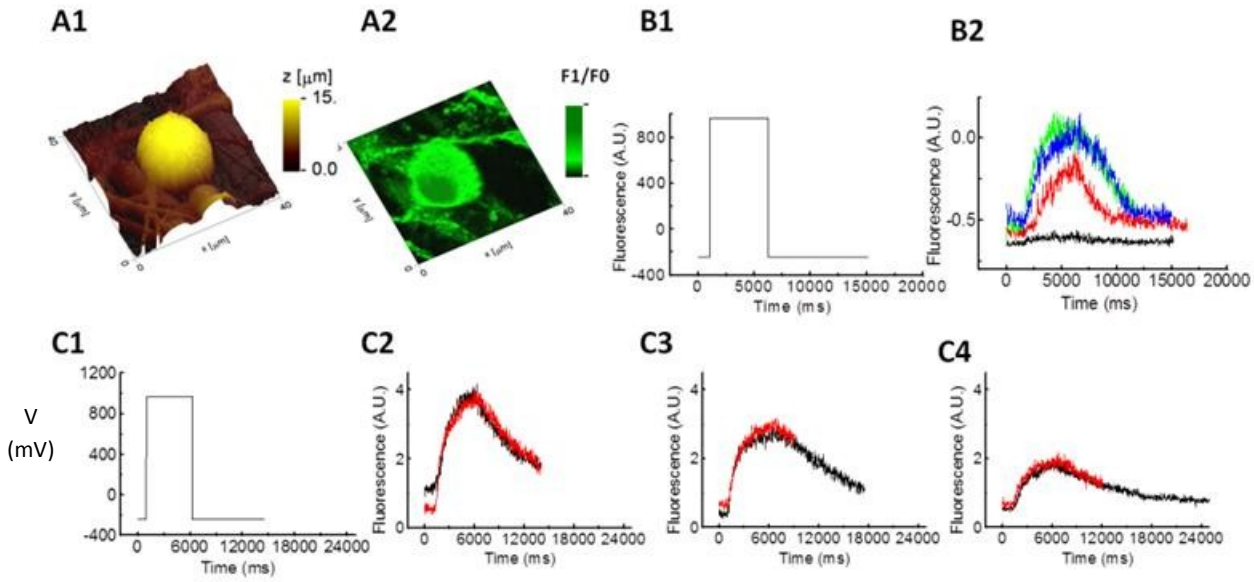

Figure 6.3. Targeting neurites with a nano-pipette. **(A1)** Topographical image of a DRG neuron. **(A2)** Surface confocal fluorescence image of DRG. **(B1)** & **(B2)** voltage delivery of capsaicin and responses from 4 different points respectively. **(C1)** voltage delivery of capsaicin. **(C2)**, **(C3)** & **(C4)**. Delivery of capsaicin to three different points twice.

In order to demonstrate the reproducibility and possible variation in calcium entry after repeated application to the same point over the course of experiments capsaicin has been delivered to the same location at the same voltage several times and the rate of fluorescence increase was recorded (see Figure 6.4). The response of cells were reproducible with relatively small variability and these responses were blocked by using a ruthenium blocker.

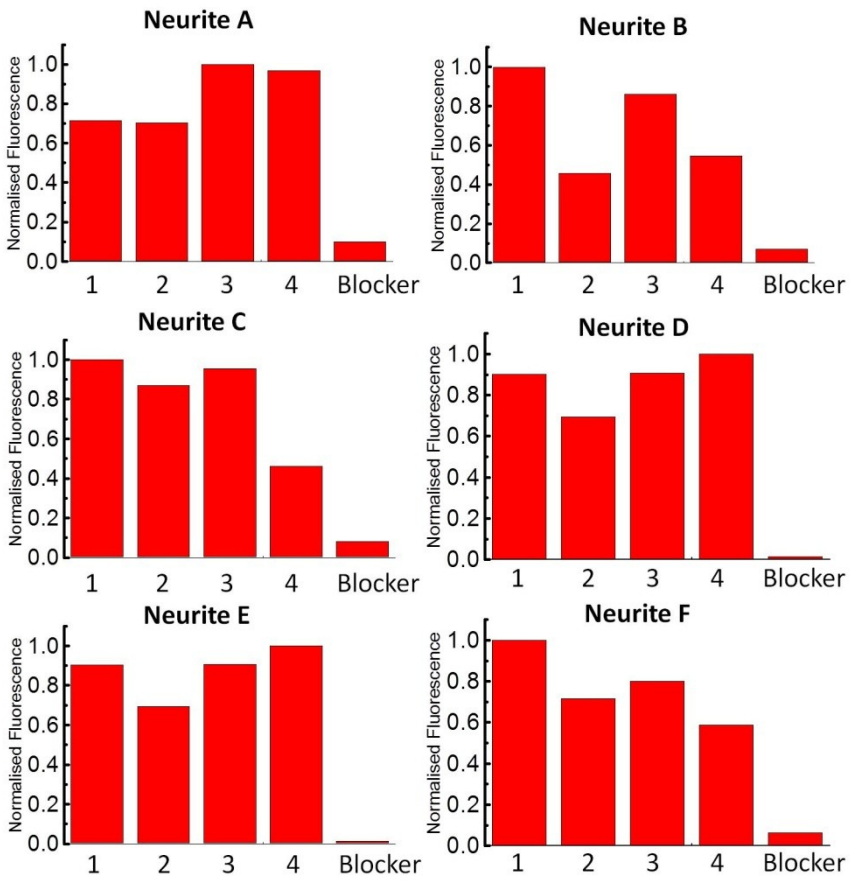

Figure 6.4. Multiple delivery of capsaicin to the same regions. +800 mV was applied to the SICM nano-pipette, on 6 neuronal structures over time (Neurites A-F), in a sequence. Red bars show normalised fluorescence of the rate of calcium entry over 1 second of application. 10 mM ruthenium red blocker was added to the bath before the last application and fluorescence measurement. The X axis shows the number of application to the same location.

By taking advantage of the rate of entry, it is possible to optimise the delivery protocol to keep the delivery duration to a minimum level to prevent desensitisation of receptors, and also overloading of the structure.

“To illustrate this the experimental protocol was designed and optimised to allow sequential drug delivery from point to point, in a way to give enough time for every structure to recover, before repeating the stimulation on the same point. Neurites from topographical and fluorescence image of 100 micron region were selected and targeted. Figure 6.5 shows normalised recordings from 4 different points within a 100 µM scanning area, at different voltages (amount of capsaicin delivered). The increase in fluorescence has been measured and plotted. The reliability and reproducibility of point delivery is demonstrated. From the graphs it is clear that the signal is saturated at around 600-700 mV of voltage indicating that the activation of most TRPV1 channels are within that voltage range. Figure 6.5**(B)** shows the full trace of multi-dosing for several points at different voltages.

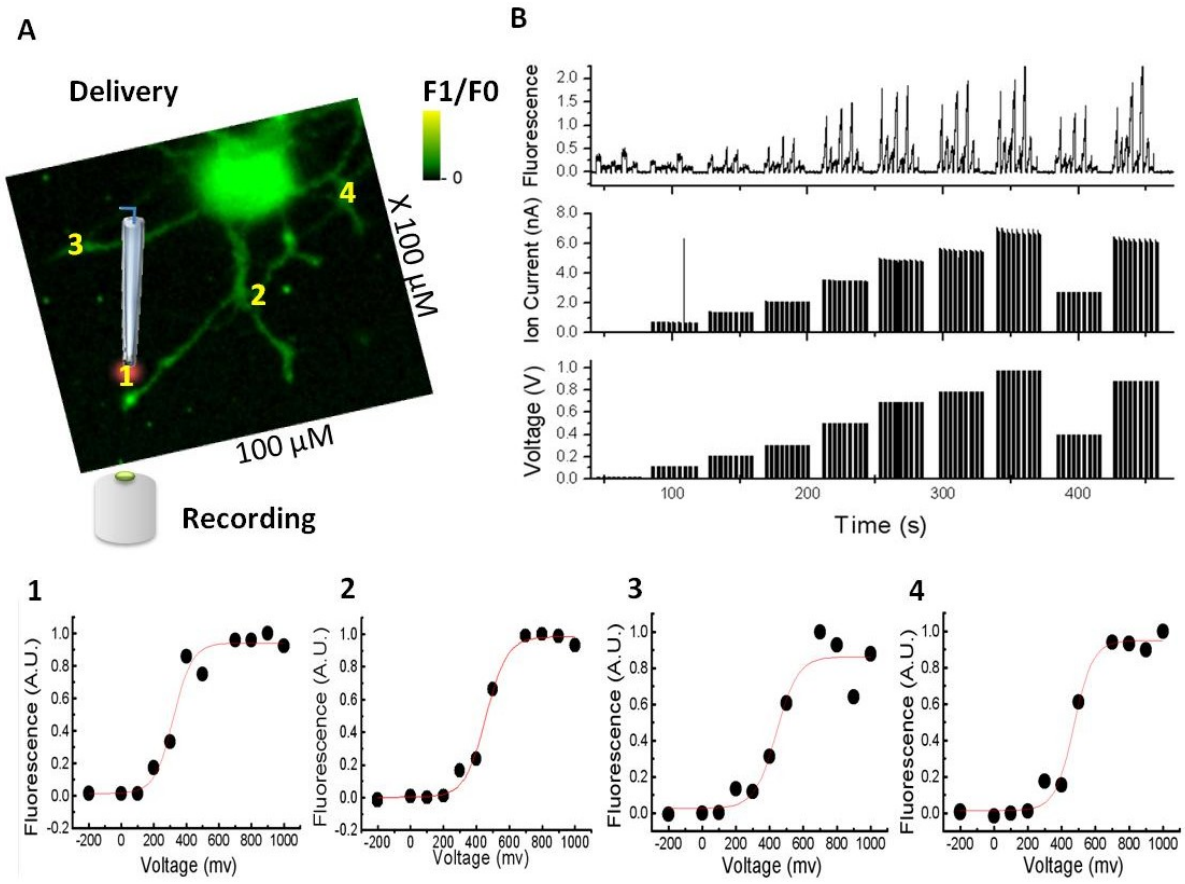

Figure 6.5. Local delivery of capsaicin to the neurites of a sensory neuron with voltage. **(A)** schematic of local delivery of chemicals to DRG neurites and simultaneous fluorescence recording. **(B)** High throughput multi-point delivery of capsaicin and simultaneous recording of fluorescence signal at different voltages. **1**, **2**, **3** and **4** show the rate of fluorescence increase as a function of voltage from 4 different points.

Figure 6.5 **(B)** demonstrates how the data was collected from multiple points using multiple different parameters in a single experiment. The histogram shows the full trace of voltage, ion current and fluorescence response." Adapted with permission from (Babakinejad et al.) Copyright (2013) American Chemical Society.

Figure 6.6 represents zoomed in sections of a large set of data, to illustrate the relationship between current, voltage and fluorescence responses on different neuritis. The histograms represent multi-point capsaicin delivery applied sequentially to 8 different points. Different voltages have been applied to the nano-pipette in order to apply capsaicin to eight dendritic structures. The dosing sequence has been kept constant throughout the experiment. The rate of entry could be calculated from the slope of fluorescence response (top panels of each figure), indicating the rate of increase of the response. DC current is recorded to ensure there is no blockage or disturbance in the delivery (Voltage and Ion-current have a linear relationship). At lower voltages/currents the delivery of chemical is expected to be lower which leads to reduced fluorescence response, and faster recovery of receptors.

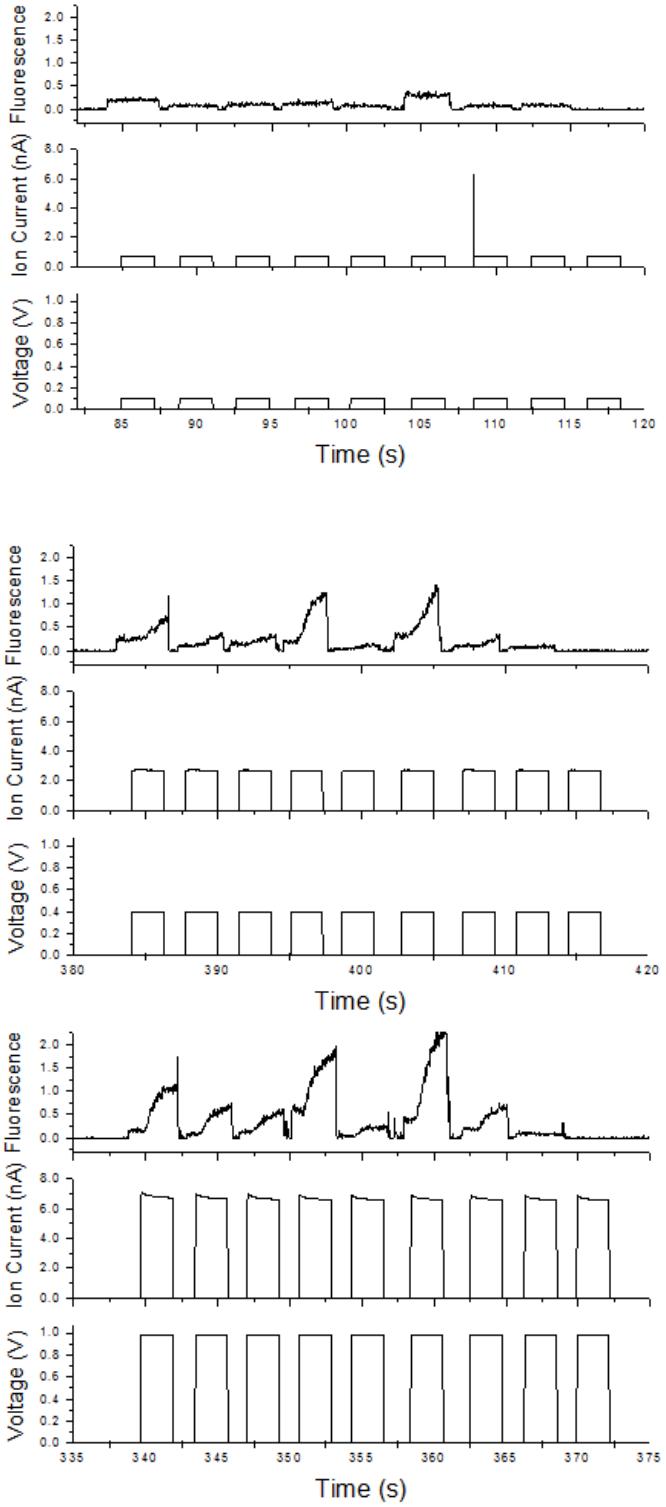

Figure 6.6. Multi-point delivery of capsaicin via a nano-pipette at different voltages to the neuronal structures with simultaneous recording of the fluorescence responses. Histograms show voltage delivery of capsaicin to 8 different neuronal structures (Last point is on the coverslip), and recording the fluorescence response under the pipette at each point. The -

same process was repeated at 3 different voltages. Top trace of each histogram is the fluorescence response. The ion current is recorded to ensure there was no blockage in the pipette and the bottom shows the amount of voltage/chemical delivery.

Hundreds of dose response curves from the same sample can be obtained using this procedure. This method of application is significant as it increases the yield of experiments dramatically. It would also allow to study neuronal plasticity, and the effect of agonist and antagonist on the same structure over time that is not generally feasible with global drug application methods.

Considerations

In order to minimise leakage and thereby affecting down-stream structures, a balance between duration of application and applied concentration should be considered for every type of cell and receptor under investigation. Spontaneous activities and signal fluctuations in processes and signals sent by nearby neurons are factors that can affect recordings. Keeping external factors such as the electrode condition, dilution factor, pH, and distance constant as well as by monitoring the ion current to ensure open passage for chemical delivery, variability in application can be kept to a minimum. Very high concentrations of a drug at the tip of the pipette could desensitise ion channels. It should be noted that spontaneous responses can occur at any time that can affect the base line fluorescence value. Current artefacts, electro-osmotic effects and iontophoresis of ions in solution other than the drug should also be taken into account.

References

Babakinejad,B., Jonsson,P., Lopez,C.A., Actis,P., Novak,P., Takahashi,Y., Shevchuk,A., Anand,U., Anand,P., Drews,A., Ferrer-Montiel,A., Klenerman,D., and Korchev,Y.E. (2013). Local delivery of molecules from a nanopipette for quantitative receptor mapping on live cells. Anal. Chem. *85*, 9333-9342.

Bíró ,T., Brodie,C., Modarres,S., Lewin,N.E., ACS ,P., and Blumberg,P.M. (1998). Specific vanilloid responses in C6 rat glioma cells. Molecular Brain Research *56*, 89-98.

Camprubi-Robles,M., Planells-Cases,R., and Ferrer-Montiel,A. (2009). Differential contribution of SNARE-dependent exocytosis to inflammatory potentiation of TRPV1 in nociceptors. FASEB J. *23*, 3722-3733.

Caterina,M.J., Schumacher,M.A., Tominaga,M., Rosen,T.A., Levine,J.D., and Julius,D. (1997). The capsaicin receptor: a heat-activated ion channel in the pain pathway. Nature *389*, 816-824.

Lambert,J.W. and Sum,A.K. (2006). Molecular dynamics study of the properties of capsaicin in an 1-octanol/water system. J. Phys. Chem. B *110*, 2351-2357.

McLatchie,L.M. and Bevan,S. (2001). The effects of pH on the interaction between capsaicin and the vanilloid receptor in rat dorsal root ganglia neurons. Br. J. Pharmacol. *132*, 899-908.

Nusser,Z. (2012). Differential subcellular distribution of ion channels and the diversity of neuronal function. Current Opinion in Neurobiology *22*, 366-371.

Ralevic,V., Jerman,J.C., Brough,S.J., Davis,J.B., Egerton,J., and Smart,D. (2003). Pharmacology of vanilloids at recombinant and endogenous rat vanilloid receptors. Biochemical Pharmacology *65*, 143-151.

Shevchuk,A.I., Novak,P., Takahashi,Y., Clarke,R., Miragoli,M., Babakinejad,B., Gorelik,J., Korchev,Y.E., and Klenerman,D. (2011). Realizing the biological and biomedical potential of nanoscale imaging using a pipette probe. Nanomedicine. (Lond) *6*, 565-575.

Studer,M. and McNaughton,P.A. (2010). Modulation of single-channel properties of TRPV1 by phosphorylation. J. Physiol *588*, 3743-3756.

Szallasi Arpad, Daniel N.Cortrigt, Charles A.Blum, and Samer R.Eid (2007). The vanilloid receptor TRPV1: 10 years from channel cloning to antagonist proof-of-concept. Nat Rev Drug Discov *6*, 357-372.

Tominaga,M., Caterina,M.J., Malmberg,A.B., Rosen,T.A., Gilbert,H., Skinner,K., Raumann,B.E., Basbaum,A.I., and Julius,D. (1998). The Cloned Capsaicin Receptor Integrates Multiple Pain-Producing Stimuli. Neuron *21*, 531-543.

Wood,J.N., Winter,J., James,I.F., Rang,H.P., Yeats,J., and Bevan,S. (1988). Capsaicin-induced ion fluxes in dorsal root ganglion cells in culture. J. Neurosci. *8*, 3208-3220.

CHAPTER 7

Other experiments

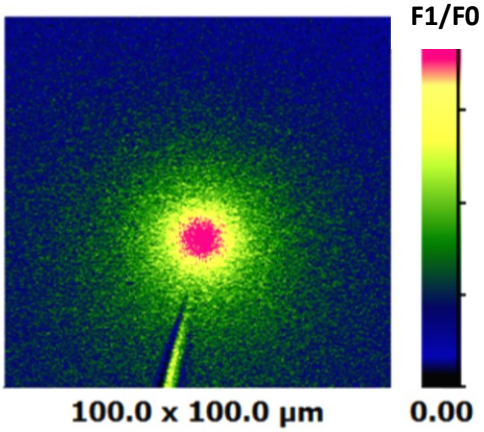

*Image of Calcium release from the SICM nano-pipette, detected with fluo-4 in the bath.

In this chapter I will show the injection of a single neuron with fluorescence dye. I will discuss the sensitivity of ion current passed through the nano-pipette and faraday current measured by an electrochemical nano-electrode to changes in temperature. I will also discuss the development of carbon nano-heating element and its potential in the study of heat sensitive receptors. Local depolarization of dendritic structure with a voltage pulse will also be demonstrated.

Micro-injection of a neuron

Neuronal networks in tissue culture dishes are complex and elaborated. The ability to label single neurons with fluorescence dye would be advantageous and makes it possible to distinguish specific neuronal structures from the unlabeled ones and to decipher specific structural and functional relationship.

The goal of my thesis was to develop multifunctional probes for neuroscience, and here I show that nano-pipette can be deployed as well as a nano-injector (Adam Seger et al., 2012). The SICM nano-pipette was filled with cell impermeable Alexa Fluor 488 dye, before mounting the pipette on the pressure holder, and approach to the DRG cell body using feedback distance system. Next, the pipette was moved down manually to penetrate into the cell membrane for about 5 microns. Between 2-3 kPa pressure was then applied to deliver the dye to the cell body. Injection of the dye to the cell body was immediately visible with the camera. Figure 7.1 show different frames, taken over time to illustrate how the fluorescence dye is distribute across the neuritis of the injected neuron. With this method different neurons can be labelled with different dyes, and their processes can be followed fluorescently to identify connects and branches.

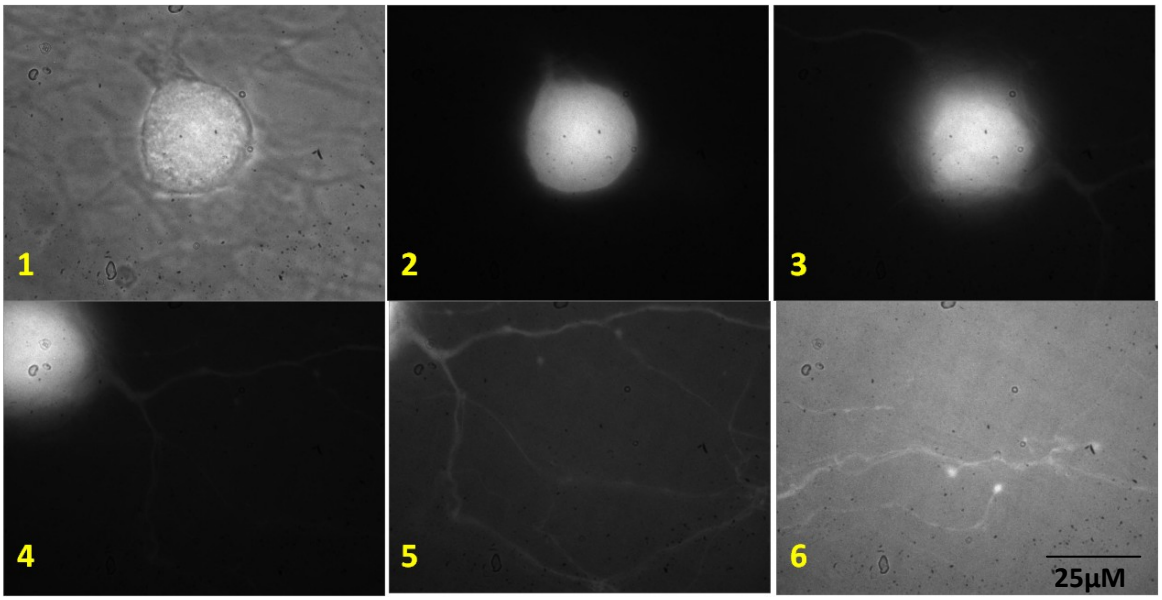

Figure 7.1. Injection of a fluorescent dye to the body of a DRG neuron **(A & B)** Frames (1) to (6) show different fluorescent images obtained from a loaded neuronal body and its associated neuritis after injection with the cell impermeable dye.

Voltage depolarisation of membrane

The SICM nano-pipette maybe used for local voltage depolarisation of the membrane in order to trigger voltage sensitive channels. Here a preliminary experiment to explore this possibility is shown. Further investigation is necessary to establish the possibility of using this method. Here the nano-pipette was positioned to approach to a fine neuronal dendrite. The feedback system was switched off, to keep the pipette stationary right above the dendrite (50 nm). Voltage bias of 10 V was applied to the tip of the nano-pipette. Figure 7.2. Shows the fluorescence response associated with voltage depolarisation of voltage sensitive channels and calcium entry. For this experiment, voltage was applied externally and from the ground electrode in order to be able to apply voltages of higher than 1 V.

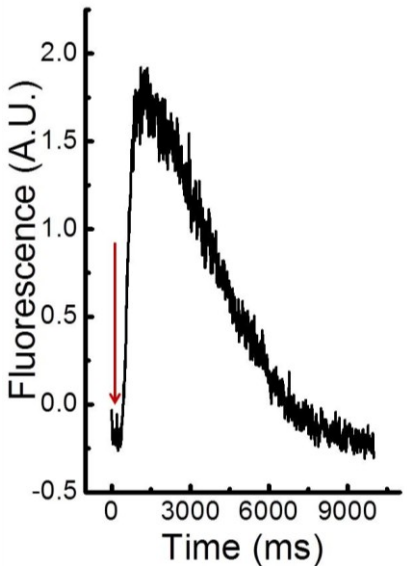

Figure 7.2. Local voltage depolarisation of sensory neurons neurite. Fluorescence response of a DRG neurite under the pipette as a result of a 10 V voltage pulse. Arrow indicates the moment the voltage pulse was applied.

Torch Effect: focus & enhancment of receptor response

In local delivery experiments, the opening of the ion channels, can lead to calcium entry that can propagate and activate downstream receptors. The medium for imaging experiments contains calcium that is readily available throughout the solution. It would be desiarable to be able to stimulate receptors under the nano-pipette and at the same time to keep the delivery and activation localised to the region of delivery. An effective approach to confine the response in calcium imaging experiments after local delivery is to remove calcium ions from the bath solution by adding EDTA and instead provide the calcium through the nano-pipette. In the case of capsaicin delivery, calcium and capsaicin can be delivered under the same positive potential from the nano-pipette electrode. Therefore the stimulant and the chemical necessary for depolarisation can be provided at the same time creating a so called

"torch effect". In this configuration, calcium entry only should occur at the area of stimulation, and as calcium entry is necessary for the firing of the neurons, this will keep other regions silent. This approach prevents downstream signalling effects which could interfere with mapping studies of receptors of interest. Using a higher calcium content solution in the nano-pipette can also help to enhance the intensity of the signal. Figure 7.3 shows calcium application from a nano-pipette tip to a bath solution containing calcium sensitive dye. By increasing the concentration of EDTA in the medium, calcium delivery is focalised to the tip of the nano-pipette.

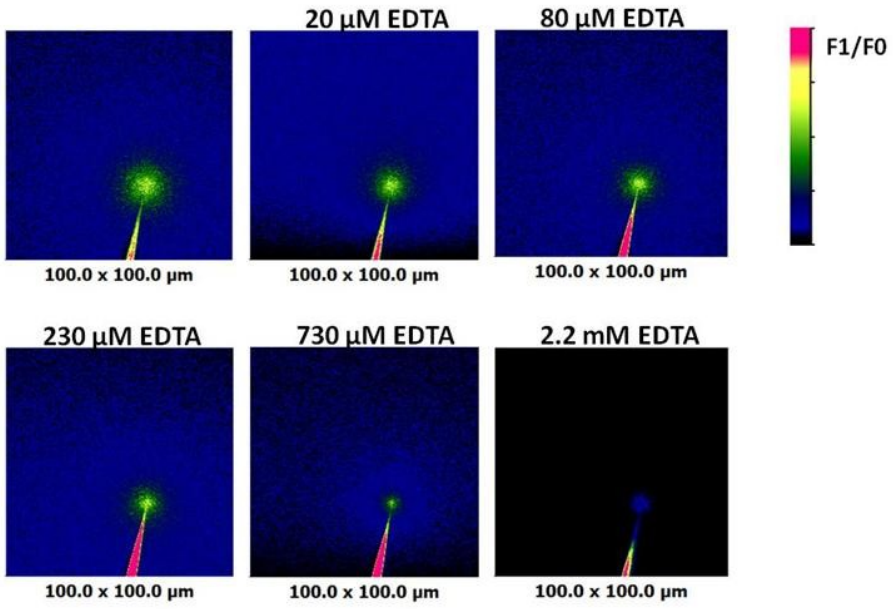

Figure 7.3. Ejection of calcium ions from the tip of the pipette using voltage. Fluorescence images of fluo-4 in the bath. Nano-pipette contain HBSS (2mM Ca^{2+}) while 1 Volt was applied to the pipette vs ground electrode, to eject the positive ions and Calcium from the nano-pipette tip **(1)**. Bath solution contained calcium free medium. Increasing concentration of EDTA was added to the bath to focus the calcium concentration to the tip of the nano-pipette **(2-5)**.

Ion current as temperature sensor

Thermal sensing at a cellular level has biological relevance in the study of metabolic activities in fat cells (Clark et al., 1986). Kim and colleagues have reported fabrication of a micro-pipette capable of measuring thermal fluctuation with high resolution 2 μm), which is capable of measuring steady thermal ±0.01 °C (Shrestha et al., 2011).

The electrochemical currents as well as the ion current are both sensitive to temperature changes and it should possible to calibrate and measure local changes in temperature with high sensitivity. To demonstrate this, warm PBS solution was added to a petri-dish, and a SICM nano-pipette filled with PBS was immersed (+200 mV applied to the SICM nano-pipette), and the ion current was monitored while the temperature dropped, which was measured with a thermometer probe in the bath. Figure 7.4 shows changes in the ion current as the solution temperature returns to room temperature, showing a linear dependency between the ion current and temperature changes.

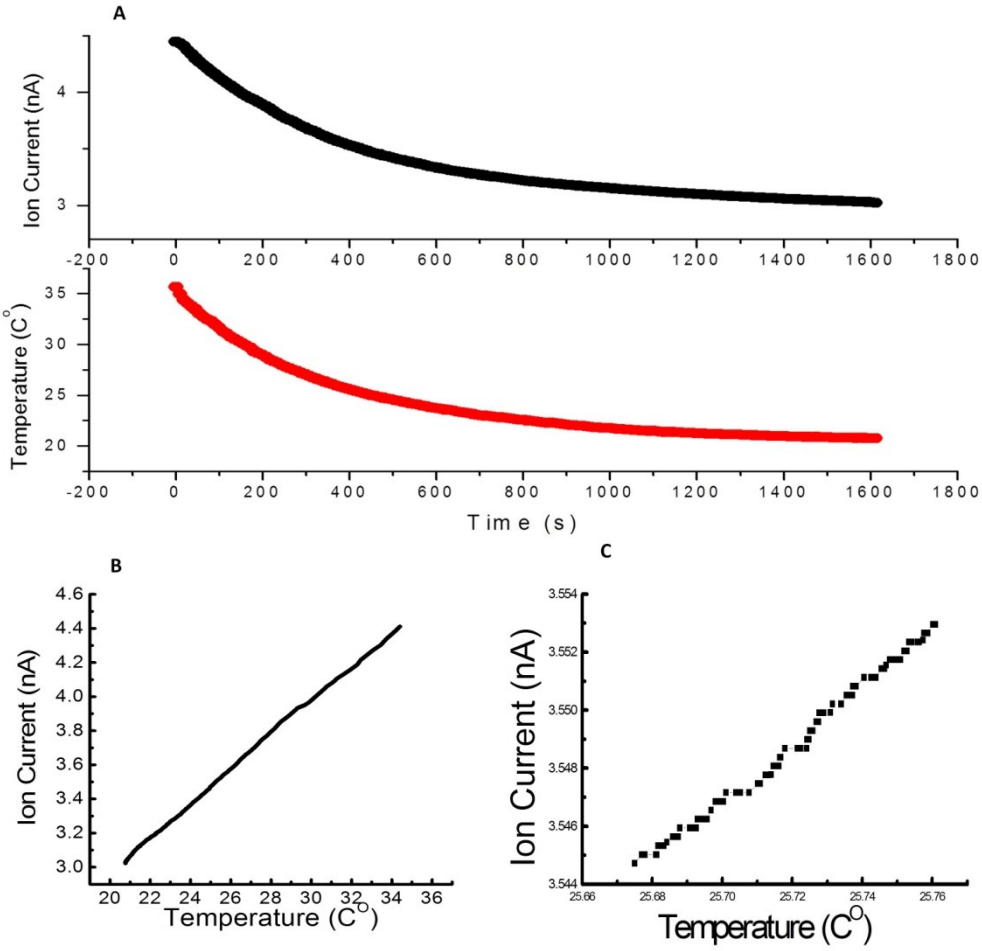

Figure 7.4. Graphs represent the relationship between temperature and ion current in the pipette. **(A)** Simultanious recording of temperature and ion current over a long period. **(B)** & **(C)** the linear relationship between temperature changes and ion current changes over large and small temperature changes respectively.

The experiment described in figure 7.4 was repeated in a solution containing ferrocenmethanol with a SICM nano-pipette and an electrochemical carbon probe (Figure 7.5 **(A)**), to assess the sensitivity of faraday current and ion current to changes in temperature and their relationships with each other (Figure **(5B)**).

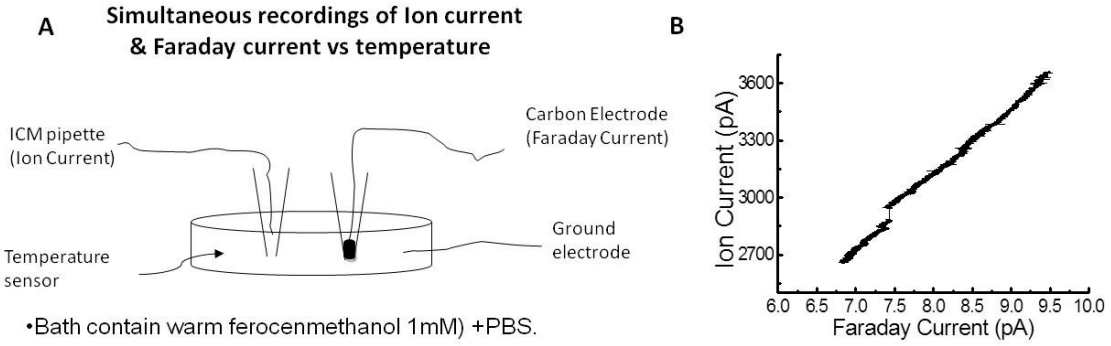

Figure 7.5. The influence of temperature changes on ion current and faraday current. **(A)** Cartoon represents the set-up for simultaneous ion current and faraday current **(B)** Electrochemical and and ion current measurements of SICM and SECM probes immersed in a warm solution (1mM FcCH2OH+PBS), representing how ion current and faraday current change with relation to each other as the temperature drops towards room temperature.

Development of a nano-heater

Qin and colleagues have developed an optical approach and used an infrared diode laser as a heat source and have also demonstrated the relations. A double barrel quartz pipette (theta glass) was coated with carbon with the intention to build a connection between each barrel at the tip of the pipette (Figure 7.6 **(B)**). The resistance between the two barrels was measured with a voltmeter, to confirm this connection, by placing a wire inside each barrel. A resistance of about ~10 kΩ was selected for experiment. Once a connection was confirmed, the wires were connected to an external voltage generator instrument, for the application of voltage to the double barrel carbon probe. Heat is expected to be generated at the area of highest resistance (The tip, Figure 7.6 **(A)**). The carbon electrode was then placed in a bath solution. Generation of bubbles was observed under the optical microscope

at the tip of the nano-heating element when high voltages were applied. Figure 7.6 **(C)** is a visual representation of heat generation near the tip taken a thermal camera. The graph shows the variation in heat generation at different voltages (Figure 7.6 **(C)** & **(D)).** TRPV1 transfected HEK cells, which are known to be heat sensitive, were subsequently used to demonstrate the potential use of carbon heater for stimulation of heat sensitive receptors. The double barrel probe was mounted on the SICM set up and brought to proximity of a HEK cell membrane manually, before the application of voltage to generate heat at the tip heat that led to the calcium entry in to the HEK cells and a fluorescence response (Figure 7.6 **(E)**).

Further experiments are required to calibrate the heating probe. The SICM ion sensitivity to temperature changes discussed in in figure 7.4 can be utilised for calibration. This can be done by bringing a SICM nano-pipette -under the feedback control- to the proximity of the heating element in solution, and by monitor changes in ion current at different voltages applied to the nano-heater.

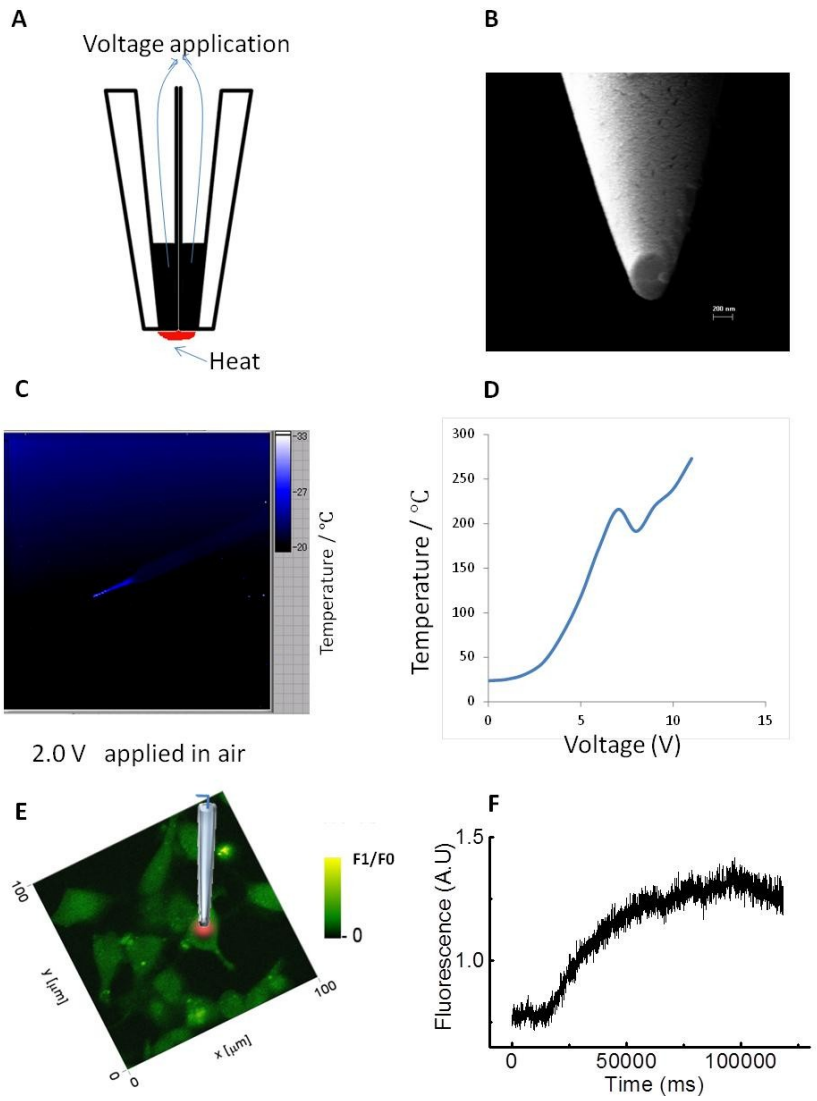

Figure 7.6. A nano-heating element**. (A)** The cartoon representation of a nano-heating carbon probe with heat generated at the tip (red). **(B)** An SEM image of the tip of a double barrel quartz electrode. **(C)** A thermal camera image of a carbon nano-heater in air taken with a TVS-8500 thermal camera. **(D)** The relationship of voltage and temperature generated at the tip of the nano-heater measured by the thermal camera. The resistance of the nano-heater has changed at around 200 degrees which might have been because of the over heating. **(E)** The heat invoked calcium response of TRPV1 HEK cells upon heat generation at the heating element tip. **(F)** Cartoon illustration of a TRPV1 HEK cell stimulated by a nano-heater.

References

Adam Seger,R., Actis,P., Penfold,C., Maalouf,M., Vilozny,B., and Pourmand,N. (2012). Voltage controlled nano-injection system for single-cell surgery. Nanoscale *4*, 5843-5846.

Clark,D.G., Brinkman,M., and Neville,S.D. (1986). Microcalorimetric Measurements of Heat-Production in Brown Adipocytes from Control and Cafeteria-Fed Rats. Biochemical Journal *235*, 337-342.

Shevchuk,A.I., Novak,P., Takahashi,Y., Clarke,R., Miragoli,M., Babakinejad,B., Gorelik,J., Korchev,Y.E., and Klenerman,D. (2011). Realizing the biological and biomedical potential of nanoscale imaging using a pipette probe. Nanomedicine. (Lond) *6*, 565-575.

Shrestha,R., Choi,T.Y., Chang,W., and Kim,D. (2011). A High-Precision Micropipette Sensor for Cellular-Level Real-Time Thermal Characterization. Sensors *11*, 8826-8835.

CHAPTER 8

Conclusions and future directions

The delivery of chemicals through a nano-pipette, under iontophoresis and pressure application was characterised. In collaboration with Dr Peter Jonsson (University of Cambridge) we developed a theoretical model that precisely describes the concentration profile of reagents being delivered from a nano-pipette. A key component in this approach was the integration of the nano-pipette into a SICM. This provided the distance control required for the quantitative reagents delivery. This integration allowed the local stimulation of transfected TRPV1 HEK cells and DRG sensory neurons through the local application of capsaicin. Using this method, cells can be stimulated rapidly and quantitatively, and dose response curves can be obtained locally with sub-cellular resolution. Furthermore, cells were less prone to agonist-induced desensitization compared with dosing in the bulk solution. I demonstrated as well the amenability of automated, multi-point delivery and recording of fluorescence response with a laser confocal microscope.

The use of *in vitro* primary neuronal cultures for high-throughput and clinically relevant, therapeutic drug screenings has been unwieldy, and unpractical because of the complex cell culture preparation and the limited availability of specific cell types (Melli and Hoeke, 2009). The fast multi-dosing application SICM set-up is most suitable for repeated application and

highly specific, targeted pharmacological experiments and provides the option to obtain hundreds of dose response curves for various points within few minutes. The implementation of a long range x-y piezos in to the SICM set-up in the future could provide a drug delivery platform for large scale experiments. In academic settings, I envision this technique to be applied in the mapping of receptors on the surface of living cells and making a contribution in the study of synaptic plasticity.

In parallel with the application of nano-pipettes as a delivery tool, we have developed a novel method for the creation of carbon nano-electrodes embedded in quartz nano-pipettes. I characterized these nano-electrodes using electrochemical methods and demonstrated that their size can be precisely adjusted within the range 5-200 nm by simply changing the nano-pipette pulling parameters. These nano-electrodes have been used for high-resolution electrochemical imaging of living cells as well as for the detection of neurotransmitters release form PC12 cells. These nano-electrodes are currently used in the lab to map the metabolism of brain slices and to detect reactive oxygen species within a single cell.

I believe that the two main methodologies developed during my thesis could be ultimately combined to comprise a device capable of controlled, rapid reagents delivery and simultaneous measurement of the cellular response. This should increase yield of data collected from *in vitro* assays which is particularly important for primary culture preparations.

Brain functions at the nano-scale and the novel multifunctional nano-probe, such as the ones developed during my thesis- will ultimately allow neuroscientists to study brain function with an unprecedented level of details (Cooper and Nadeau, 2009).

I believe that the SICM has the capacity to incorporate recent technological advances, and would predict the future set ups, to be used to study the nano-physiology of neurons to make a significant contribution to the advancement of biomedical sciences in general and neuroscience research in particular.

References

Cooper,D.R. and Nadeau,J.L. (2009). Nanotechnology for in vitro neuroscience. Nanoscale *1*, 183-200.

Melli,G. and Hoeke,A. (2009). Dorsal root ganglia sensory neuronal cultures: a tool for drug discovery for peripheral neuropathies. Expert Opinion on Drug Discovery *4*, 1035-1045.

List of References

Actis,P., Tokar,S., Clausmeyer,J., Babakinejad,B., Mikhaleva,S., Cornut,R., Takahashi,Y., Lopez,C.A., Novak,P., Shevchuck,A.I., Dougan,J.A., Kazarian,S.G., Gorelkin,P.V., Erofeev,A.S., Yaminsky,I.V., Unwin,P.R., Schuhmann,W., Klenerman,D., Rusakov,D.A., Sviderskaya,E.V., and Korchev,Y.E. (2014). Electrochemical Nanoprobes for Single-Cell Analysis. Acs Nano *8*, 875–884.

Adam Seger,R., Actis,P., Penfold,C., Maalouf,M., Vilozny,B., and Pourmand,N. (2012). Voltage controlled nano-injection system for single-cell surgery. Nanoscale *4*, 5843-5846.

Ainla,A., Jansson,E.T., Stepanyants,N., Orwar,O., and Jesorka,A. (2010). A microfluidic pipette for single-cell pharmacology. Anal. Chem. *82*, 4529-4536.

Alivisatos,A., Andrews,A.M., Boyden,E.S., Chun,M., Church,G.M., Deisseroth,K., Donoghue,J.P., Fraser,S.E., Lippincott-Schwartz,J., Looger,L.L., Masmanidis,S., McEuen,P.L., Nurmikko,A.V., Park,H., Peterka,D.S., Reid,C., Roukes,M.L., Scherer,A., Schnitzer,M., Sejnowski,T.J., Shepard,K.L., Tsao,D., Turrigiano,G., Weiss,P.S., Xu,C., Yuste,R., and Zhuang,X. (2013). Nanotools for Neuroscience and Brain Activity Mapping. Acs Nano *7*, 1850-1866.

Amatore,C., Arbault,S., Guille,M., and Lemaitre,F. (2008). Electrochemical monitoring of single cell secretion: Vesicular exocytosis and oxidative stress. Chemical Reviews *108*, 2585-2621.

Amemiya,S., Bard,A.J., Fan,F.R., Mirkin,M.V., and Unwin,P.R. (2008). Scanning Electrochemical Microscopy. Annual Review of Analytical Chemistry *1*, 95-131.

Anand,U., Otto,W., Facer,P., Zebda,N., Selmer,I., Gunthorpe,M., Chessell,I., Sinisi,M., Birch,R., and Anand,P. (2008). TRPA1 receptor localisation in the human peripheral nervous system and functional studies in cultured human and rat sensory neurons. Neuroscience Letters *438*, 221-227.

Angle,M.R. and Schaefer,A.T. (2012). Neuronal recordings with solid-conductor intracellular nanoelectrodes (SCINEs). PloS one *7*, e43194.

Avdic,A., Lugstein,A., Wu,M., Gollas,B., Pobelov,I., Wandlowski,T., Leonhardt,K., Denuault,G., and Bertagnolli,E. (2011). Fabrication of cone-shaped boron doped diamond and gold nanoelectrodes for AFM-SECM. Nanotechnology *22*.

Azevedo,F.A., Carvalho,L.R., Grinberg,L.T., Farfel,J.M., Ferretti,R.E., Leite,R.E., Jacob Filho,W., Lent,R., and Herculano-Houzel,S. (2009). Equal Numbers of Neuronal and Nonneuronal Cells Make the Human Brain an Isometrically Scaled-Up Primate Brain. Journal of Comparative Neurology *513*, 532-541.

Babakinejad,B., Jonsson,P., Lopez,C.A., Actis,P., Novak,P., Takahashi,Y., Shevchuk,A., Anand,U., Anand,P., Drews,A., Ferrer-Montiel,A., Klenerman,D., and Korchev,Y.E. (2013). Local delivery of molecules from a nanopipette for quantitative receptor mapping on live cells. Anal. Chem. *85*, 9333-9342.

Bagher P, Polo-Parada L, and Segal SS (11 A.D.). Microiontophoresis and micromanipulation for intravital fluorescence imaging of the microcirculation. JoVE.

Banks,D.J., Balachandran,W., Richards,P.R., and Ewins,D. (2002). Instrumentation to evaluate neural signal recording properties of micromachined microelectrodes inserted in invertebrate nerve. Physiological Measurement *23*, 437-448.

Bard,A.J., Li,X., and Zhan,W. (2006). Chemically imaging living cells by scanning electrochemical microscopy. Biosensors & Bioelectronics *22*, 461-472.

Betzig,E., Patterson,G.H., Sougrat,R., Lindwasser,O.W., Olenych,S., Bonifacino,J.S., Davidson,M.W., Lippincott-Schwartz,J., and Hess,H.F. (2006). Imaging intracellular fluorescent proteins at nanometer resolution. Science *313*, 1642-1645.

Bhargava,A., Lin,X., Novak,P., Mehta,K., Korchev,Y., Delmar,M., and Gorelik,J. (2013). Super-resolution Scanning Patch Clamp Reveals Clustering of Functional Ion Channels in Adult Ventricular Myocyte. Circulation Research *112*.

Binnig,G., Quate,C.F., and Gerber,C. (1986). Atomic Force Microscope. Physical Review Letters *56*, 930-933.

Bíró ,T., Brodie,C., Modarres,S., Lewin,N.E., ACS ,P., and Blumberg,P.M. (1998). Specific vanilloid responses in C6 rat glioma cells. Molecular Brain Research *56*, 89-98.

Bruckbauer,A., James,P., Zhou,D., Yoon,J.W., Excell,D., Korchev,Y., Jones,R., and Klenerman,D. (2007). Nanopipette delivery of individual molecules to cellular compartments for single-molecule fluorescence tracking. Biophys. J. *93*, 3120-3131.

Bruckbauer,A., Zhou,D., Kang,D.J., Korchev,Y.E., Abell,C., and Klenerman,D. (2004). An addressable antibody nanoarray produced on a nanostructured surface. J. Am. Chem. Soc. *126*, 6508-6509.

Camprubi-Robles,M., Planells-Cases,R., and Ferrer-Montiel,A. (2009). Differential contribution of SNARE-dependent exocytosis to inflammatory potentiation of TRPV1 in nociceptors. FASEB J. *23*, 3722-3733.

Caterina,M.J., Schumacher,M.A., Tominaga,M., Rosen,T.A., Levine,J.D., and Julius,D. (1997). The capsaicin receptor: a heat-activated ion channel in the pain pathway. Nature *389*, 816-824.

Chang,K.C., Chiang,Y.W., Yang,C.H., and Liou,J.W. (2012). Atomic force microscopy in biology and biomedicine. Tzu Chi Medical Journal. 24, 162 -169.

Chen,C.C., Zhou,Y., and Baker,L.A. (2012). Scanning Ion Conductance Microscopy. Annual Review of Analytical Chemistry *5*, 207-228.

Clark,D.G., Brinkman,M., and Neville,S.D. (1986). Microcalorimetric Measurements of Heat-Production in Brown Adipocytes from Control and Cafeteria-Fed Rats. Biochemical Journal *235*, 337-342.

Comstock,D.J., Elam,J.W., Pellin,M.J., and Hersam,M.C. (2010). Integrated Ultramicroelectrode-Nanopipet Probe for Concurrent Scanning Electrochemical Microscopy and Scanning Ion Conductance Microscopy. Analytical Chemistry *82*, 1270-1276.

Cooper,D.R. and Nadeau,J.L. (2009). Nanotechnology for in vitro neuroscience. Nanoscale *1*, 183-200.

Cui,Y., Wei,Q.Q., Park,H.K., and Lieber,C.M. (2001). Nanowire nanosensors for highly sensitive and selective detection of biological and chemical species. Science *293*, 1289-1292.

Gonsalves,M., Barker,A.L., Macpherson,J.V., Unwin,P.R., O'Hare,D., and Winlove,C.P. (2000). Scanning electrochemical microscopy as a local probe of oxygen permeability in cartilage. Biophysical Journal *78*, 1578-1588.

Gorelik,J., Gu,Y., Spohr,H.A., Shevchuk,A.I., Lab,M.J., Harding,S.E., Edwards,C.R., Whitaker,M., Moss,G.W., Benton,D.C., Sanchez,D., Darszon,A., Vodyanoy,I., Klenerman,D., and Korchev,Y.E. (2002). Ion channels in small cells and subcellular structures can be studied with a smart patch-clamp system. Biophys. J. *83*, 3296-3303.

Gorelik,J., Yang,L.Q., Zhang,Y., Lab,M., Korchev,Y., and Harding,S.E. (2006). A novel Z-groove index characterizing myocardial surface structure. Cardiovasc. Res. *72*, 422-429.

Hansma,P.K., Drake,B., Marti,O., Gould,S.A.C., and Prater,C.B. (1989). The Scanning Ion-Conductance Microscope. Science *243*, 641-643.

Herr,N.R., Kile,B.M., Carelli,R.M., and Wightman,R. (2008). Electroosmotic Flow and Its Contribution to Iontophoretic Delivery. Analytical Chemistry *80*, 8635-8641.

Hooke, R. Micrographia: or some physiological descriptions of minute bodies, made by magnifying glasses with observations and inquiries thereupon. 1665. John Martyn, Printer to the Royal Society, London.
Ref Type: Generic

Hu,H., Xie,S., Meng,X., Jing,P., Zhang,M., Shen,L., Zhu,Z., Li,M., Zhuang,Q., and Shao,Y. (2006). Fabrication and characterization of submicrometer- and nanometer-sized double-barrel pipets. Analytical Chemistry *78*, 7034-7039.

Isik,S. and Schuhmann,W. (2006). Detection of nitric oxide release from single cells by using constant-distance-mode scanning electrochemical microscopy. Angewandte Chemie-International Edition *45*, 7451-7454.

Jonsson,P., McColl,J., Clarke,R.W., Ostanin,V.P., Jonsson,B., and Klenerman,D. (2012). Hydrodynamic trapping of molecules in lipid bilayers. Proc. Natl. Acad. Sci. U. S. A *109*, 10328-10333.

Juncker,D., Schmid,H., and Delamarche,E. (2005). Multipurpose microfluidic probe. Nat. Mater. *4*, 622-628.

Kirby,B.J. and Hasselbrink,E.F., Jr. (2004). Zeta potential of microfluidic substrates: 1. Theory, experimental techniques, and effects on separations. Electrophoresis *25*, 187-202.

Korchev,Y.E., Bashford,C.L., Milovanovic,M., Vodyanoy,I., and Lab,M.J. (1997). Scanning ion conductance microscopy of living cells. Biophys. J. *73*, 653-658.

Kovacs,P., Denes,V., Kellenyi,L., and Hernadi,I. (2005). Microiontophoresis electrode location by neurohistological marking: Comparison of four native dyes applied from current balancing electrode channels. J. Pharmacol. Toxicol. Methods *51*, 147-151.

Krol,S., Macrez,R., Docagne,F., Defer,G., Laurent,S., Rahman,M., Hajipour,M.J., Kehoe,P.G., and Mahmoudi,M. (2013). Therapeutic Benefits from Nanoparticles: The Potential Significance of Nanoscience in Diseases with Compromise to the Blood Brain Barrier. Chemical Reviews *113*, 1877-1903.

Kueng,A., Kranz,C., Lugstein,A., Bertagnolli,E., and Mizaikoff,B. (2003). Integrated AFM-SECM in tapping mode: Simultaneous topographical and electrochemical imaging of enzyme activity. Angewandte Chemie-International Edition *42*, 3238-3240.

Kurulugama,R.T., Wipf,D.O., Takacs,S.A., Pongmayteegul,S., Garris,P.A., and Baur,J.E. (2005). Scanning electrochemical microscopy of model neurons: Constant distance imaging. Analytical Chemistry *77*, 1111-1117.

Kwak,J. and Bard,A.J. (1989). Scanning Electrochemical Microscopy - Theory of the Feedback Mode. Analytical Chemistry *61*, 1221-1227.

Kwiat,M., Stein,D., and Patolsky,F. Nanotechnology meets electrophysiology. Current Opinion in Biotechnology (2013).

Lab,M.J., Bhargava,A., Wright,P.T., and Gorelik,J. (2013). The scanning ion conductance microscope for cellular physiology. Am. J. Physiol Heart Circ. Physiol *304*, H1-11.

Lalley,P.M. (1994). The excitability and rhythm of medullary respiratory neurons in the cat are altered by the serotonin receptor agonist 5-methoxy-N,N, dimethyltryptamine. Brain Res. *648*, 87-98.

Lalley,P. (1999). Microiontophoresis and Pressure Ejection. In Modern Techniques in Neuroscience Research, U.Windhorst and H.+.Johansson, eds. Springer Berlin Heidelberg), pp. 193-212.

Lambert,J.W. and Sum,A.K. (2006). Molecular dynamics study of the properties of capsaicin in an 1-octanol/water system. J. Phys. Chem. B *110*, 2351-2357.

Lefrou,C. and Cornut,R. (2010). Analytical Expressions for Quantitative Scanning Electrochemical Microscopy (SECM). Chemphyschem *11*, 547-556.

Li,N., Tourovskaia,A., and Folch,A. (2003). Biology on a chip: microfabrication for studying the behavior of cultured cells. Critical reviews in biomedical engineering *31*, 423-488.

Loh,O., Lam,R., Chen,M., Moldovan,N., Huang,H., Ho,D., and Espinosa,H.D. (2009). Nanofountain-probe-based high-resolution patterning and single-cell injection of functionalized nanodiamonds. Small *5*, 1667-1674.

Macpherson,J.V., Unwin,P.R., Hillier,A.C., and Bard,A.J. (1996). In-situ imaging of ionic crystal dissolution using an integrated electrochemical/AFM probe. Journal of the American Chemical Society *118*, 6445-6452.

McCreery,R.L. (2008). Advanced carbon electrode materials for molecular electrochemistry. Chemical Reviews *108*, 2646-2687.

McLatchie,L.M. and Bevan,S. (2001). The effects of pH on the interaction between capsaicin and the vanilloid receptor in rat dorsal root ganglia neurons. Br. J. Pharmacol. *132*, 899-908.

Meister,A., Gabi,M., Behr,P., Studer,P., Voros,J., Niedermann,P., Bitterli,J., Polesel-Maris,J., Liley,M., Heinzelmann,H., and Zambelli,T. (2009). FluidFM: combining atomic force microscopy and nanofluidics in a universal liquid delivery system for single cell applications and beyond. Nano Lett. *9*, 2501-2507.

Melli,G. and Hoeke,A. (2009). Dorsal root ganglia sensory neuronal cultures: a tool for drug discovery for peripheral neuropathies. Expert Opinion on Drug Discovery *4*, 1035-1045.

Miao,W.J., Ding,Z.F., and Bard,A.J. (2002). Solution viscosity effects on the heterogeneous electron transfer kinetics of ferrocenemethanol in dimethyl sulfoxide-water mixtures. Journal of Physical Chemistry B *106*, 1392-1398.

Mirkin,M.V., Fan,F.R.F., and Bard,A.J. (1992). Scanning Electrochemical Microscopy .13. Evaluation of the Tip Shapes of Nanometer Size Microelectrodes. Journal of Electroanalytical Chemistry *328*, 47-62.

Neher,E. and Sakmann,B. (1976). Single-Channel Currents Recorded from Membrane of Denervated Frog Muscle-Fibers. Nature *260*, 799-802.

Nicoll,R.A., Malenka,R.C., and Kauer,J.A. (1990). Functional comparison of neurotransmitter receptor subtypes in mammalian central nervous system. Physiol Rev. *70*, 513-565.

Nikolaev,V.O., Moshkov,A., Lyon,A.R., Miragoli,M., Novak,P., Paur,H., Lohse,M.J., Korchev,Y.E., Harding,S.E., and Gorelik,J. (2010). Beta2-adrenergic receptor redistribution in heart failure changes cAMP compartmentation. Science *327*, 1653-1657.

Nogala,W., Velmurugan,J., and Mirkin,M.V. (2012). Atomic Force Microscopy of Electrochemical Nanoelectrodes. Analytical Chemistry *84*, 5192-5197.

Novak,P., Li,C., Shevchuk,A.I., Stepanyan,R., Caldwell,M., Hughes,S., Smart,T.G., Gorelik,J., Ostanin,V.P., Lab,M.J., Moss,G.W., Frolenkov,G.I., Klenerman,D., and Korchev,Y.E. (2009).

Nanoscale live-cell imaging using hopping probe ion conductance microscopy. Nat. Methods *6*, 279-281.

Nusser,Z. (2012). Differential subcellular distribution of ion channels and the diversity of neuronal function. Current Opinion in Neurobiology *22*, 366-371.

Piper,J.D., Li,C., Lo,C.J., Berry,R., Korchev,Y., Ying,L., and Klenerman,D. (2008). Characterization and application of controllable local chemical changes produced by reagent delivery from a nanopipet. J. Am. Chem. Soc. *130*, 10386-10393.

Qasaimeh,M.A., Ricoult,S.G., and Juncker,D. (2013). Microfluidic probes for use in life sciences and medicine. Lab Chip *13*, 40-50.

Ralevic,V., Jerman,J.C., Brough,S.J., Davis,J.B., Egerton,J., and Smart,D. (2003). Pharmacology of vanilloids at recombinant and endogenous rat vanilloid receptors. Biochemical Pharmacology *65*, 143-151.

Raman,A., Trigueros,S., Cartagena,A., Stevenson,A., Susilo,M., Nauman,E., and Contera,S.A. (2011). Mapping nanomechanical properties of live cells using multi-harmonic atomic force microscopy. Nature Nanotechnology *6*, 809-814.

Rheinlaender,J., Geisse,N.A., Proksch,R., and Schaeffer,T.E. (2011). Comparison of Scanning Ion Conductance Microscopy with Atomic Force Microscopy for Cell Imaging. Langmuir *27*, 697-704.

Rheinlaender,J., Geisse,N.A., Proksch,R., and Scha¦êffer,T.E. (2010). Comparison of Scanning Ion Conductance Microscopy with Atomic Force Microscopy for Cell Imaging. Langmuir *27*, 697-704.

Robinson,D.L., Hermans,A., Seipel,A.T., and Wightman,R. (2008). Monitoring rapid chemical communication in the brain. Chemical Reviews *108*, 2554-2584.

Robinson,J.T., Jorgolli,M., Shalek,A.K., Yoon,M.H., Gertner,R.S., and Park,H. (2012). Vertical nanowire electrode arrays as a scalable platform for intracellular interfacing to neuronal circuits. Nat Nano *7*, 180-184.

Rodolfa,K.T., Bruckbauer,A., Zhou,D., Korchev,Y.E., and Klenerman,D. (2005). Two-component graded deposition of biomolecules with a double-barreled nanopipette. Angew. Chem. Int. Ed Engl. *44*, 6854-6859.

Rust,M.J., Bates,M., and Zhuang,X. (2006). Sub-diffraction-limit imaging by stochastic optical reconstruction microscopy (STORM). Nat. Methods *3*, 793-795.

Sanchez,D., Anand,U., Gorelik,J., Benham,C.D., Bountra,C., Lab,M., Klenerman,D., Birch,R., Anand,P., and Korchev,Y. (2007). Localized and non-contact mechanical stimulation of dorsal root ganglion sensory neurons using scanning ion conductance microscopy. J. Neurosci. Methods *159*, 26-34.

Sanchez,D., Johnson,N., Li,C., Novak,P., Rheinlaender,J., Zhang,Y., Anand,U., Anand,P., Gorelik,J., Frolenkov,G.I., Benham,C., Lab,M., Ostanin,V.P., Schaffer,T.E., Klenerman,D., and Korchev,Y.E. (2008). Noncontact measurement of the local mechanical properties of living cells using pressure applied via a pipette. Biophys. J. *95*, 3017-3027.

Schermelleh,L., Carlton,P.M., Haase,S., Shao,L., Winoto,L., Kner,P., Burke,B., Cardoso,M., Agard,D.A., Gustafsson,M.G., Leonhardt,H., and Sedat,J.W. (2008). Subdiffraction multicolor imaging of the nuclear periphery with 3D structured illumination microscopy. Science *320*, 1332-1336.

Shah,M. and Haylett,D.G. (2000). Ca2+ channels involved in the generation of the slow afterhyperpolarization in cultured rat hippocampal pyramidal neurons. Journal of Neurophysiology *83*, 2554-2561.

Shevchuk,A.I., Frolenkov,G.I., Sanchez,D., James,P.S., Freedman,N., Lab,M.J., Jones,R., Klenerman,D., and Korchev,Y.E. (2006). Imaging proteins in membranes of living cells by high-resolution scanning ion conductance microscopy. Angew. Chem. Int. Ed Engl. *45*, 2212-2216.

Shevchuk,A.I., Novak,P., Takahashi,Y., Clarke,R., Miragoli,M., Babakinejad,B., Gorelik,J., Korchev,Y.E., and Klenerman,D. (2011). Realizing the biological and biomedical potential of nanoscale imaging using a pipette probe. Nanomedicine. (Lond) *6*, 565-575.

Shevchuk,A.I., Novak,P., Taylor,M., Diakonov,I.A., Ziyadeh-Isleem,A., Bitoun,M., Guicheney,P., Lab,M.J., Gorelik,J., Merrifield,C.J., Klenerman,D., and Korchev,Y.E. (2012). An alternative mechanism of clathrin-coated pit closure revealed by ion conductance microscopy. The Journal of Cell Biology *197*, 499-508.

Shin,W. and Gillis,K.D. (2006). Measurement of changes in membrane surface morphology associated with exocytosis using scanning ion conductance microscopy. Biophysical Journal *91*, L63-L65.

Shrestha,R., Choi,T.Y., Chang,W., and Kim,D. (2011). A High-Precision Micropipette Sensor for Cellular-Level Real-Time Thermal Characterization. Sensors *11*, 8826-8835.

Simon,D.T., Kurup,S., Larsson,K.C., Hori,R., Tybrandt,K., Goiny,M., Jager,E.W., Berggren,M., Canlon,B., and Richter-Dahlfors,A. (2009). Organic electronics for precise delivery of neurotransmitters to modulate mammalian sensory function. Nat. Mater. *8*, 742-746.

Spaine,T.W. and Baur,J.E. (2001). A positionable microcell for electrochemistry and scanning electrochemical microscopy in subnanoliter volumes. Analytical Chemistry *73*, 930-938.

Stone T.W. (1985). Microiontophoresis And Pressure Ejection. The International Brain Research Organization).

Stosiek,C., Garaschuk,O., Holthoff,K., and Konnerth,A. (2003). In vivo two-photon calcium imaging of neuronal networks. Proceedings of the National Academy of Sciences of the United States of America *100*, 7319-7324.

Studer,M. and McNaughton,P.A. (2010). Modulation of single-channel properties of TRPV1 by phosphorylation. J. Physiol *588*, 3743-3756.

Sun,P., Laforge,F.O., and Mirkin,M.V. (2007). Scanning electrochemical microscopy in the 21st century. Phys. Chem. Chem. Phys. 9, 802-823.

Sviderskaya,E.V., Easty,D.J., Lawrence,M.A., Sanchez,D.P., Negulyaev,Y.A., Patel,R.H., Anand,P., Korchev,Y.E., and Bennett,D.C. (2009). Functional neurons and melanocytes induced from immortal lines of postnatal neural crest-like stem cells. FASEB J. *23*, 3179-3192.

Szallasi Arpad, Daniel N.Cortrigt, Charles A.Blum, and Samer R.Eid (2007). The vanilloid receptor TRPV1: 10 years from channel cloning to antagonist proof-of-concept. Nat Rev Drug Discov *6*, 357-372.

Takahashi,Y., Shevchuk,A.I., Novak,P., Babakinejad,B., Macpherson,J., Unwin,P.R., Shiku,H., Gorelik,J., Klenerman,D., Korchev,Y.E., and Matsue,T. (2012). Topographical and electrochemical nanoscale imaging of living cells using voltage-switching mode scanning electrochemical microscopy. Proc. Natl. Acad. Sci. U. S. A *109*, 11540-11545.

Takahashi,Y., Shevchuk,A.I., Novak,P., Murakami,Y., Shiku,H., Korchev,Y.E., and Matsue,T. (2010). Simultaneous noncontact topography and electrochemical imaging by SECM/SICM featuring ion current feedback regulation. J. Am. Chem. Soc. *132*, 10118-10126.

Takahashi,Y., Shevchuk,A.I., Novak,P., Murakami,Y., Shiku,H., Korchev,Y.E., and Matsue,T. (2010). Simultaneous Noncontact Topography and Electrochemical Imaging by SECM/SICM Featuring Ion Current Feedback Regulation. Journal of the American Chemical Society *132*, 10118-10126.

Takahashi,Y., Shiku,H., Murata,T., Yasukawa,T., and Matsue,T. (2009). Transfected Single-Cell Imaging by Scanning Electrochemical Optical Microscopy with Shear Force Feedback Regulation. Analytical Chemistry *81*, 9674-9681.

Tian,B., Cohen-Karni,T., Qing,Q., Duan,X., Xie,P., and Lieber,C.M. (2010). Three-Dimensional, Flexible Nanoscale Field-Effect Transistors as Localized Bioprobes. Science *329*, 830-834.

Tominaga,M., Caterina,M.J., Malmberg,A.B., Rosen,T.A., Gilbert,H., Skinner,K., Raumann,B.E., Basbaum,A.I., and Julius,D. (1998). The Cloned Capsaicin Receptor Integrates Multiple Pain-Producing Stimuli. Neuron *21*, 531-543.

Vilozny,B., Actis,P., Seger,R., and Pourmand,N. (2011). Dynamic Control of Nanoprecipitation in a Nanopipette. Acs Nano *5*, 3191-3197.

Westerink,R. and Ewing,A. (2008). The PC12 cell as model for neurosecretion. Acta Physiologica *192*, 273-285.

Willig,K.I., Rizzoli,S.O., Westphal,V., Jahn,R., and Hell,S.W. (2006). STED microscopy reveals that synaptotagmin remains clustered after synaptic vesicle exocytosis. Nature *440*, 935-939.

Wirth,C. and Luscher,H.R. (2004). Spatiotemporal evolution of excitation and inhibition in the rat barrel cortex investigated with multielectrode arrays. Journal of Neurophysiology *91*, 1635-1647.

Wong,D.K.Y. and Xu,L.Y.F. (1995). Voltammetric Studies of Carbon Disk Electrodes with Submicrometer-Sized Structural Diameters. Analytical Chemistry *67*, 4086-4090.

Wood,J.N., Winter,J., James,I.F., Rang,H.P., Yeats,J., and Bevan,S. (1988). Capsaicin-induced ion fluxes in dorsal root ganglion cells in culture. J. Neurosci. *8*, 3208-3220.

Xie,C., Lin,Z., Hanson,L., Cui,Y., and Cui,B. (2012). Intracellular recording of action potentials by nanopillar electroporation. Nature Nanotechnology *7*, 185-190.

Ying,L., Bruckbauer,A., Rothery,A.M., Korchev,Y.E., and Klenerman,D. (2002). Programmable delivery of DNA through a nanopipet. Anal. Chem. *74*, 1380-1385.

Ying,L., Bruckbauer,A., Zhou,D., Gorelik,J., Shevchuk,A., Lab,M., Korchev,Y., and Klenerman,D. (2005). The scanned nanopipette: a new tool for high resolution bioimaging and controlled deposition of biomolecules. Phys. Chem. Chem. Phys. *7*, 2859-2866.

Ying,L., White,S.S., Bruckbauer,A., Meadows,L., Korchev,Y.E., and Klenerman,D. (2004). Frequency and voltage dependence of the dielectrophoretic trapping of short lengths of DNA and dCTP in a nanopipette. Biophys. J. *86*, 1018-1027.

Yoon,I., Hamaguchi,K., Borzenets,I.V., Finkelstein,G., Mooney,R., and Donald,B.R. (2013). Intracellular Neural Recording with Pure Carbon Nanotube Probes. PloS one *8*, e65715.

Zhang,J. and Mifflin,S.W. (1997). Influences of excitatory amino acid receptor agonists on nucleus of the solitary tract neurons receiving aortic depressor nerve inputs. J. Pharmacol. Exp. Ther. *282*, 639-647.

Appendix: Summary of permission for third party copyright works

Page Number	Type of work:.	Source work	Copyright holder & year	Permission to re-use
Page 18	Figure	Nature Nanotechnology (2012) 7(3):180-4.	© Robinson et al 2012 published by Nature Nanotechnology	✓
Page 21, 55	Figure	Nanomedicine. (2011) 6, 565-575.	© Shevchuk et al 2011 published by Future Medicine	✓
Page 21	Figure	J. Neuroscience Methods (2007) 159, 26-34.	©Sanchez et al 2007 Biophysical Journal	✓
Page 42	Figure	Tzu Chi Medical Journal (2012). 24, -169.	© Chang et al 2012 published by Tzu Chi Medical Journal	✓
Page 43	Figure	Nature Nanotechnology (2011) 6, 809-814.	© Raman et al 2011 published by Nature Nanotechnology	✓
Page 46	Figure	Langmuir (2012) 27, 697-704.	©Rheinlaender et al 2011 Published by ACS Publications	✓
Page 68	Figure	Angewante Chemi (2011) 28, 9638-9642.	© Takahashi et al 2011 published by John Wiley and Sons Publications	✓
Page 84, 86, 88	Figure	Proceedings of the National Academy of Sciences (2012) 109, 11540-11545.	© Takahashi et al 2012 published by PNAS	✓
Chapter 4	Figure & Text	ACS Nano (2014)., 8 (1), 875–884.	© Actis et al 2014 published by ACS Publications	✓
Chapter 5 &6	Figure & Text	Analytical Chemistry (2013) 85, 9333-9342.	© Babakinejad et al 2013 published by ACS Publications	✓

This is a License Agreement between Babak Babakinejad ("You") and Nature Publishing Group ("Nature Publishing Group"). The license consists of your order details, the terms and conditions provided by Nature Publishing Group, and the payment terms and conditions.

Get the printable license.

License Number	3335940683363
License date	Feb 25, 2014
Licensed content publisher	Nature Publishing Group
Licensed content publication	Nature Nanotechnology
Licensed content title	Vertical nanowire electrode arrays as a scalable platform for intracellular interfacing to neuronal circuits
Licensed content author	Jacob T. Robinson, Marsela Jorgolli, Alex K. Shalek, Myung-Han Yoon, Rona S. Gertner, Hongkun Park
Licensed content date	Jan 10, 2012
Type of Use	reuse in a dissertation / thesis
Volume number	7
Issue number	3
Requestor type	academic/educational
Format	print and electronic
Portion	figures/tables/illustrations
Number of figures/tables/illustrations	1
High-res required	no
Figures	Figure 1
Author of this NPG article	no
Your reference number	None
Title of your thesis / dissertation	Development of Multifunctional Nano-probes for Neuroscience Research
Expected completion date	Feb 2014
Estimated size (number of pages)	160
Total	**0.00 USD**

Sam Cavana [s.cavana@future-science-group.com]

Tuesday, February 25, 2014 3:44 PM

Dear Babak,

We will be happy for you to use the figures for use in your thesis in this instance.

Kind regards,

Sam

Sam Cavana
Reprint Sales Manager

future science group
tel: +44 (0)20 8371 6084 | fax: +44 (0)20 8371 6089 | www.future-science-group.com
email: s.cavana@future-science-group.com

Babakinejad, Babak

Actions

To: s.cavana@futuremedicine.com

Sent Items

Tuesday, February 25, 2014 3:40 PM

Dear Sam,

I am a coauthor on the following paper. I was wondering if you would be so kind as to give me permission to reuse two of the figures in my thesis.

Realizing the biological and biomedical potential of nanoscale imaging using a pipette probe

Andrew I Shevchuk[1], Pavel Novak[1,2], Yasufumi Takahashi[1], Richard Clarke[3], Michele Miragoli[2], Babak Babakinejad[1],Julia Gorelik[2], Yuri E Korchev[1] & David Klenerman[†3]

Regards,

Babak

This is a License Agreement between Babak Babakinejad ("You") and Elsevier ("Elsevier"). The license consists of your order details, the terms and conditions provided by Elsevier, and the payment terms and conditions.

Get the printable license.

License Number	3335940312729
License date	Feb 25, 2014
Licensed content publisher	Elsevier
Licensed content publication	Biophysical Journal
Licensed content title	Noncontact Measurement of the Local Mechanical Properties of Living Cells Using Pressure Applied via a Pipette
Licensed content author	Daniel Sánchez,Nick Johnson,Chao Li,Pavel Novak,Johannes Rheinlaender,Yanjun Zhang,Uma Anand,Praveen Anand,Julia Gorelik,Gregory I. Frolenkov,Christopher Benham,Max Lab,Victor P. Ostanin,Tilman E. Schäffer,David Klenerman,Yuri E. Korchev
Licensed content date	15 September 2008
Licensed content volume number	95
Licensed content issue number	6
Number of pages	11
Type of Use	reuse in a thesis/dissertation
Portion	figures/tables/illustrations
Number of figures/tables/illustrations	1
Format	both print and electronic
Are you the author of this Elsevier article?	No
Will you be translating?	No
Title of your thesis/dissertation	Development of Multifunctional Nano-probes for Neuroscience Research
Expected completion date	Feb 2014
Estimated size (number of pages)	160
Elsevier VAT number	GB 494 6272 12
Permissions price	0.00 USD
VAT/Local Sales Tax	0.00 USD / 0.00 GBP
Total	**0.00 USD**

This is a License Agreement between Babak Babakinejad ("You") and Elsevier ("Elsevier"). The license consists of your order details, the terms and conditions provided by Elsevier, and the payment terms and conditions.

Get the printable license.

License Number	3336090585431
License date	Feb 25, 2014
Licensed content publisher	Elsevier
Licensed content publication	Tzu Chi Medical Journal
Licensed content title	Atomic force microscopy in biology and biomedicine
Licensed content author	Kai-Chih Chang,Yu-Wei Chiang,Chin-Hao Yang,Je-Wen Liou
Licensed content date	December 2012
Licensed content volume number	24
Licensed content issue number	4
Number of pages	8
Type of Use	reuse in a thesis/dissertation
Portion	figures/tables/illustrations
Number of figures/tables/illustrations	2
Format	both print and electronic
Are you the author of this Elsevier article?	No
Will you be translating?	No
Title of your thesis/dissertation	Development of Multifunctional Nano-probes for Neuroscience Research
Expected completion date	Feb 2014
Estimated size (number of pages)	160
Elsevier VAT number	GB 494 6272 12
Permissions price	0.00 USD
VAT/Local Sales Tax	0.00 USD / 0.00 GBP
Total	**0.00 USD**

This is a License Agreement between Babak Babakinejad ("You") and Nature Publishing Group ("Nature Publishing Group"). The license consists of your order details, the terms and conditions provided by Nature Publishing Group, and the payment terms and conditions.

Get the printable license.

License Number	3335941271924
License date	Feb 25, 2014
Licensed content publisher	Nature Publishing Group
Licensed content publication	Nature Nanotechnology
Licensed content title	Mapping nanomechanical properties of live cells using multi-harmonic atomic force microscopy
Licensed content author	A. Raman, S. Trigueros, A. Cartagena, A. P. Z. Stevenson, M. Susilo, E. Nauman
Licensed content date	Nov 13, 2011
Type of Use	reuse in a dissertation / thesis
Volume number	6
Issue number	12
Requestor type	academic/educational
Format	print and electronic
Portion	figures/tables/illustrations
Number of figures/tables/illustrations	1
High-res required	no
Figures	Figure 1
Author of this NPG article	no
Your reference number	None
Title of your thesis / dissertation	Development of Multifunctional Nano-probes for Neuroscience Research
Expected completion date	Feb 2014
Estimated size (number of pages)	160
Total	**0.00 USD**

Copyright Clearance Center RightsLink®

Home | Account Info | Help

ACS Publications High quality. High impact.

Title: Comparison of Scanning Ion Conductance Microscopy with Atomic Force Microscopy for Cell Imaging

Author: Johannes Rheinlaender, Nicholas A. Geisse, Roger Proksch, and Tilman E. Schäffer

Publication: Langmuir

Publisher: American Chemical Society

Date: Jan 1, 2011

Copyright © 2011, American Chemical Society

Logged in as:
Babak Babakinejad
Account #:
3000756027

LOGOUT

PERMISSION/LICENSE IS GRANTED FOR YOUR ORDER AT NO CHARGE

This type of permission/license, instead of the standard Terms & Conditions, is sent to you because no fee is being charged for your order. Please note the following:

- Permission is granted for your request in both print and electronic formats, and translations.
- If figures and/or tables were requested, they may be adapted or used in part.
- Please print this page for your records and send a copy of it to your publisher/graduate school.
- Appropriate credit for the requested material should be given as follows: "Reprinted (adapted) with permission from (COMPLETE REFERENCE CITATION). Copyright (YEAR) American Chemical Society." Insert appropriate information in place of the capitalized words.
- One-time permission is granted only for the use specified in your request. No additional uses are granted (such as derivative works or other editions). For any other uses, please submit a new request.

If credit is given to another source for the material you requested, permission must be obtained from that source.

License Number	3336080524263
License date	Feb 25, 2014
Licensed content publisher	John Wiley and Sons
Licensed content publication	Angewandte Chemie International Edition
Licensed content title	Multifunctional Nanoprobes for Nanoscale Chemical Imaging and Localized Chemical Delivery at Surfaces and Interfaces
Licensed copyright line	Copyright © 2011 WILEY-VCH Verlag GmbH & Co. KGaA, Weinheim
Licensed content author	Yasufumi Takahashi,Andrew I. Shevchuk,Pavel Novak,Yanjun Zhang,Neil Ebejer,Julie V. Macpherson,Patrick R. Unwin,Andrew J. Pollard,Debdulal Roy,Charles A. Clifford,Hitoshi Shiku,Tomokazu Matsue,David Klenerman,Yuri E. Korchev
Licensed content date	Sep 1, 2011
Start page	9638
End page	9642
Type of use	Dissertation/Thesis
Requestor type	University/Academic
Format	Print and electronic
Portion	Figure/table
Number of figures/tables	1
Original Wiley figure/table number(s)	Adapting part of figure 1.
Will you be translating?	No
Title of your thesis / dissertation	Development of Multifunctional Nano-probes for Neuroscience Research
Expected completion date	Feb 2014
Expected size (number of pages)	160
Total	**0.00 USD**

PNAS Permissions [PNASPermissions@nas.ed...

Tuesday, February 25, 2014 7:55 PM

Permission is granted for your use of the figures as described in your message. Please cite the full article references (because this material published after 2008, a copyright notice is not needed). Let us know if you have any questions.

Best regards,
Kay McLaughlin for
Diane Sullenberger
Executive Editor
PNAS

Babakinejad, Babak

Actions

To: PNASPermissions@nas.edu

Sent Items

Tuesday, February 25, 2014 7:09 PM

Dear Sir/Madam,
I am a co-author on the following publication. I would be grateful if you could grant permission to use content (Figure 2, 3 and 4) from the following PNAS article published in Volume 109, pages 11540 -11545. http://www.pnas.org/content/109/29/11540.abstract in my PhD thesis.

Yasufumi Takahashi et al.,

Yours truly,

Babak Babakinejad